(2)

AD-A247 091

MENTATION PAGE

Form Approved
OMB No. 0704-0188

2. REPORT DATE	3. REPORT TYPE AND DATES COVERED
Nov. 30, 1991	Final Report 6/1/89-9/30-91

4. TITLE AND SUBTITLE
A Seismic and Integrated Geophysical Study of the Lithosphere of the Colorado Plateau

5. FUNDING NUMBERS
F449620-89-C-0076
61102F
2309
A2

6. AUTHOR(S)
G.R. Keller, M.R. Baker, D.I. Doser and J.H. Hinojosa

7. PERFORMING ORGANIZATION NAME(S) AND ADDRESS(ES)
University of Texas at El Paso
Department of Geological Sciences
El Paso, Texas 79968-0555

8. PERFORMING ORGANIZATION REPORT NUMBER
AFOSR-TR- 92 0009
AFGEOB2

9. SPONSORING/MONITORING AGENCY NAME(S) AND ADDRESS(ES)
Department of the Air Force
Air Force Office of Scientific Research (AFSC)
BoBolling Air Force Base, DC 20332-6448

10. SPONSORING/MONITORING AGENCY REPORT NUMBER

11. SUPPLEMENTARY NOTES

12a. DISTRIBUTION/AVAILABILITY STATEMENT
Publically Available

12b. DISTRIBUTION CODE

13. ABSTRACT *(Maximum 200 words)*

The major effort of this project was field data collection, data processing, and interpretation for the PACE (Pacific to Arizona Crustal Experiment) seismic experiment. This major cooperative study involved the University of Texas at El Paso, the Air Force Geophysical Lab, the U.S. and Canadian Geological Surveys, Stanford University, the University of Saskatchewan and the University of Arizona. The massive data set gathered during this experiment have been analyzed by a variety of techniques. The results show a gradual thickening of the crust from about 30 km in the Basin and Range to about 40 km along the southwestern margin of the Colorado Plateau. Lateral variations along the transition zone were found to be small.

Work along a long profile extending from the Nevada Test Site to White Sands Missile Range included collection of new data, waveform modeling of data from the Albuquerque, NM digital seismograph station and a crustal structure study of western New Mexico. These results document thin (~35 km) crust beneath the central portion of the Rio Grande rift, extension of the lithospheric anomaly associated with this rift well east of the physiographic rift valley, a broad transitional zone to thick crust on the western margin of the rift, and delineation of a batholithic mass in the upper crust of western New Mexico.

14. SUBJECT TERMS
Colorado Plateau, Seismic Profiling, Lithospheric Structure

15. NUMBER OF PAGES
439

16. PRICE CODE

17. SECURITY CLASSIFICATION OF REPORT	18. SECURITY CLASSIFICATION OF THIS PAGE	19. SECURITY CLASSIFICATION OF ABSTRACT	20. LIMITATION OF ABSTRACT
Unclassified	Unclassified	Unclassified	(a)

A Seismic & Integrated Geophysical Study of the Lithosphere of the Colorado Plateau

Final Report
Contact Number: F449620-89-C-0076

Principal Investigators

G. Randy Keller
Diane I. Doser
Juan H. Hinojosa
Mark R. Baker

Department of Geological Sciences
University of Texas at El Paso
El Paso, Texas 79968

Summary

The major thrust of this project was participation in the Pacific to Arizona Crustal Experiment (PACE) in the Fall of 1989. The funding provided for this major, cooperative experiment via the University of Texas at El Paso (UTEP) was vital to its overall success. Through the work of our experiment team, a subcontract to the University of Saskatchewan/Geological Survey of Canada, and the provision of drill holes and explosives, about one third of the manpower, instrumentation, and seismic sources for the main experiment was provided by UTEP. Thanks to this contribution, the experiment was executed in a timely fashion and was able to achieve its scientific objectives. The massive data set collected has shed considerable light on the Basin and Range - Colorado Plateau Transition Zone in western Arizona and the adjacent portions of the Plateau. A large number of groups were involved in this effort (See attached tables), and a set of papers reporting results will be submitted as a special section to the Journal of Geophysical Research early in 1992.

The shooting and recording geometries for the PACE experiment are shown in Figures 1 and 2. The main NE-SW trending line and short parallel line were recorded in the first deployment. A station spacing of about 330 m was obtained on the mainline, and the parallel line was occupied to test for lateral variability and to collect data for a tomographic analysis. The NW-SE trending crossline was recorded in one deployment with a very close station spacing of 100 m in the central portion of the spread with the spacing gradually increasing away from the center. The Air Force Geophysical Laboratory group recorded on the north rim of the Grand Canyon for this deployment, and the short parallel line was occuppied again to collect fan data for tomographic analysis. This deployment provided data on purely Colorado Plateau structures and extended approximately along the NTS - WSMR (White Sands Missile Range) regional seismic profile. The final deployment (Meteor crater line) was the easternmost and targeted shallow basement structures. It was suspected that such structures were more complex than generally believed and that they were capable of producing significant travel-time anomalies which could be erroneously attributed to deeper

structures. This line also provided a direct tie to COCORP (Consortium for Continental Reflection Profiling) profiling in the area. Gravity anomalies have also been evaluated as a constraint on shallow structures.

The shotpoint efficiency for the PACE-89 study was very good. Examples of record sections from the main profile are shown in Figure 3-5. Shotpoints 31 and 46 were the southwesternmost and northeasternmost sources which bracket the receivers deployed in 1989. They primarily contain information about crustal structure. The record sections shown in Figure 5 were constructed by merging the 1987 and 1989 PACE data. Mantle arrivals are clear on these record sections. The number of shots in the 1989 data set made it possible to derive earth models by inverse methods. The mainline earth model derived is shown in Figure 6. The velocity structure is depicted by velocity contours.

The earth model shown in Figure 6 shows a gradual thickening of the crust from the Basin and Range through the Transition Zone into the Colorado Plateau. Previous studies to the southeast suggested that a step (fault?) existed in the Moho at the edge of the Colorado Plateau. The detailed data from the PACE 89 experiment indicate that the travel-time anomaly giving rise to this interpretation may well have been due to a shallow structure. This gradual transition in crustal structure is indicative of ductile rather than brittle behavior. Simple shear models of crustal extension in the adjacent Basin and Range would suggest a local area of crustal thinning along the margin of the Colorado Plateau. Such features were not observed in the PACE 89 data, again suggesting that ductile behavior is dominate from mid-crustal depths downward. A deep mantle interface detected also appears to gradually deepen beneath the plateau.

The secondary thrust of this effort was work on the NTS-WSMR regional seismic profile and lithospheric transect (Figure 7). This long term effort is being undertaken with the collaboration of Los Alamos National Laboratory. The ultimate goal of this study is to record NTS sources across

the Colorado Plateau and Rio Grande Rift into the Great Plains and to observe the effects of the boundaries of these major lithospheric structures. By using large conventional explosions at WSMR, this profile can be partially reversed. A goal during this study was to obtain whatever data possible to constrain crustal structure along this profile, thus increasing our confidence that we can identify deep-seated seismic anomalies. To this end, seismic profiles across the Mogollon - Datil volcanic field area were analyzed in order to investigate the Colorado Plateau - Rio Grande Rift transition zone. The location of these profiles is shown in Figure 8 and the final seismic models are shown in Figures 9 and 10. This work was part of a doctoral dissertation by Robert V. Schneider (Appendix A) and demonstrated the presence of a broad crustal transitional zone along the eastern margin of the Colorado Plateau. Another constraint on crustal structure was provided by broadband teleseismic waveform analysis of a station located in the Rio Grande rift. This study was conducted by Brian Murphy and served as his M.S. thesis (Appendix B). Data from the Albuquerque, New Mexico digital seismic station (ANMO) were employed in this study. Long and short period, digital, three component seismograms were merged through source equalization deconvolution to derive broadband receiver functions. After stacking based on common source distance and back azimuth, the mean radial component receiver functions were analyzed by both forward and inverse modeling schemes. The final models for southwest and northwest back azimuths are shown in Figures 11 and 12. Since these results show shear wave distributions, they were compared with interstation surface wave data for the path from El Paso to Albuquerque which is contained within the Rio Grande rift. The agreement between these results was excellent. This type of work also included the operation of a broadband station in southwestern, New Mexico. Correlation with refraction and COCORP profiles in the central portion of the Rio Grande Rift would indicate that the discontinuity at 35 km in Figures 11 and 12 is the Moho.

Recording along the NTS-WSMR regional seismic profile (Figure 7) has produced data across the entire state of New Mexico and a few records in eastern Arizona. This work is the basis ot an

M.S. Thesis by Donald Roberts (Appendix C). An example of these data and the ray tracing results are shown in Figures 13 and 14. Because of the unusually long source receiver offsets being recorded, the asymptotic ray theory algorithm being employed had to be modified to account for a curved earth. The earth model shown in Figure 14 represents our synthesis of the results of this effort to date. This model reflects all of the constraints available including regional gravity anomalies. The eastern margin of the Colorado Plateau and the transition between the Rio Grande Rift and Great Plains reflect gradual thinning of the lithosphere beneath the rift. As discussed below, the thermal anomaly implied by this thinning can explain a portion of the uplift of the plateau. Another implication of this model is that the Rio Grande Rift - Great Plains boundary extends considerably further east than previously believed. Variations from the widely accepted Burdick and Helmberger upper mantle velocity structure for the western United States are depicted in Figure 14. These variations primarily consist of lithospheric thinning beneath the Rio Grande Rift and marked thickening of the lithosphere beneath the Great Plains.

The final effort during this project has been regional evaluation of the Colorado Plateau (CP) lithosphere (Appendix D). The Colorado Plateau (CP) is a coherent and elastically strong lithospheric block surrounded in part by the weaker extensional regimes of the Basin and Range Province and the Rio Grande Rift. The CP has experienced a Cenozoic uplift of about 2 km. The exact physical mechanism responsible for this isostatic uplift is still unclear. Previously proposed uplift mechanisms for the CP include, in general, some form of (i) thermal expansion, (ii) crustal thickening, and (iii) phase changes. An alternative thermomechanical uplift mechanism has been derived and evaluated. A finite difference solution to both the axisymmetric, time-dependent heat conduction equation with heat sources and the elastic flexure equation has been obtained. Heat flux boundary conditions are used at the base and sides of the model, while the upper boundary is isothermal. The time-dependent elastic thickness of the CP lithosphere model is computed at each time step, and the buoyancy produced by the heated material is used as the thermally-derived normal stress acting on

the elastic lithosphere. The initial results of this study appear to indicate that the 2 km of uplift of the CP were produced by at least two sources of uplift, the first associated with the regional heating of the western Cordillera, and the second associated with the flexural response of the CP lithosphere to radial heating at the sides.

PACE - 89 PARTICIPANTS

USGS	Refraction Crew
	Flagstaff Personnel
	Teleseismic Group
UTEP/Canadians	Randy Keller
	Jesus Bocanegra
	Diane Doser
	Mark Baker
	Steven Harder
	Donald Roberts
	Carlos Montana
	Abdul Suleiman
	Ronald Barrow
	Zolie Hajnal and student assistants
	Bob Schiemann
	Tim Cartwright
University of Arizona	Roy Johnson
	Field assistants
Standford University	George Thompson
	John Howie
	Tom Parsons
Air Force Geophysics Lab	John Cipar
	Lorraine Wolf
	Field assistants
Northern Arizona University	Paul Morgan
	Dave Brumbau

TYPES OF PACE SEISMIC STUDIES

Refraction:	**Jill McCarthy and Will Kohler -- *USGS***
	G. Randy Keller, Diane Doser, Mark Baker, Carlos Montana, and Bashir Durrani -- *UTEP*
	John Cipar, Lorraine Wolf, and Susan D'Annolfo -- *AFGL*
	Zoltan Hajnal -- *Univ. Saskatchewan*
Reflection:	**George Thompson, John Howie, and Tom Parsons -- *Stanford***
	Roy Johnson and Ken Hartman - *Arizona*
Teleseismic:	**H.M. Iyer, John Evans, and Phil Dawson -- *USGS***
	David Brumbau -- *Northern Arizona Univ.*
Receiver Functions:	**Stan Ruppert and Harley Benz -- *Stanford & USGS***

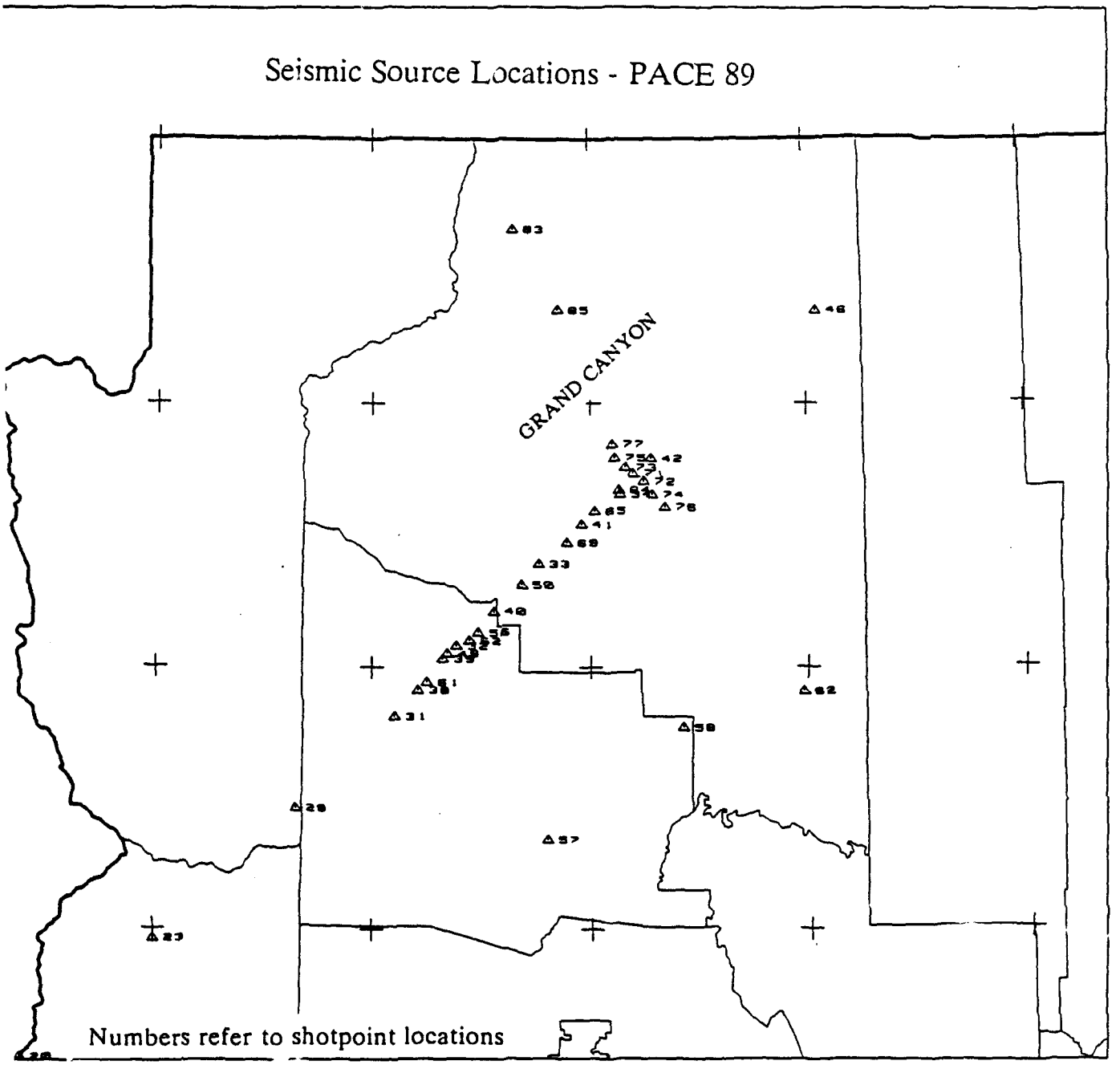
Seismic Source Locations - PACE 89
GRAND CANYON
Numbers refer to shotpoint locations

Figure 1

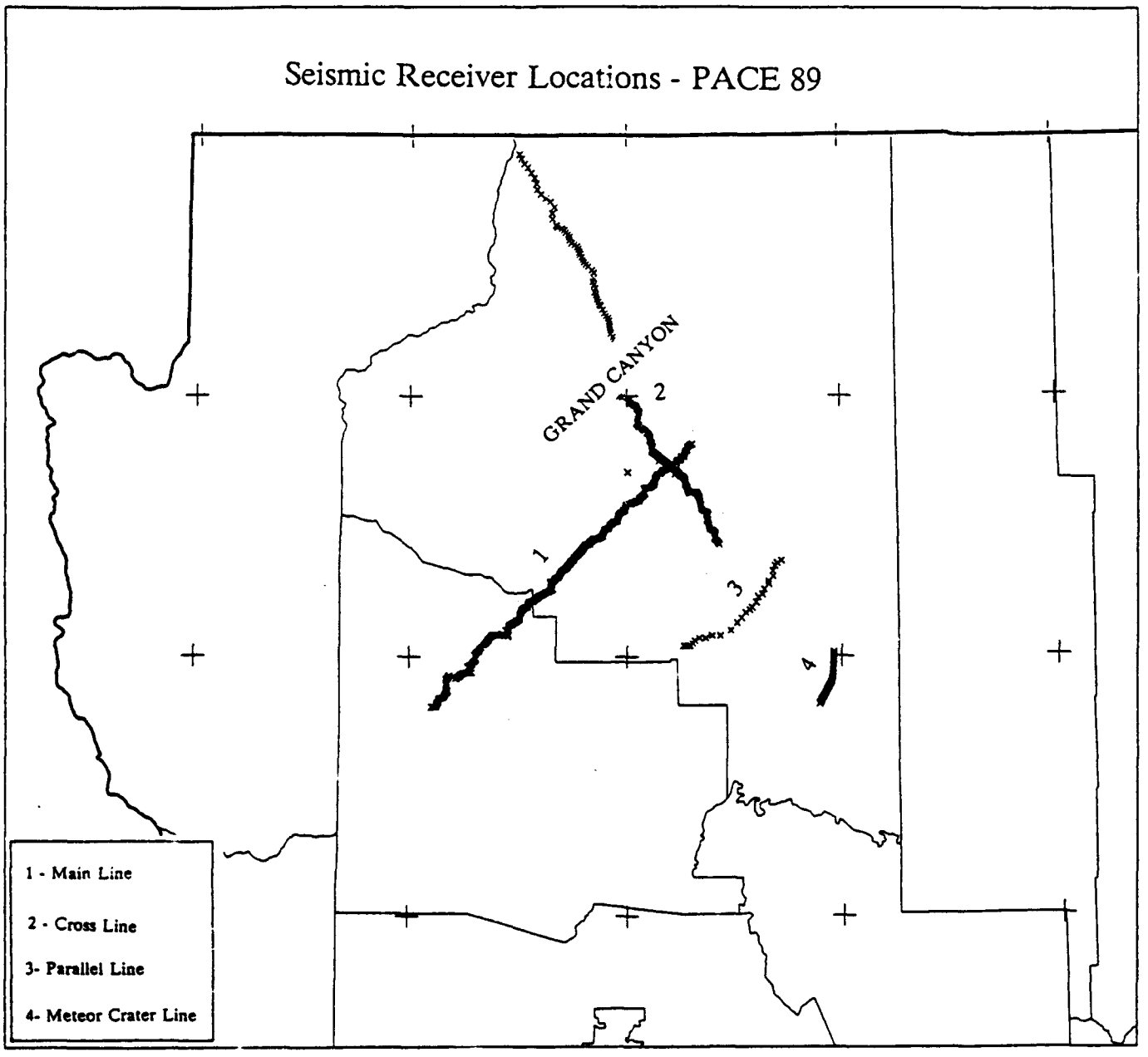
Seismic Receiver Locations - PACE 89
GRAND CANYON
1
2
3
4
1 - Main Line
2 - Cross Line
3- Parallel Line
4- Meteor Crater Line

Figure 2

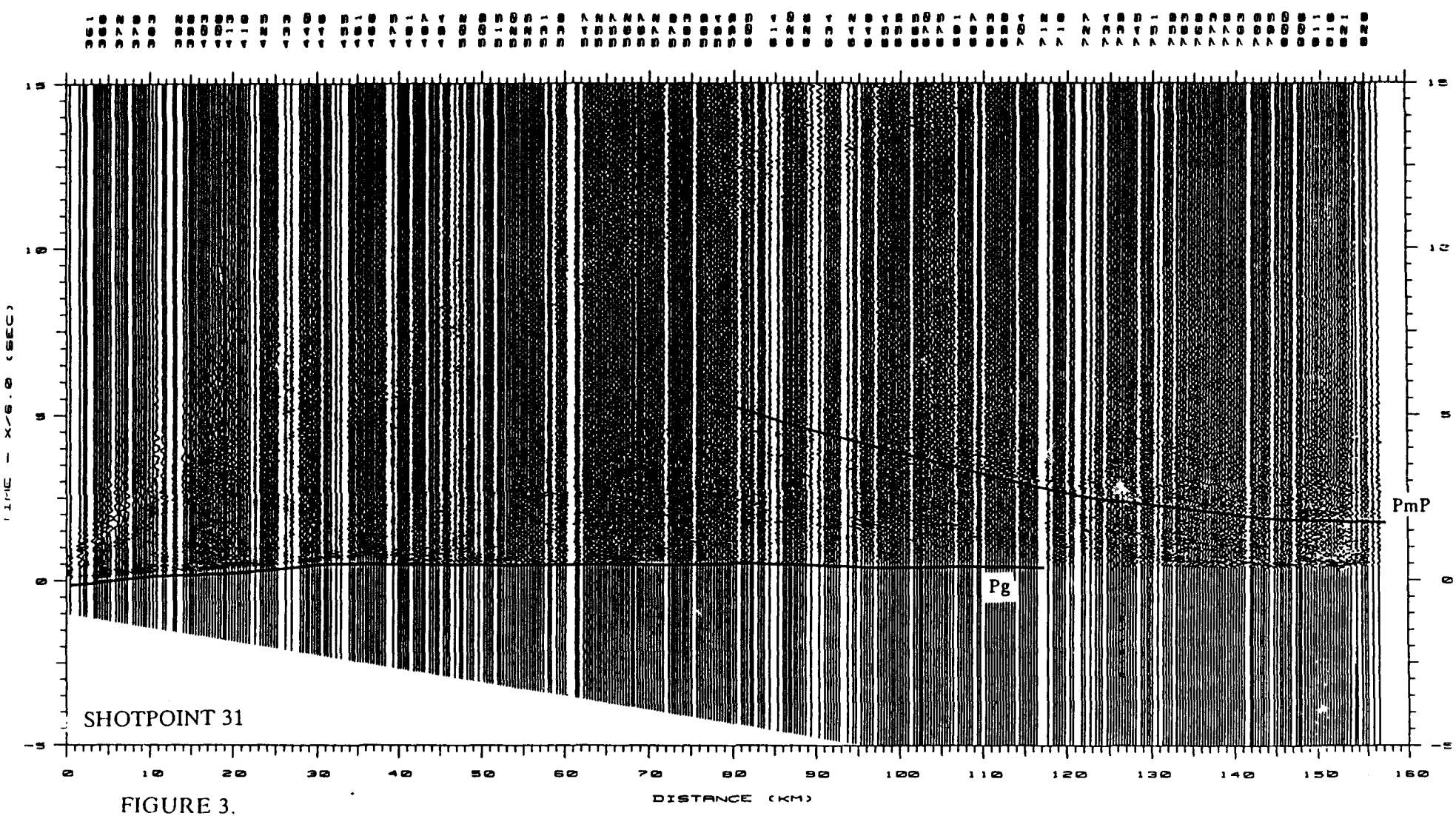

FIGURE 3.

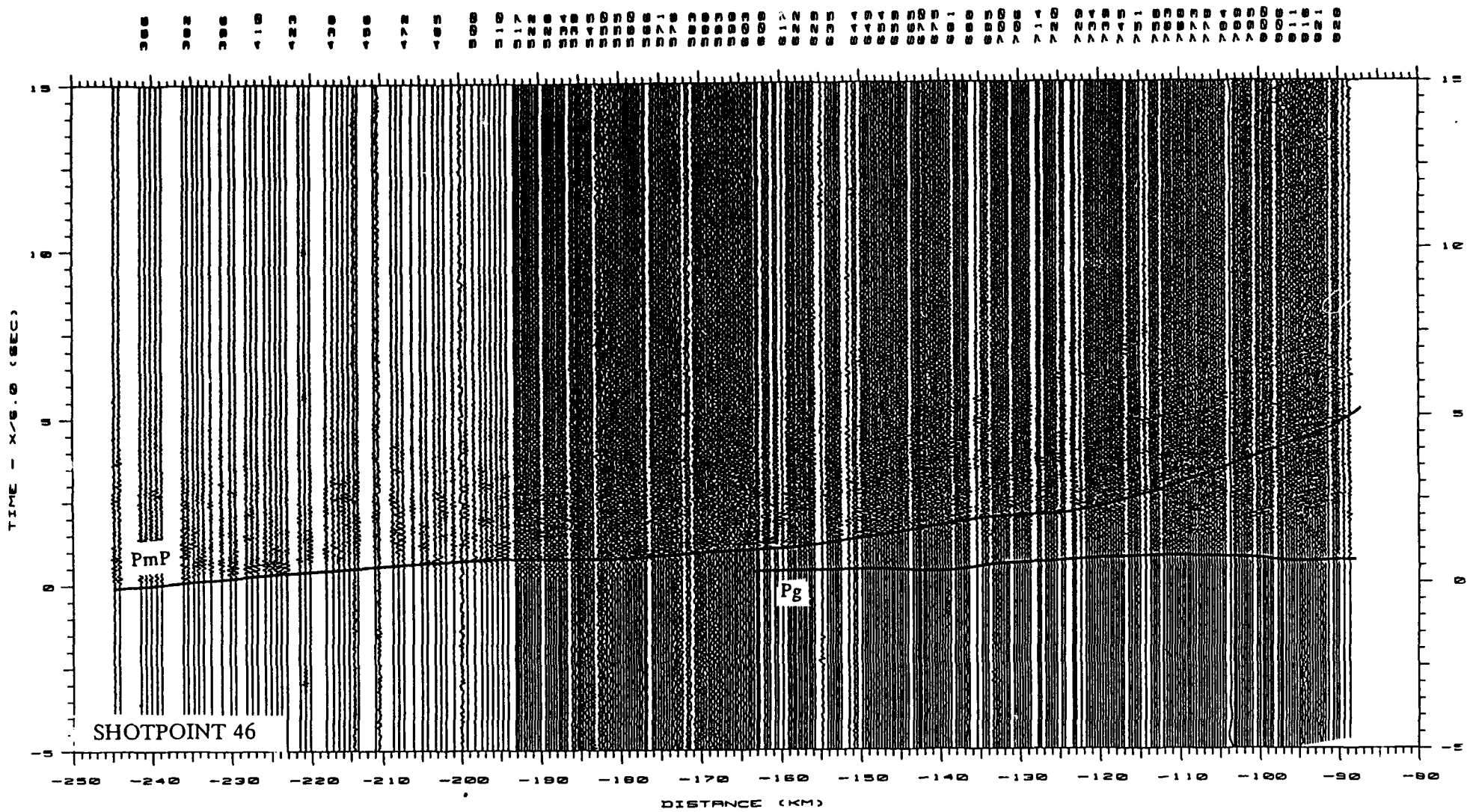
PmP
Pg
SHOTPOINT 46
TIME - X/6.0 (SEC)
DISTANCE (KM)
-250
-240
-230
-220
-210
-200
-190
-180
-170
-160
-150
-140
-130
-120
-110
-100
-90
-80

FIGURE 4.

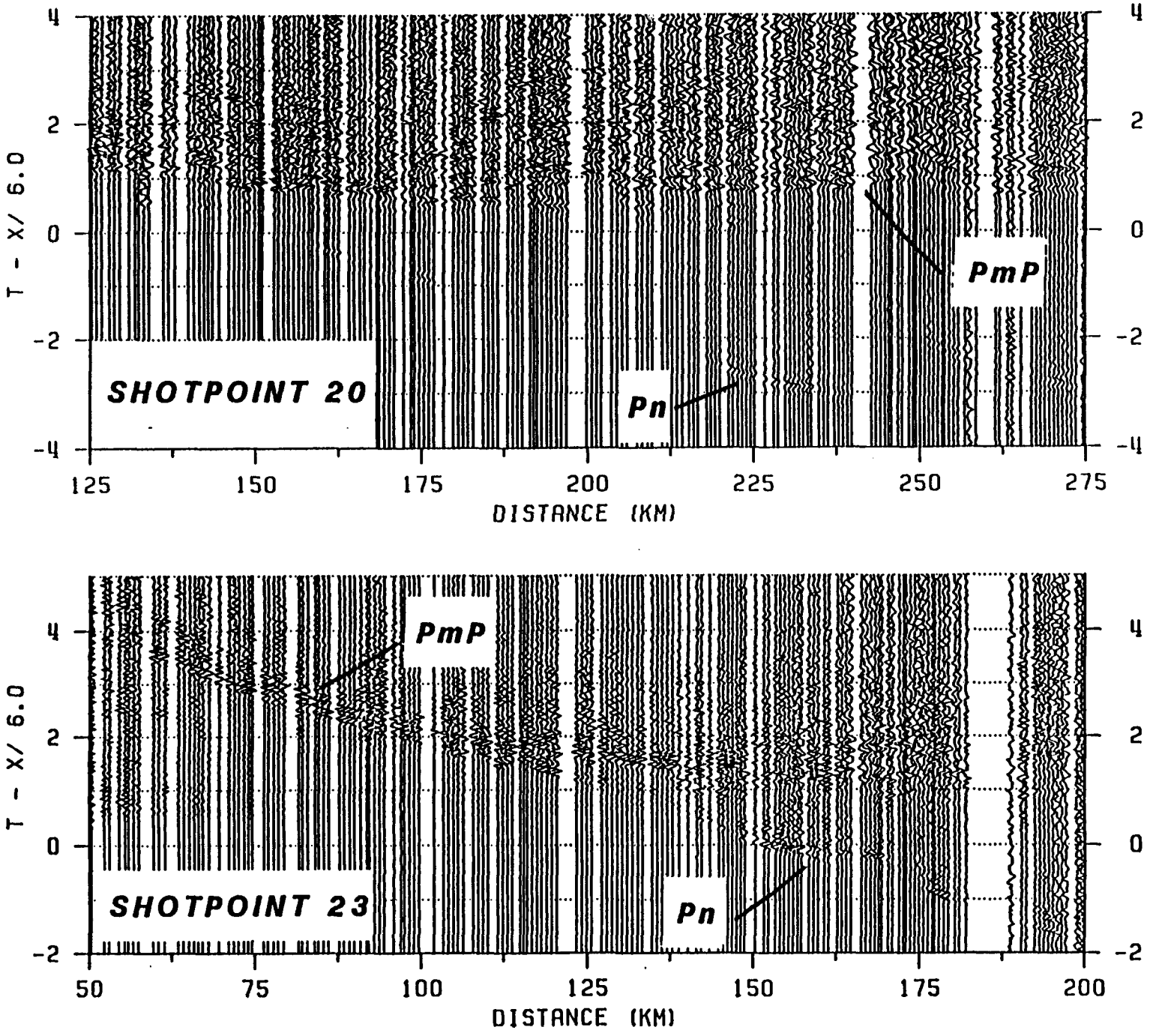
T - X/ 6.0
4
2
0
-2
-4
SHOTPOINT 20
Pn
PmP
125
150
175
200
225
250
275
DISTANCE (KM)
SHOTPOINT 23
PmP
Pn
50
75
100
125
150
175
200
DISTANCE (KM)

FIGURE 5.

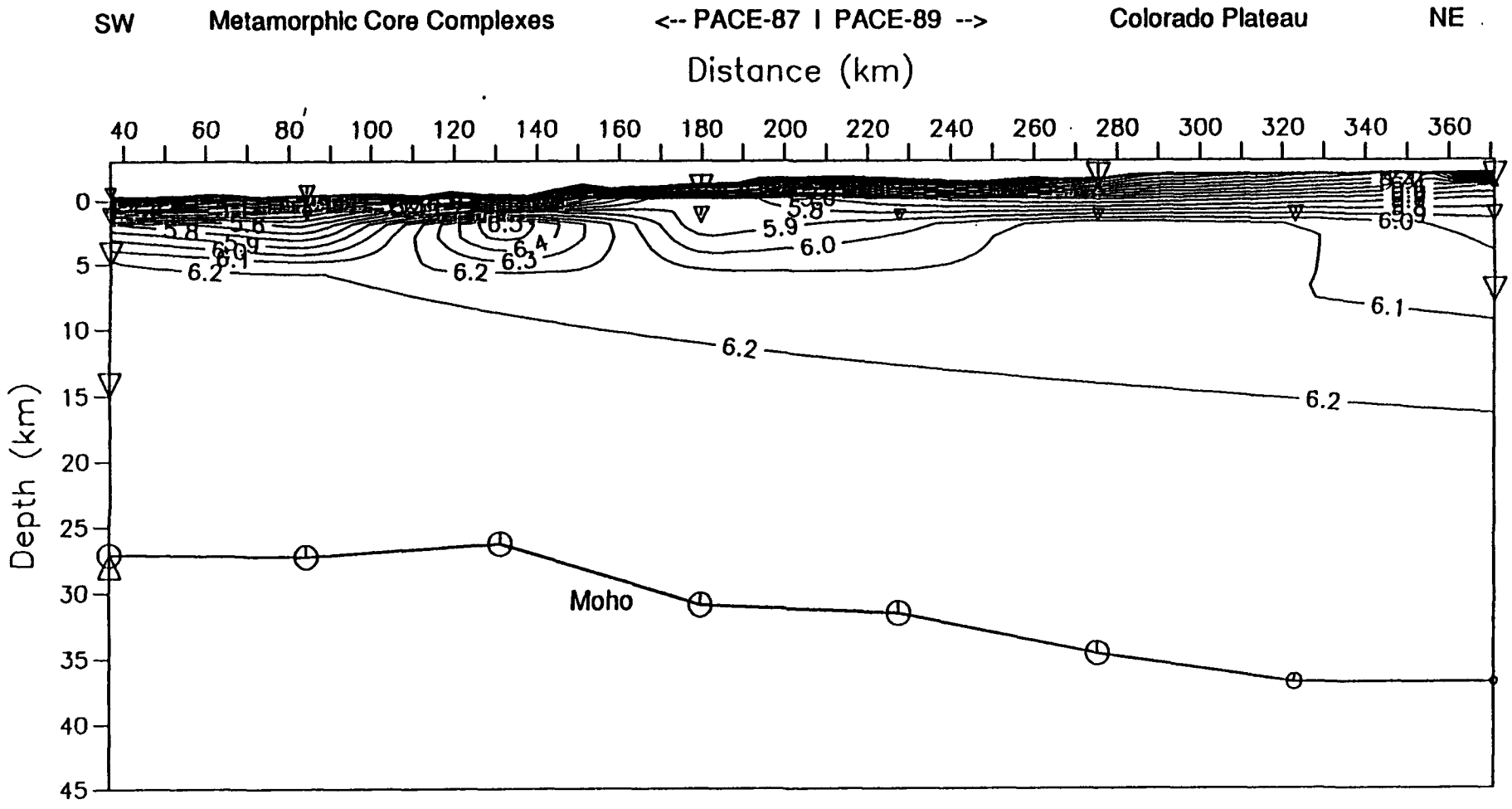

FIGURE 6. Velocity contours for the merged PACE 1987-1989 crustal model derived from the Zelt inversion routine. The profile extends from the Colorado River (left) to the Navajo Indian Reservation (right). Note the increase in crustal thickness from 28 km beneath the metamorphic core complexes to approximately 39 km beneath the Colorado Plateau. Also note the low crustal velocities (6.2-6.4 km/s) in the middle and lower crust. Triangles and circles mark velocity and structural node points; the larger the symbol the greater the resolution.

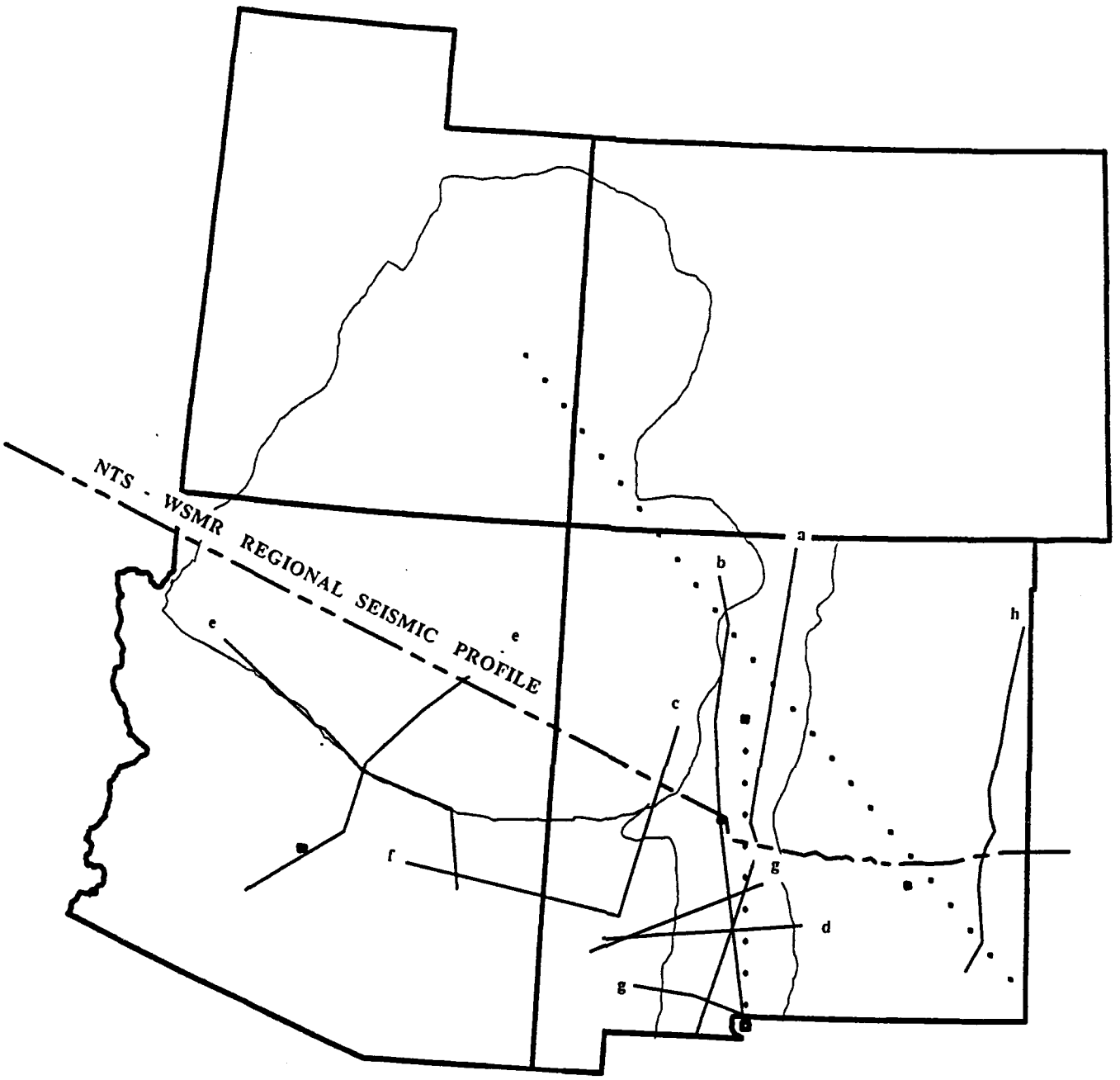

Figure 7. Previous seismic surveys completed within the Rio Grande Rift and neighboring provinces along with the projection of the NTS-WSMR Regional Seismic Profile.

The solid lines represent seismic refraction surveys: a) Olsen et al, 1979; b) Toppozada and Sanford, 1976; c) Schneider, 1990; d) Cook et al, 1979; e) 2 lines, Warren, 1969; f) Gish, 1981; g) 3 lines, Sinno et al, 1986; and h) Stewart and Pakiser, 1962. The long dotted line is the teleseismic line of Davis et al, 1984, and the short dotted line within the rift is the surface wave dispersion experiment of Keller et al, 1979.

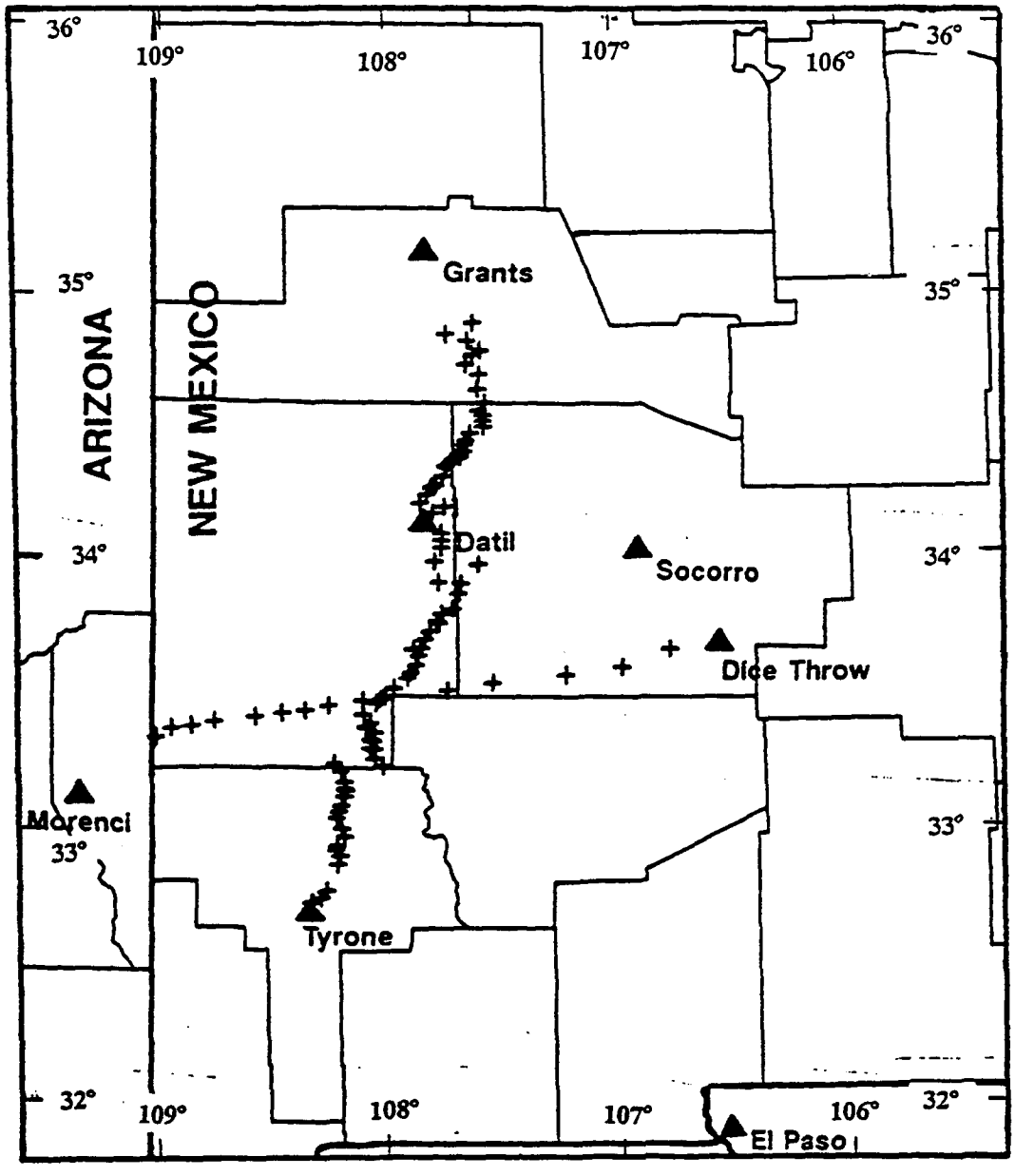

Figure 8. Location of seismic refraction lines used in the present study. The east-west trending line is from Jaksha (1982). Locations of seismic recording stations are indicated by a (+).

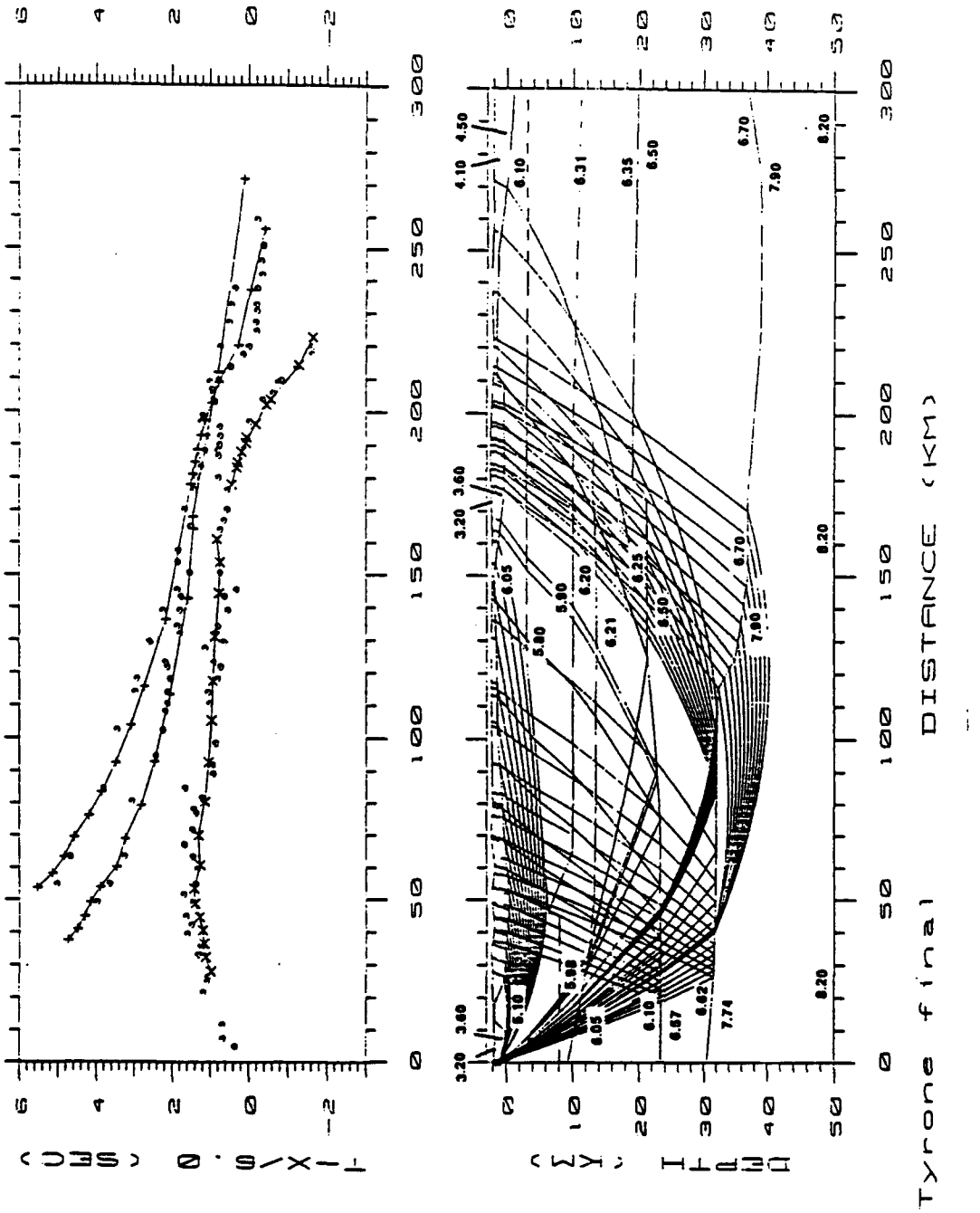

Figure 9. Ray-tracing model for Tyrone-Acoma line, final configuration. Velocities are in km/sec. Symbols: o = observed arrivals; + = calculated reflected arrivals; x = calculated refracted arrivals.

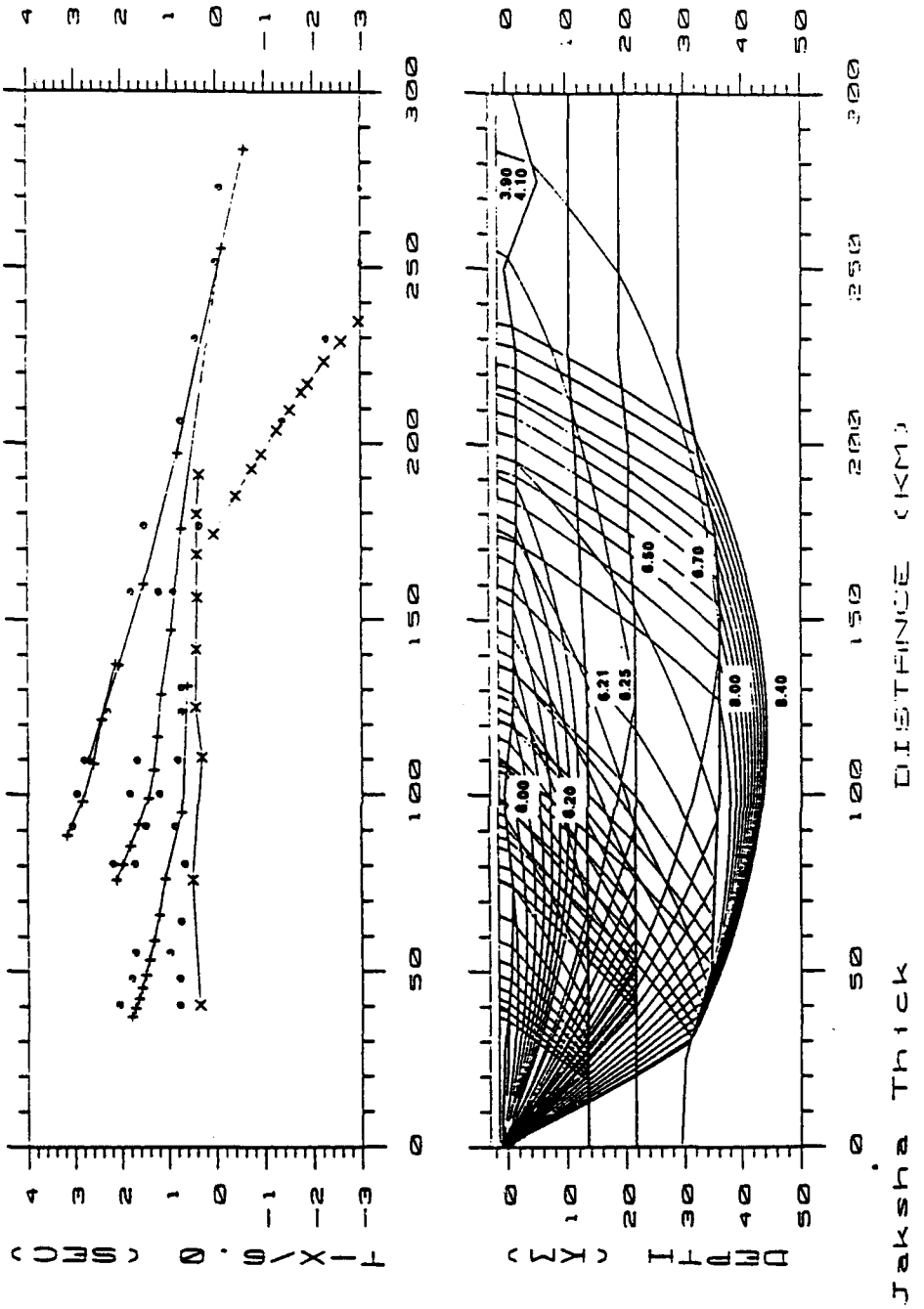

Figure 10. Thickened crust seismic ray-tracing model for the Jaksha (1982) refraction line using re-picked arrivals for this study. Symbols: o = observed arrivals; + = calculated reflection arrivals; x = calculated refraction arrivals. Velocities are in km/sec.

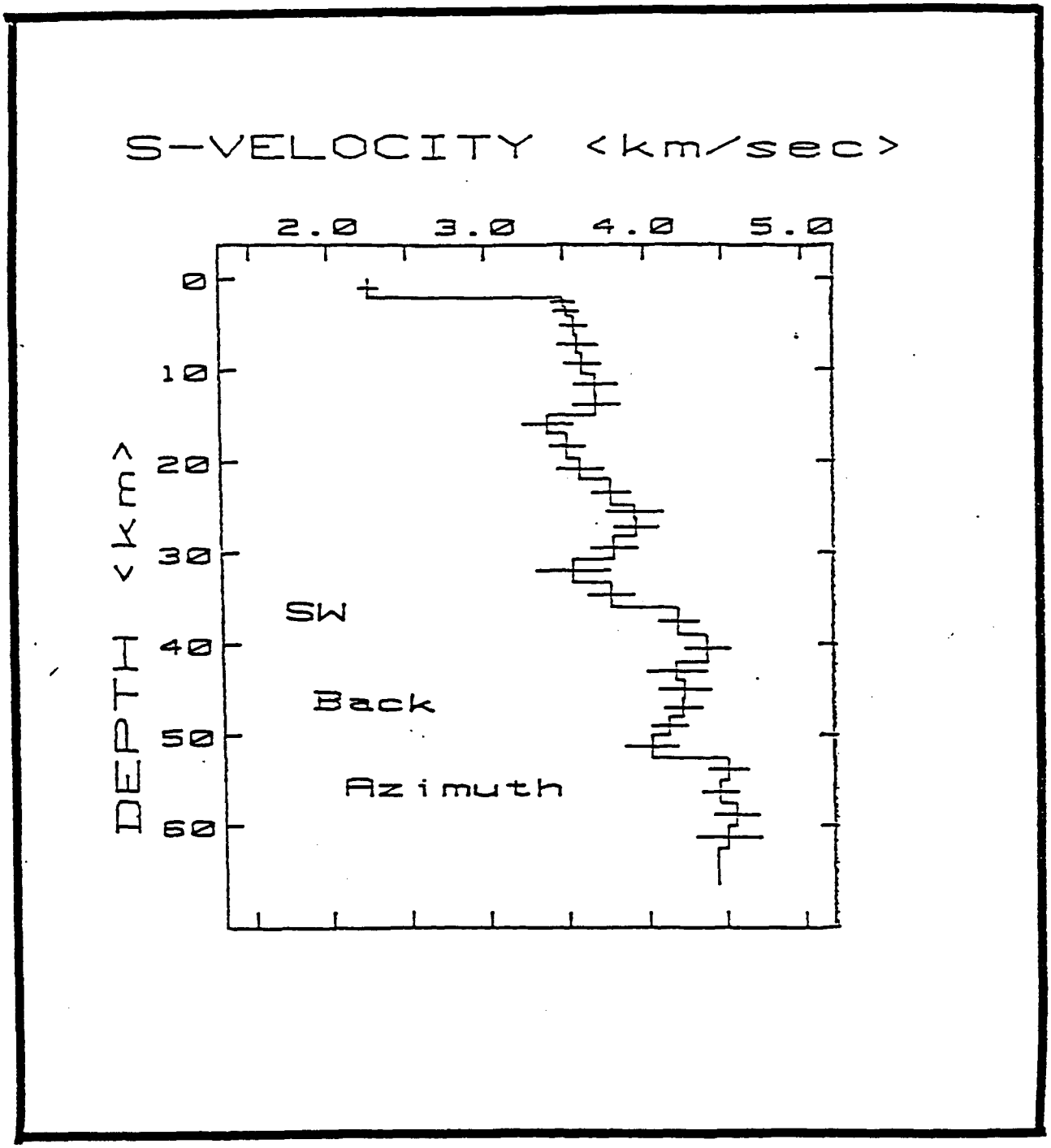

Figure 11. Final S-wave velocity model for southwest back azimuth. Error bars represent +/- 2 standard errors.

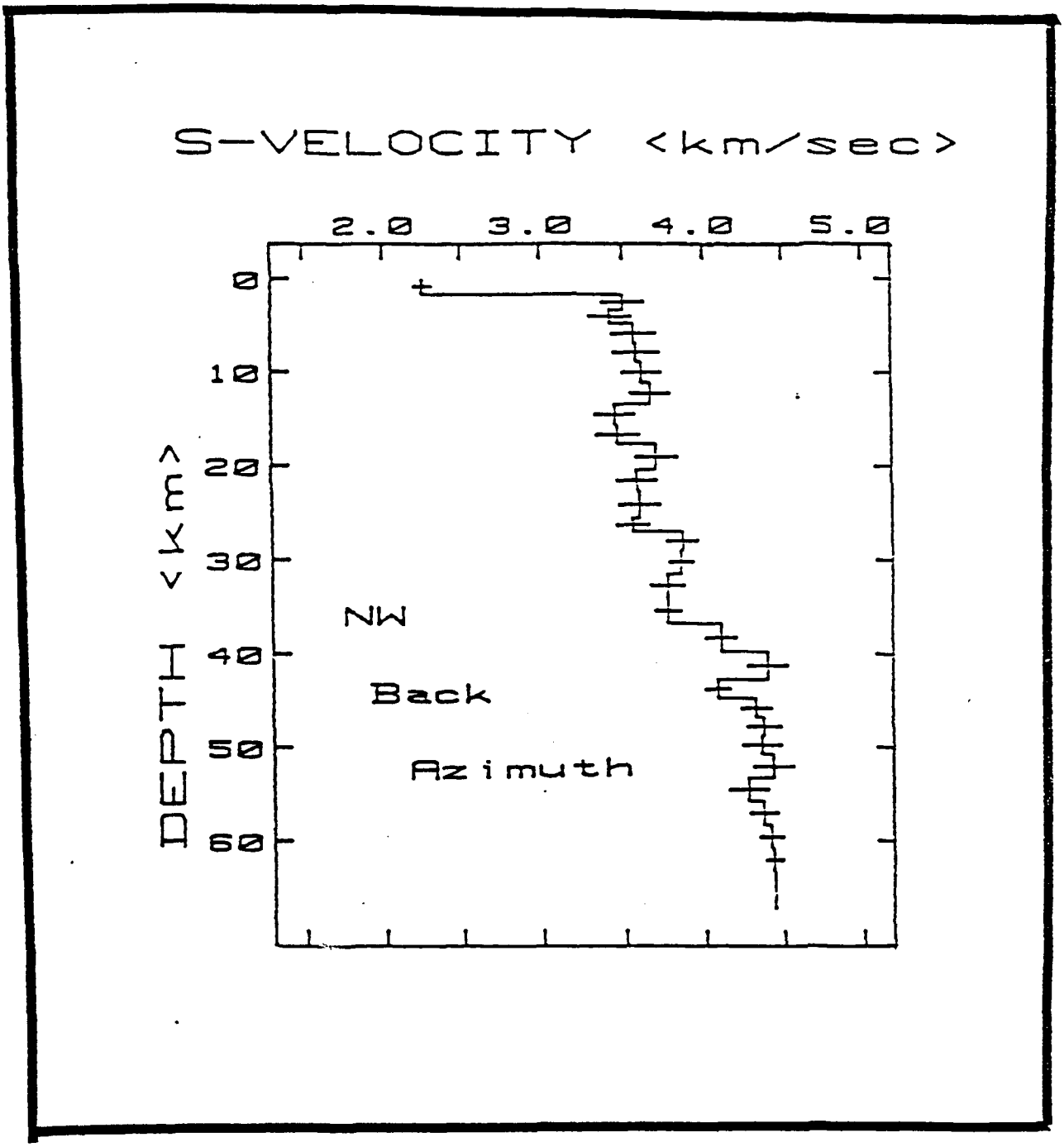

Figure 12. Final S-wave velocity model for northwest back azimuth. Error bars represent +/- 2 standard errors.

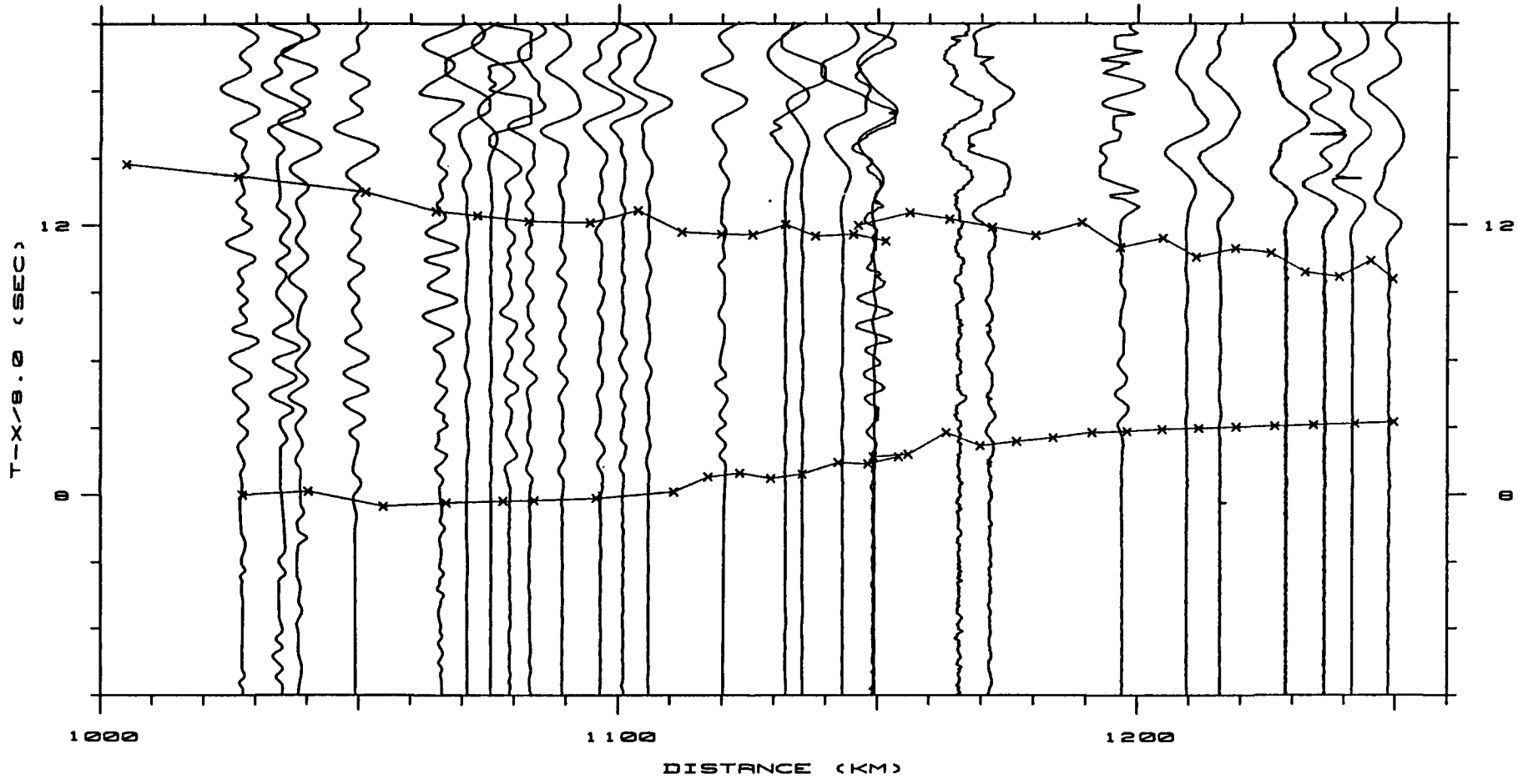

Figure 13. Observed seismic sections with modeled arrival branches.

All stations with an offset of less than 1149 km recorded shot NTS2. All stations with larger offsets recorded NTS4. The station at R = 1149 km was occupied for both shots. Shotpoint NTS4 is located 7.5 km closer to the array than shotpoint NTS2.

Figure 14. Final seismic model plotted as a "curved" earth with the modeled raysets.

The layer immediately below the Moho discontinuity represents the lithospheric upper mantle which is in turn underlain by the low velocity zone (LVZ) of the uppermost asthenosphere. This survey was able to resolve the crustal regions beneath the Rio Grande rift and the deeper structure under the Colorado Plateau/Rio Grande rift transition.

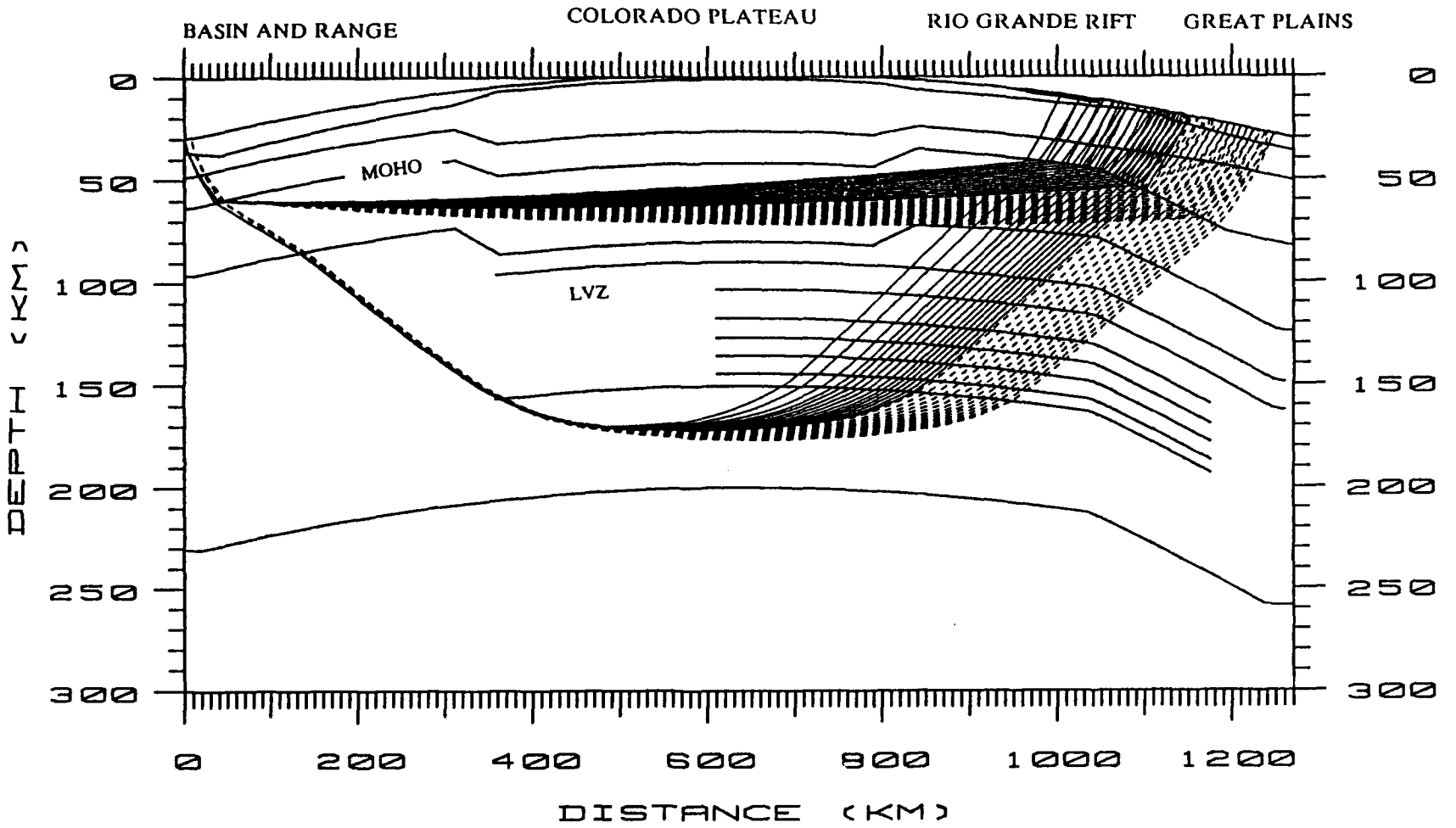

A Long Range Seismic Refraction Survey Across the Rio Grande Rift and its Transition Zones in Central New Mexico

Donald G. Roberts
Department of Geological Sciences
The University of Texas at El Paso,
El Paso, TX 79968

Appendix C

INTRODUCTION

Most researchers in the geosciences have come to recognize the Rio Grande Rift (RGR) of the southwestern U.S. (Figure 1) as a separate, distinguishable geologic province of the North American continent. Scientists have gathered considerable amounts of geological and geophysical data along the over 1000 km extent of the rift. In many cases, care was taken to restrict surveys to within the rift borders in order to isolate the rift structure and morphology from that of neighboring provinces. As a result, knowledge of the intra-rift crustal structure and history has greatly increased over the last fifteen years. Yet very few works have examined the transition zones to the east or west.

The purpose of this research is to expand on these previous works by using long offset seismic data to examine the transition zone between the southern RGR and the neighboring Great Plains (GP) province to the east. The profile of recordings begins southeast of Socorro, NM, and extends eastward to near the Texas-New Mexico border (Figure 2). The surface expression of rifting within this region extends as far east as the western extreme of the Sacramento and Pedernal Uplifts (Chapin, 1971) but no seismic investigations have examined the transition at depth.

The profile was chosen so it would have a near radial orientation to the Nevada Test Site (NTS). The large nuclear explosions created at NTS provide excellent seismic sources and the resultant long offsets (>1000 km) make it possible to examine the structure of the transition region to depths below the low velocity zone in the upper mantle. The investigation targeted these depths because it is presumed that the RGR-GP transition extends into

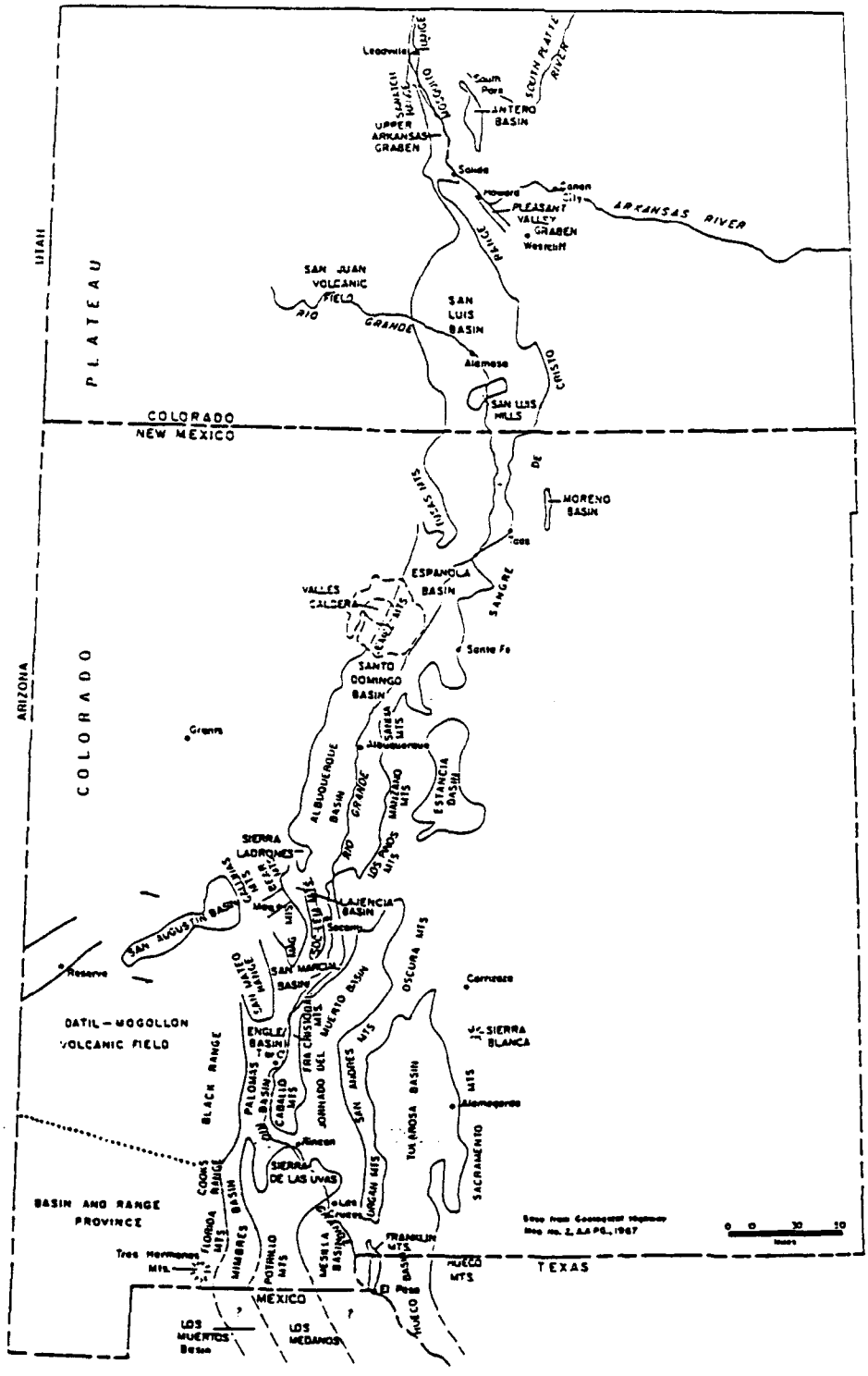

Figure 1. Regional setting of the Rio Grande Rift from Chapin (1975).

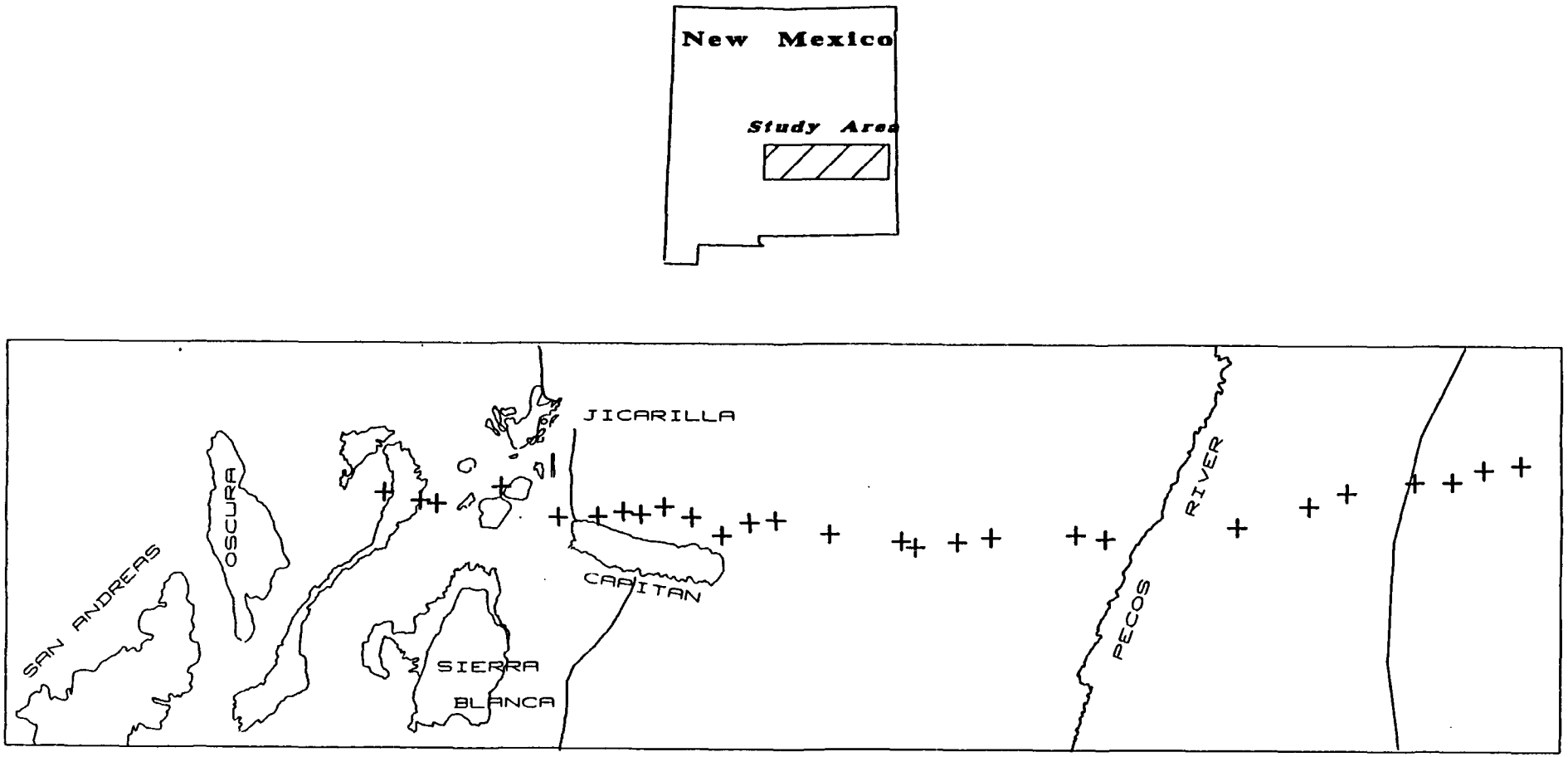

Figure 2. Geologic setting of study area.

The north-south line at the eastern end of the figure corresponds to the refraction line of Stewart and Pakiser (1962).

the deep lithosphere and asthenosphere. Eventually, these data will be merged with other data to complete a continuous line of refractions stations from the Nevada Test Site (NTS) through the White Sands Missile Range of New Mexico and over to the Texas border (Figure 3). The complete project is named the NTS-WSMR Regional Seismic Profile.

However, these long offsets also present a problem. Since the ultimate objective of the survey was to analyze the rift/craton transition, the chosen modeling technique had to accept two-dimensional structures. The method chosen for this survey was a 2-D ray tracing algorithm based on asymptotic ray theory (ART) (Cerveny et al., 1977; Cerveny, 1979). Since all of the station offsets in this work were over 900 km, some type of compensation had to be made for the curvature of the earth. Conventional earth "flattening" transforms involve various techniques of modifying a homogeneous, flat earth model so that the results obtained from the specific modeling algorithm approximate those expected from a homogeneous, spherical earth model (Chapman, 1973). The two-dimensional nature of the models used in ART make such a transformation difficult, if not impossible. To alleviate this problem, a new technique for compensating for the curvature was developed and implemented for this study.

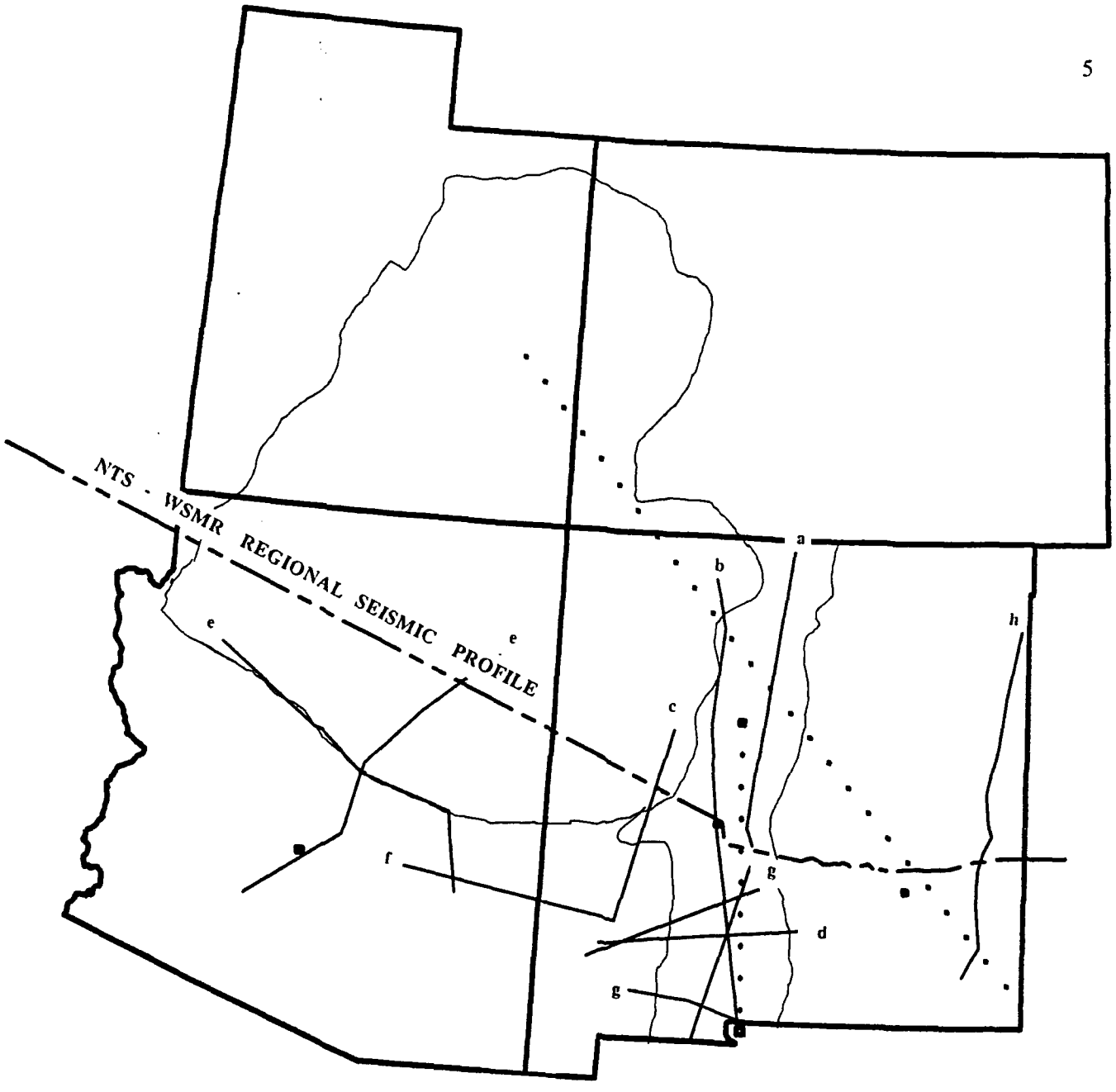

Figure 3. Previous seismic surveys completed within the Rio Grande Rift and neighboring provinces along with the projection of the NTS-WSMR Regional Seismic Profile.

The solid lines represent seismic refraction surveys: a) Olsen et al, 1979; b) Toppozada and Sanford, 1976; c) Schneider, 1990; d) Cook et al, 1979; e) 2 lines, Warren, 1969; f) Gish, 1981; g) 3 lines, Sinno et al, 1986; and h) Stewart and Pakiser, 1962. The long dotted line is the teleseismic line of Davis et al, 1984, and the short dotted line within the rift is the surface wave dispersion experiment of Keller et al, 1979.

STRUCTURAL SETTING

The Rio Grande Rift (RGR) is a mid- to late-Cenozoic extensional feature located between the Colorado Plateau (CP) and the Basin and Range (BR) provinces to the west, the Southern Rocky Mountains (SRM) to the north and northeast, and the Great Plains (GP) to the east (Figure 1). It extends south from Leadville, Colorado, along a series of re-activated Pennsylvanian and Laramide (and possibly Pre-Cambrian) fault scarps (Cordell, 1978; and others) and continues to at least the US-Mexico border and probably beyond. Tweto (1979) describes the northern section (Taos, New Mexico, to Leadville) as two end-to-end grabens paralleling Laramide structures in a north-northwesterly direction. Gravity surveys over the northernmost Upper Arkansas basin indicate that the basin pinches out about 20 km north of Leadville. This marks the widely accepted northern terminus of the rift "proper," but effects of the rifting (e.g., faulting and volcanism) extend north to the Wyoming border (Tweto, 1979).

The central portion of the rift is comprised of another nearly end-to-end series of grabens trending in a north-northeasterly direction from Socorro, New Mexico, to Taos. This directional change is due, in part, to a complex series of transverse normal faults resulting in a right-lateral, en echelon offset between the basins (Kelley, 1979). Throughout the region, the eastern boundary of the rift is clearly marked by a series of high, sharp uplifts making the en echelon fault patterns very obvious. However, the western boundary is much more obscure with most boundary and transverse faults buried or poorly defined (Kelley, 1979).

As it extends south from Socorro, the rift's structural character changes

somewhat. A series of three or four wide, parallel grabens replaces the single, narrow grabens of the north. The total width of these basins is roughly 2.5 times that of the northern and central segments (Chapin, 1979) and, therefore, the southern Rio Grande Rift appears structurally similar to the Basin and Range province. South of the Datil-Mogollon volcanic field, the rift grades almost imperceptibly into the southern Basin and Range. On the eastern flank, the clear boundary faults of the central segment become buried under the northernmost sediments of the Jornado del Muerto Basin and the rift boundary appears to jump eastward to the western edge of the Jicarilla Mountains, Sierra Blanca, and the Sacramento Mountains. Still farther south, this eastern boundary becomes somewhat controversial itself. Seager and Morgan (1979) exclude the Salt Basin of west Texas and southern New Mexico from their definition of the "mature" region of the rift since it lacks Cenozoic volcanics and appears to have more normal heat flow values (Swanberg, 1979). But Veldhuis and Keller (1980) use a series of gravity profiles across the region as well as the leveling surveys of Reilinger et al (1979), to include the Salt Basin as part of the rift system. Both accounts, however, seem to agree that this argument is one of degree and depends mainly upon one's definition of the rift proper. The southernmost extension of the rift appears to lie near Villa Ahumada in the Los Muertos Basin of northern Chihuahua, and in the Presidio Basin of west Texas (Seager and Morgan, 1979).

PREVIOUS GEOPHYSICAL WORK

Seismic

Several seismic experiments have been completed within the rift during the last 15 years (Figure 3). Toppozada and Sanford (1976) re-examined data recorded along a profile extending from the GASBUGGY nuclear explosion of 1967. They modeled the crust as two plane layers over a half space with a 2^{o} northward dip. The top layer was 19 km thick with a velocity of 6.15 km/s. The bottom crustal layer averaged 21 km thick with a velocity of 6.5 km/s. This placed the half space (assumed to be the mantle) at an average depth of 40 km with a P-wave velocity of 7.9 km/s. However, these authors did note that the survey transected both the Colorado Plateau and the Rio Grande Rift (Figure 3) and, therefore, represents an average of the crustal structure within each province. Since the crust within the Colorado Plateau is certainly no thicker than 50 km, the authors concluded that the rift crust should be no thinner than 30 km at the Pg/Pn crossover point about 50 km west of Albuquerque.

Olsen et al. (1979) monitored the DICE THROW III conventional explosion at White Sands Missile Range (WSMR) with a seismic array extending 350 km from Socorro to the New Mexico-Colorado border (Figure 3). Using the same Moho dip as Toppozada and Sanford, they modeled this section of crust (which lies completely within the rift) as 3 layers over a half space. From the surface down, their earth model results were: 3.2 km at 4.3 km/sec, 18.2 km at 6.0 km/sec, and 12.3 km at 6.4 km/sec. The Moho depth ranged from 37 km in the north to 29 km in the south and the upper mantle velocity was 7.75 km/sec.

Sinno et al. (1986) conducted a thorough refraction experiment in the southern rift (Figures 3, 4, and 5). Their work consisted of a reversed E-W profile (Cross Line), a different, unreversed E-W profile (Pipe Line Road Line), and an unreversed N-S profile (Axial Line). The crustal model shown in Figure 5 summarizes the results of their survey. The reversed Cross Line showed no significant dip along the Moho and an upper mantle velocity of 7.7 km/s. To match this constraint at the Cross/Axial intersection point and its own arrival times and amplitudes, the Axial Line was modeled with an upper mantle velocity of 7.7 km/s and a Moho depth ranging from 32 km in the north to 28 km in the south (an apparent dip of just less than 2^{o}). The Pipe Line Road section was then tied to the Axial Line resulting in an upper mantle velocity of 7.7 km/s and a Moho depth of 32 km in the west and 28 km in the east (approx. 2.5^{o} of dip).

Another refraction line within the southern rift extends from Santa Rita to Cloudcroft. This line was first interpreted and published by Cook et al. (1979) and later re-interpreted by Daggett (1982) due to some processing errors in the first version (Figure 3). The final model suggests a mantle depth of 29 km and an upper mantle velocity of 7.7 km/s and is in excellent agreement with the results of Sinno et al. (1986).

Two surface wave dispersion experiments have been conducted within the rift and, while these experiments lack the resolution of a typical seismic refraction experiment, their results agree with the refraction work and provide some constraints for S-wave velocities. Keller et al. (1979) modeled the region between Las Cruces, NM, and Durango, CO (Figure 3). Their results show a 35 km thick crust underlain by upper mantle with an S-wave velocity

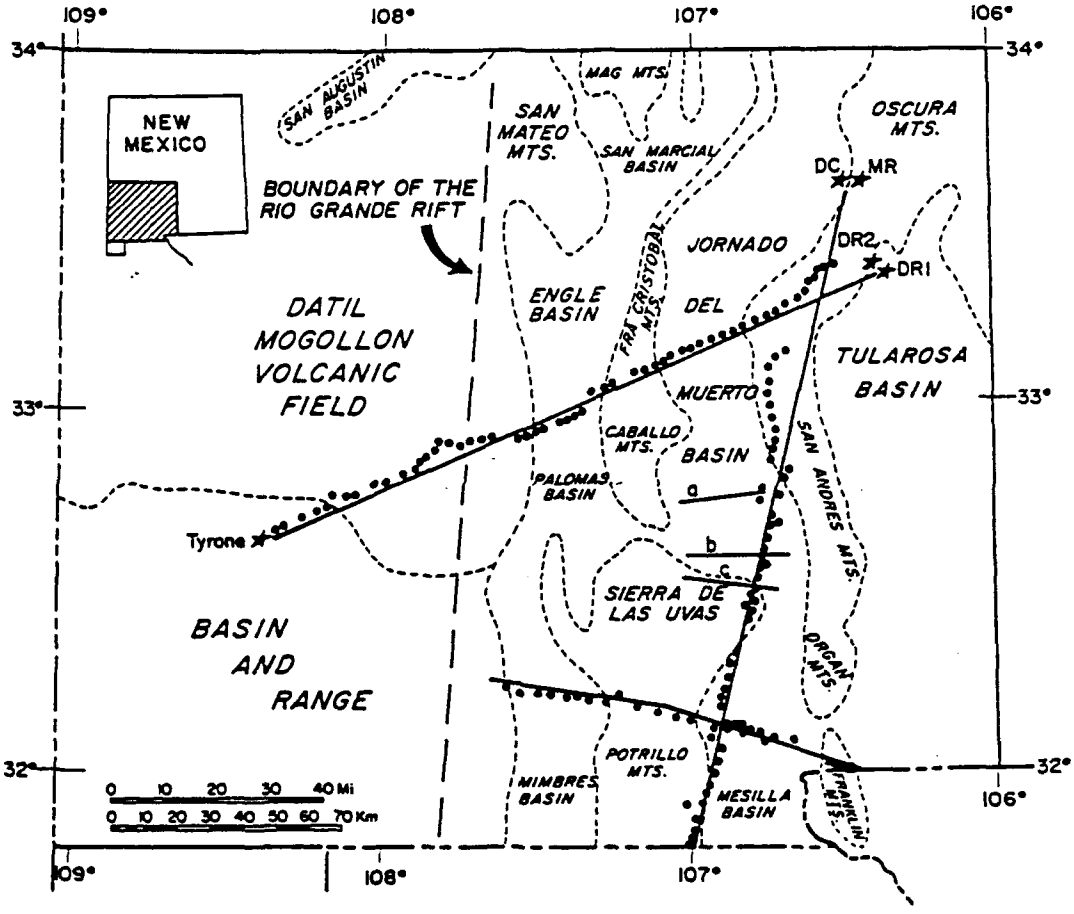

Figure 4. Location of refraction profiles conducted by Sinno et al (1986).

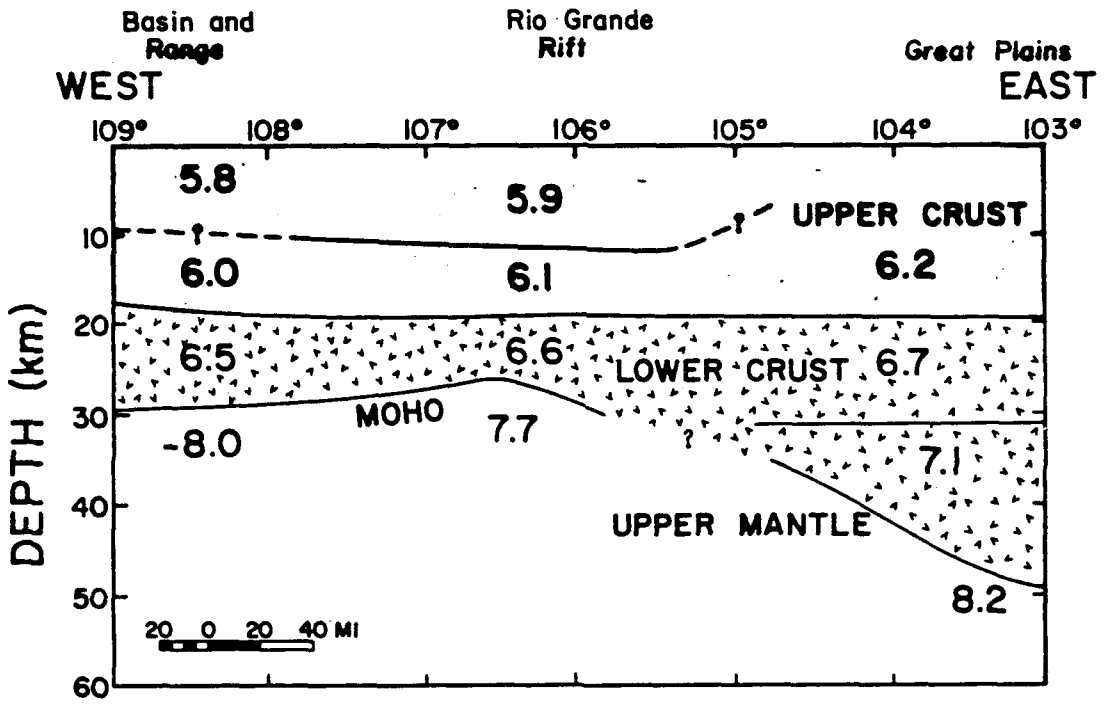

Figure 5. Southern Rio Grande Rift crustal model from Sinno et al (1986).

of 4.4 km/s and, assuming a Poisson's ratio of 0.25, a P-wave velocity of 7.7 km/s. However, since the waves traveled partly through the Colorado Plateau and partly through the rift, the Moho may be shallower within the rift. If so, then these data match fairly well with those of Olsen et al. (1979) and Sinno et al. (1986). Using WWSSN stations at El Paso (EPT) and Albuquerque (ALQ), Sinno and Keller (1986) were able to model structures completely within the rift (Figure 3). However, since their inversion technique could not resolve the Moho as a distinct interface, they opted to use an averaged P-wave velocity deduced from refraction studies along with their S-wave data to compute a Poisson's ratio for the various crustal layers. Their results are presented in Table 1 and represent an average of rift structures between Albuquerque and El Paso.

Average P Wave Model		Surface Wave Model	Poisson's Ratio
Thickness, km	P velocity, km/s	S velocity, km/s	
2.12	4.29	1.74 (SD 0.02)	--
18.25	5.99	3.49 (SD 0.39)	0.24
12.20	6.48	3.64 (SD 0.54)	0.27
(upper mantle)	7.77	4.25 (SD 0.02)	0.29

Table 1. Calculated Poisson's Ratio's for the Rio Grande rift from Sinno and Keller (1986).

Davis et al. (1984) monitored a 20-station teleseismic line extending from Moab, UT, to near Odessa, TX (Figure 3). The line transected the rift in a NW-SE direction near the Valles Caldera and provided a first look at the deep (40-100 km) structure of the region. Using both a least squares

inversion technique and downward continuation of the P-wave delay data, they predicted the existence of an anomalous low velocity zone centered on the rift. The data strongly favored a mantle anomaly over a lower crustal anomaly. The best fit in both analyses was a low velocity "bulge" between 70 and 200 km depth with a lateral extent of 500 km. This suggests that the interface near 70 km is the lithosphere/asthenosphere boundary. This model also fits well with observed gravity profiles in the rift but requires very little density contrast within the LVZ, suggesting that the low velocities are caused by a small fraction of partial melt having little effect on density.

Non-seismic

Cordell (1978) provides a thorough overview of the geophysical characteristics of the rift with particular emphasis on non-seismic investigations. Regional gravity surveys along the rift axis delineate the major boundary faults of the various grabens. These faults also seem to align fairly well with lineations in the aeromagnetic data (Cordell, 1978). These magnetic lineations follow the rift and therefore separate the Great Plains from the Colorado Plateau. Since the magnetic lineations, or basement grains, of the Plateau do not coincide with those of the Great Plains, some authors have inferred that the Plateau was sutured onto the craton during Pre-Cambrian time and later tectonic activity, such as the recent rifting, has occurred along this weaker suture zone (Cordell, 1978).

The Rio Grande Rift can be clearly delineated on surface heat flow maps. Reiter el al. (1975) compiled approximately 100 heat flow measurements from within New Mexico, Colorado, Utah, and Arizona. A contour map of their data in New Mexico and Colorado (Figure 6) showed a major

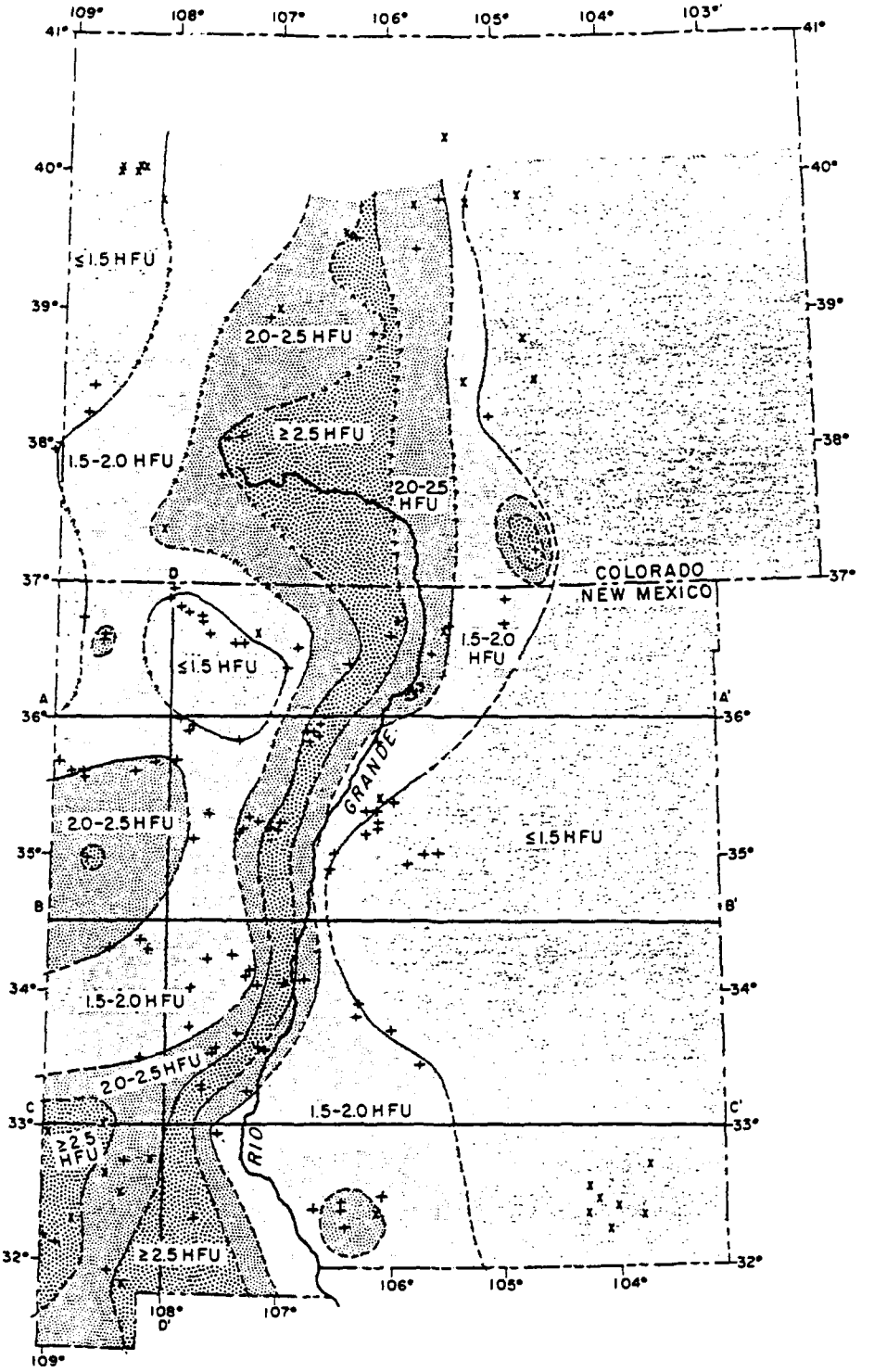

Figure 6. Heat flow in New Mexico and Colorado from Reiter et al (1975).

geothermal anomaly coincident with the western edge of the RGR. A series of profiles across this map indicated that throughout New Mexico the RGR could be easily distinguished from its neighboring provinces to the east and west. In addition, the data revealed a north to south warming trend west of the rift axis. The authors attributed this anomalous heat flow to some type of thermal source, presumably a mantle upwarp, or bulge, under the western edge of the rift.

Swanberg (1979) used chemical geothermometry to compute heat flow values in west Texas, New Mexico, and southern Colorado. This technique added about 10,000 new heat flow data points for the region and resulted in the heat flow map shown in Figure 7. The map is very similar to that of Reiter et al. (1975) but Swanberg suggested that most of the anomalous flow is a product of the the Quaternary faulting associated with the rift, especially in the southern section. This means that the thermal waters were heated by a normal thermal gradient within the basins and then forced to the surface along the bounding fault scarps.

Daggett (1982) assumed that all heat flow values greater than 125 mW/m^2 (3 HFU) in southern New Mexico were associated with localized forced convection along the fault scarps. He compiled bore hole heat flow data from several sources and produced heat flow profiles across the southern and central portions of the rift (Figure 8). He excluded values greater than 3 HFU and plotted all values within a 1.5^{o}-2^{o} band of latitude along a single profile. From these profiles he concluded that the southern RGR was geothermally indistinguishable from the southern BR but the central RGR had an anomalous heat flow of 20 mW/m^2 for a lateral distance of 80 km with a 25 km transition zone to the east and west.

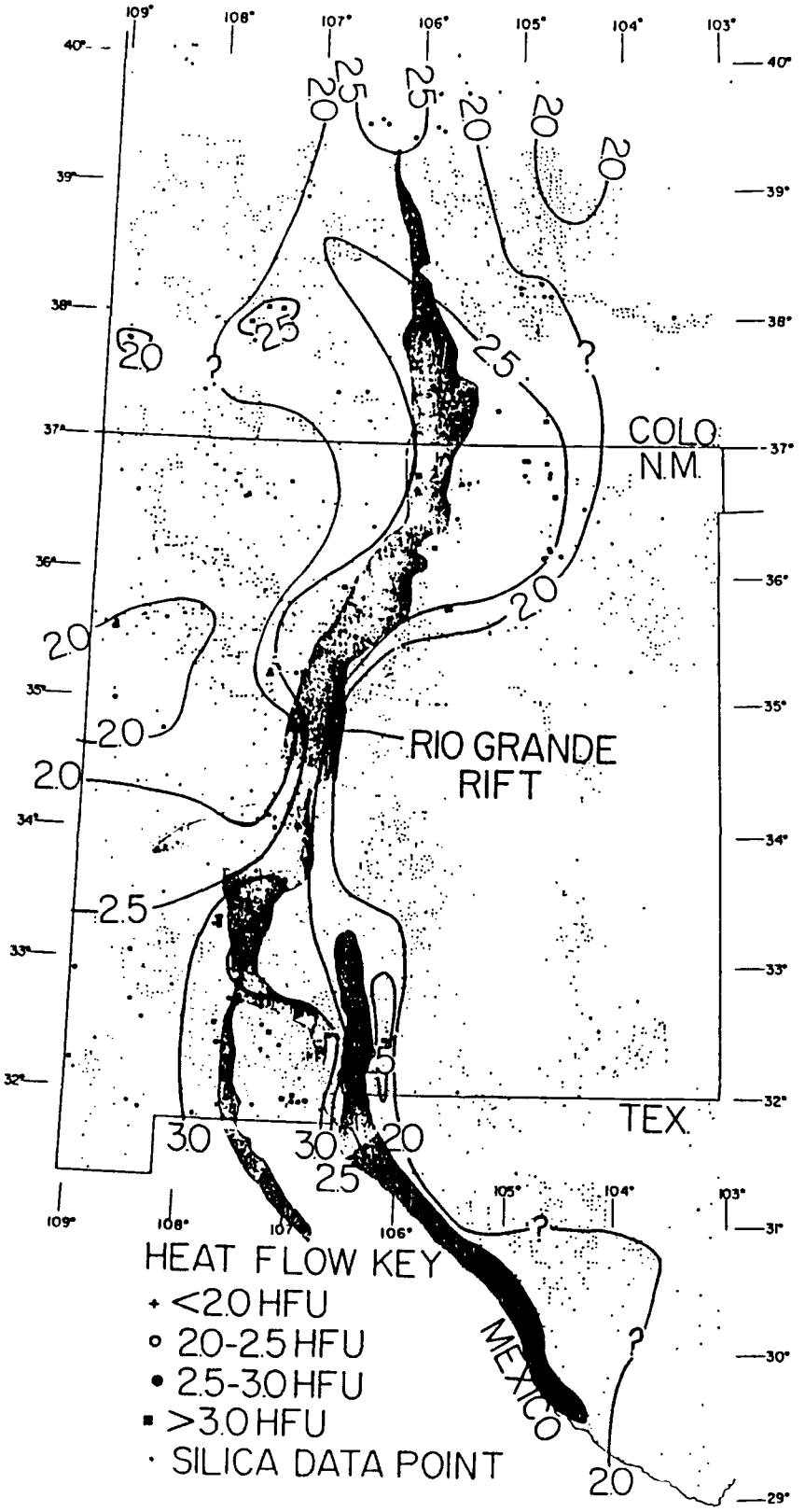

Figure 7. Heat flow map of New Mexico and Colorado from Swanberg (1972).

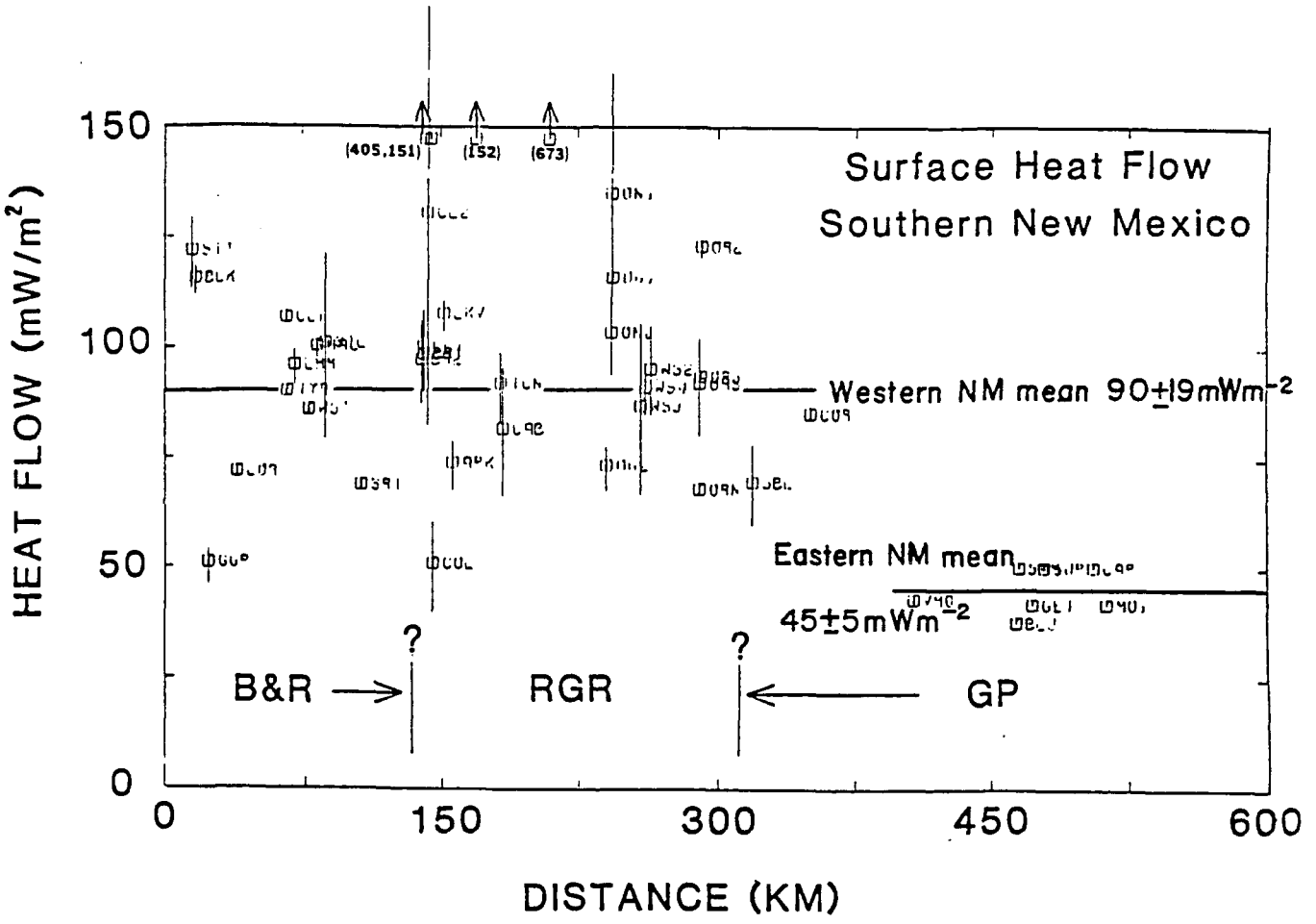

Figure 8. Heat flow profile across the southern Rio Grande Rift and its neighboring provinces (from Daggett, 1982).

Several E-W trending gravity profiles along the entire length of the rift demonstrate the north to south widening and smearing of rift structures as compared to the flanking provinces. Cordell (1978) compiled a series of profiles at 1^{o} intervals from 37^{o}N to 32^{o}N latitude (Figure 9). They extended from 111^{o}W to 102^{o}W longitude and, therefore, incorporate the entire width of the rift and portions of the flanking provinces. In all but the southernmost profile, the rift is centered within a large (approx. -100 mgals compared to adjacent areas) regional gravity low extending from near 110^{o}W or 111^{o}W longitude to 104^{o}W or 103^{o}W longitude. Superimposed on this anomaly is a smaller wavelength (approx. 100 km) gravity high also centered on the Rio Grande valley. In the southern profile, the gravity high becomes much wider and the result is simply a smaller amplitude for the regional low (Cordell, 1978; Seager and Morgan, 1979). Both of these anomalies have been attributed to basically the same phenomena, i.e., the upwarp of one characteristic unit into another. Cordell (1978) and Seager and Morgan (1979) attribute the negative anomaly to upwarp of the asthenospheric LVZ into the upper mantle and/or lateral density variations within this region due to thermal and convective forces. The smaller, positive anomaly appears to be an extension of this process via magmatic intrusion of high density mantle material into the relatively low density lower crust, i.e., crustal thinning.

Daggett et al. (1986) modeled a gravity profile across the southern rift at 32^{o}N latitude and also along the Pipe Line Road and Cross Line seismic lines of Sinno et al. (1986). The first extends along 32^{o}N latitude from 108^{o}W to 104^{o}W longitude, beginning in the southern RGR, crossing the Diablo Plateau, and into the western half of the Delaware basin. Both their profile and a similar profile by Veldhuis and Keller (1980) show that the rift grades

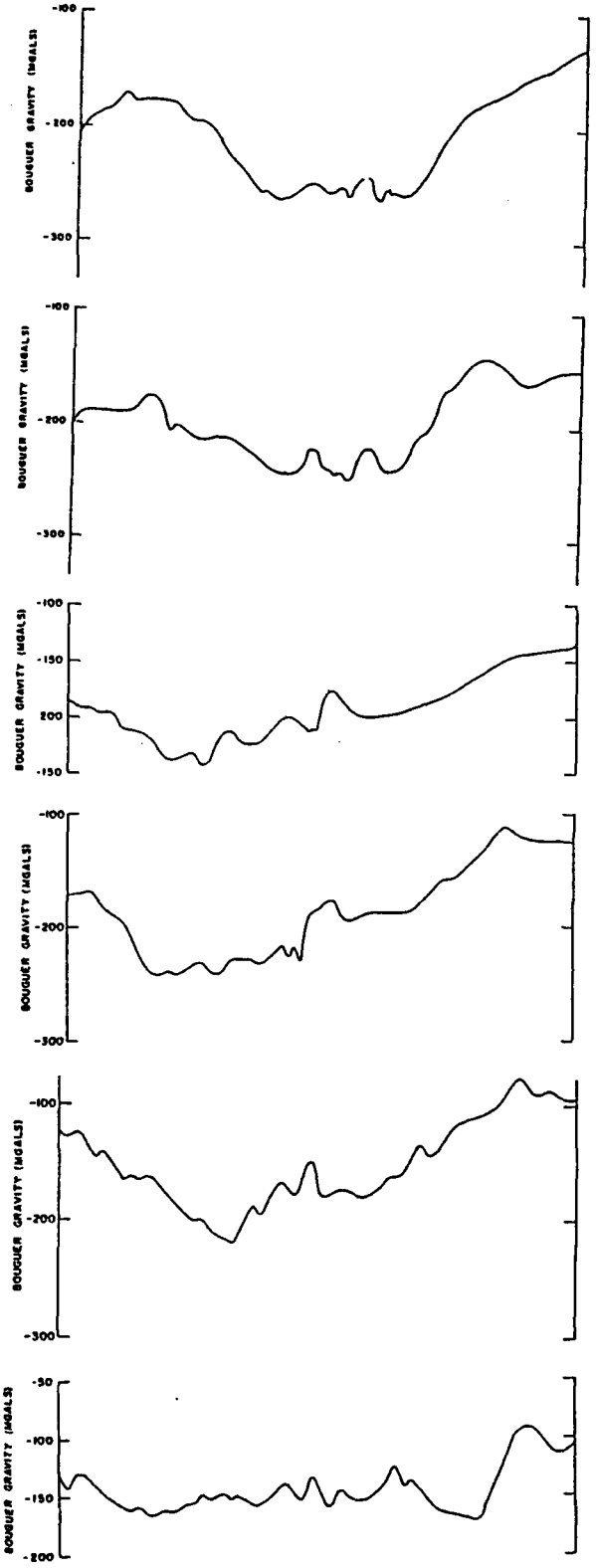

Figure 9. Gravity profiles across New Mexico from Cordell (1978).

The profiles extend from 111°W to 102°W longitude and at 1° intervals. The top profile was at 37°N and the bottom profile at 32°N latitude.

into the Great Plains just to the east of the Diablo Plateau. Daggett et al. (1986) modeled the anomaly over the Plateau as being due to both an intracrustal feature and a mantle upwarp but were unable to discriminate between the two. In either case, the transition between the rift's anomalously low density upper mantle (3.15 gm/cm^3) and the Great Plains mantle (3.3 gm/cm^3) occurred at approximately 105^oW longitude.

Summary and discussion

Recent geophysical investigations have shown that seismically and non-seismically, the RGR is a distinguishable feature extending from central Colorado into northern Chihuahua, Mexico. Basically, the rift is manifested by a mantle upwarp between the tectonically stable Great Plains and the other southwestern provinces. The rift is characterized by a relatively narrow positive gravity anomaly along its axis, a broader gravity low over the same region, higher surface heat flow and thinner crust than the surrounding provinces, and low upper mantle seismic velocities. The refraction lines of Olsen et al. (1979) and Sinno et al. (1986) show that crustal structure along the axis of the rift appears fairly consistent throughout New Mexico. If the dip of just less than 2^o found by Sinno et al. (1986) is applied to the data of Olsen et al. (1979), then an upper mantle velocity of 7.7 km/sec exists along the entire rift axis in New Mexico. The combination of this with the other seismic lines within the central and southern rift shows that the M-discontinuity seems to reach its shallowest point within the vicinity of El Paso (Figure 10), coinciding well with a large, positive regional gravity anomaly (Figure 11).

These data within the rift have enabled geophysicists to distinguish the rift

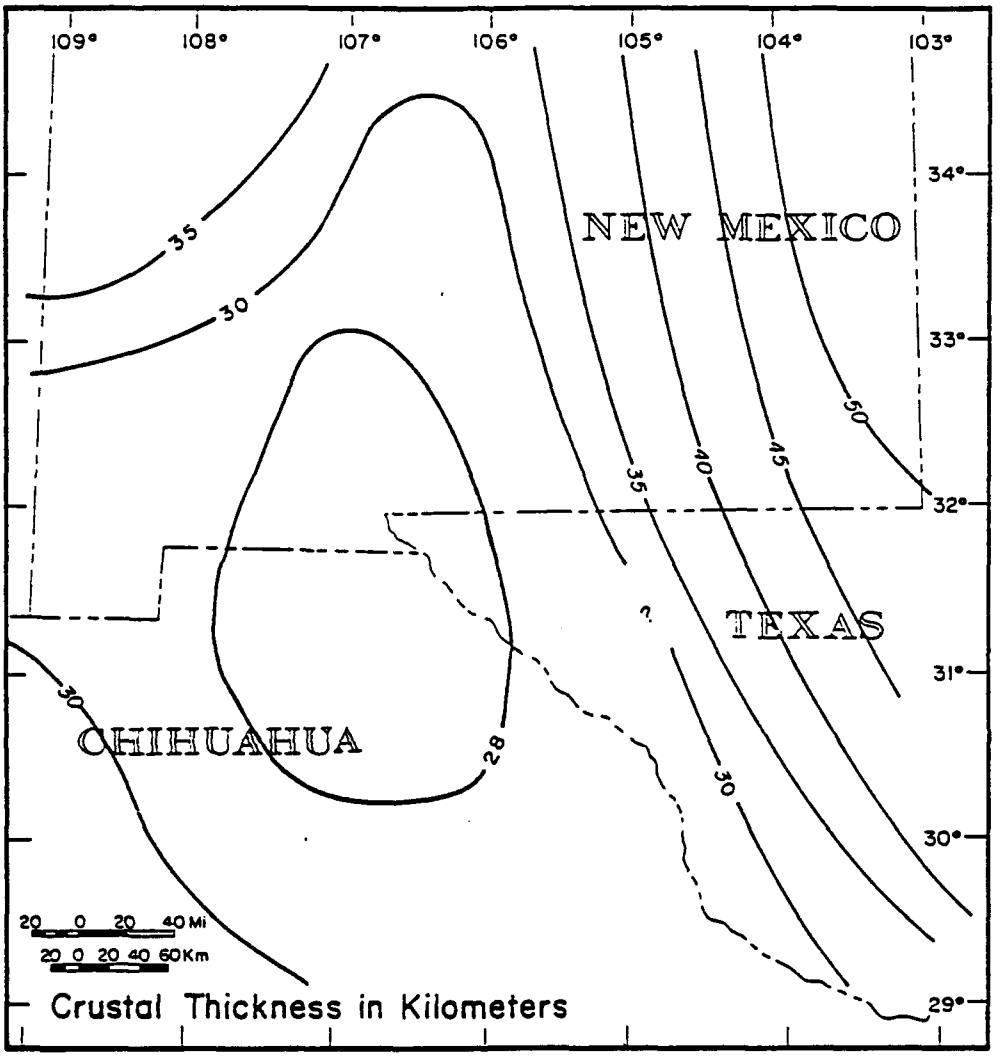

Figure 10. Contour map of depth to Moho in southern Rio Grande Rift from Keller et al (1990).

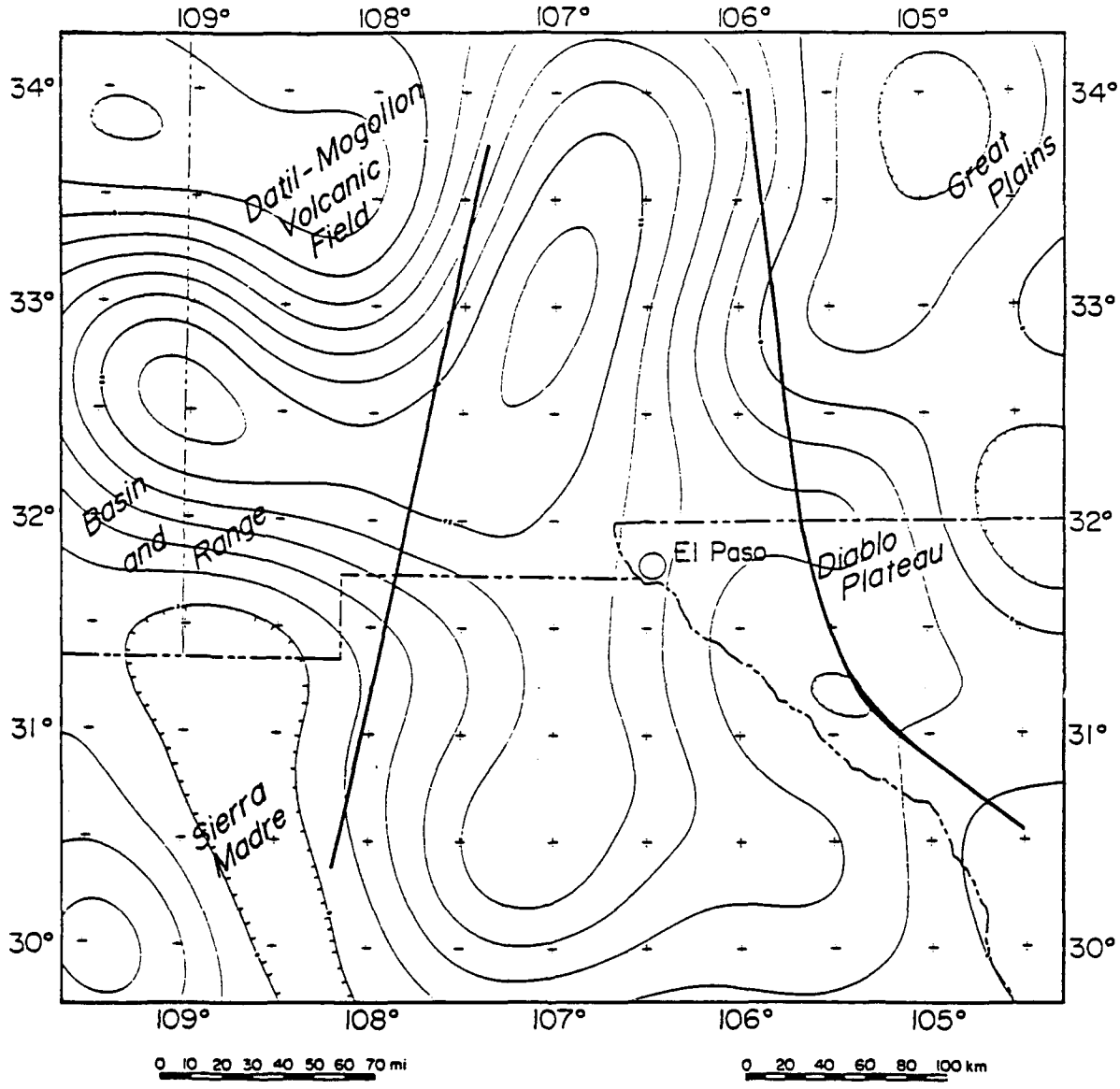

Figure 11. Regional bouguer gravity map of the southern Rio Grande Rift from Keller et al (1990).

from its neighboring provinces, but very little work has been done through the transition zones to the east or west. The previously cited works of Toppozada and Sanford (1976) and Keller et al. (1979) extended from the Colorado Plateau into the rift but lacked sufficient resolution to accurately define the transition. Gish et al. (1981) began a refraction line in what might be considered the extreme western edge of the RGR and progressed westward through portions of the Datil-Mogollon volcanic field (DMVF) and into the Basin and Range of Arizona (Figure 3). This resulted in analysis of the CP-BR transition but contributed little to knowledge of the rift. Jaksha (1982) monitored the DICE THROW explosion at WSMR with a widely spaced seismic line extending from WSMR to Morenci, AZ (Figure 3). The line was reversed with mine shots near Morenci and the results indicated a crustal thickness of 33 km, no significant dip along the Moho, and a Pn velocity of 7.98 km/s. This crustal thickness agrees well with results from within the rift but the Pn velocity is much higher. An unreversed refraction survey extending from Santa Rita, NM, to Grants, NM (Harden, 1982), showed a crustal thickness of 35 km and a Pn velocity of 7.97 km/s. These last two surveys indicate that the upper mantle velocity within the DMVF is more "normal" than that of the rift but apparently the crustal thickness is about the same.

No refraction or surface wave dispersion studies have been completed across the eastern flank of the rift. However, the teleseismic study by Davis et al. (1984, Figure 3), the various gravity profiles across the southern rift (Figure 9), and the published heat flow data (Figures 6, 7, and 8) do provide some indication of the location and gross structure of the transition. Stewart and Pakiser (1962) monitored the GNOME nuclear explosion in southeastern

New Mexico with a seismic array that trended roughly due north (Figure 3). Their data revealed a four layer crust: 4.2 km at 4.93 km/s, 15 km at 6.14 km/s, 11.9 km at 6.72 km/s, and 19.7 km at 7.1 km/s. This placed the Moho at a depth of 50.8 km with an upper mantle P-wave velocity of 8.23 km/s. This work indicates that the easternmost plains of New Mexico are well within the Great Plains province and that the anomalous crustal and upper mantle structures associated with the southern RGR terminate somewhere west of 104°W longitude.

THE STUDY AREA

At its western extreme, the seismic array fielded for this survey ties with the intra-rift refraction profiles of Sinno et al. (1986) and Olsen et al. (1979) while its eastern end crosses the teleseismic line of Davis et al. (1984) and the Great Plains refraction profile analyzed by Stewart and Pakiser (1962, Figure 3). The array trends nearly east-west along latitude 33.7°N from 106.3°W to 104°W longitude yielding station offsets of about 1000 km to 1200 km (Figure 2). The westernmost stations lie at the northern limit of the Oscura Uplift approximately 13 km east of the Jornado del Muerto basin and 40 km ESE of Socorro, NM. Progressing eastward, the profile crosses the Claunch Sag, a downwarped, mid-Permian evaporite basin which forms a rough connection between the larger Estancia and Tularosa basins. A series of Tertiary laccoliths and stocks border the sag to the east. The seismic profile weaves between several of these intrusions and climbs the western flank of the Mescalero Arch, a structural high which roughly follows the axis of the ancient Pedernal Mountains. From there, the seismic line continues eastward along the northern flank of the Capitan intrusion, down the gently dipping Pecos Slope, and onto the Permian shelf of eastern New Mexico (Kelley and Thompson, 1964; Kelley, 1972). As previously mentioned, the RGR's eastern boundary must lie somewhere within the western half of this region.

DATA ACQUISITION

The seismic data gathered for this survey was recorded during five separate deployments (Table 2). The scarcity of seismic equipment on any given shot date required the use of several different types of recorders and seismometers. Table 3 lists the various configurations used for this survey.

SHOTS							
SHOT NAME	DATE	TIME (GMT)	LOCATION N LAT	W LON	ELEV	# OF OCCUPIED STATIONS	# OF SUCCESSFUL STATIONS
NTS1	12 Jun 85	15:15:00.082	37.248	116.489	6250	13	3
NTS2	25 Jul 85	14:00:00.0876	37.297	116.438	6400	21	18
NTS3	5 Jun 86	15:04:00.064	37.098	116.016	4250	15	8
----	17 Jun 86	----	----	----	----	16	0
NTS4	24 Sep 87	15:00:00.055	37.228	116.375	6700	16	10

Table 2. NTS blasts used as sources for this survey.

STATION CONFIGURATIONS

Configuration number	Recorder	Type	Seismometer	Natural Frequency
1	Sprengnether DR-100, 100 sps, clock trigger	digital	Mark Products L-4, vertical component	1 Hz undamped
2	Sprengnether DR-100, 100 sps, clock trigger	digital	Sprengnether S-7000, vertical component	1 Hz damped
3	Sprengnether DR-100, 100 sps, clock trigger	analog	Sprengnether S-6000, vertical component	1 Hz damped
4	Sprengnether MEQ-800, smoked-drum paper record, manual trigger	analog	Sprengnether S-7000, vertical component	1 Hz damped
5	Sprengnether MEQ-800, smoked-drum paper record, manual trigger, plus FM tape recorder	analog	Sprengnether S-7000, vertical component	1 Hz damped

Table 3. Station configurations used during this survey.

On the day of a scheduled blast, approximate shot times were requested from the appropriate authority and field crews activated as many recording stations as possible. Each crew was responsible for four to seven stations spread out over distances up to 35 km. The various recorders had recording windows ranging from twenty minutes to four hours. If a blast was postponed for more than just a few minutes, each crew was responsible for resetting each

of its stations as necessary. Due to the frequency and erratic nature of the shot postponements, difficult station access, and communication difficulties, many stations did not record successfully. This resulted in fewer successful traces than hoped but enough data was recovered to continue the project. Table 4 lists the pertinent information associated with each of the successful stations. The offset distances were computed by first determining the arc distance between the shot and receiver and then transforming this angular distance into kilometers by approximating the earth as a perfect sphere with a radius of 6371 km. Some of the traces in Table 4 were eventually editted from the final sections to decrease redundancy in certain regions. As Figure 3 indicates, the seismic profile is not exactly radial to the NTS. The maximum difference in azimuthal angle from the shot to the recorders is 2.4^{o}, 3.8^{o}, and 2.8^{o} for the NTS1/NTS2, NTS3, and NTS4 sections, respectively.

SUCCESSFUL STATIONS						
STATION NAME	SHOT NAME	CONF. #	LOCATION N LA.	W LON	ELEV	OFFSET (KM)
P3	NTS2	4	33.729	105.978	5556	1027
P4	NTS2	4	33.714	105.894	5300	1035
P2	NTS2	4	33.708	105.856	5506	1038
T3	NTS2	4	33.742	105.708	6640	1049
PDE.P4	NTS1	4	33.683	105.575	6470	1066
STONE	NTS2	1	33.678	105.532	6400	1067
ENCINOSO	NTS2	1	33.685	105.483	6257	1071
CANNING	NTS2	1	33.694	105.424	6140	1076
RADIO	NTS2	1	33.690	105.383	6020	1079
BM5997	NTS2	2	33.705	105.329	5997	1083
HARRISON	NTS2	2	33.684	105.266	5620	1089
SERRANO	NTS2	2	33.649	105.198	5438	1097
SMOOTS	NTS2	2	33.674	105.133	5156	1101
SEC29	NTS2	2	33.679	105.072	4924	1106
SECO	NTS2	3	33.694	105.016	4810	1110
PDE.T3	NTS1	4	33.651	104.948	4640	1120
NOWHERE	NTS2	1	33.637	104.782	4165	1132
PDE.T2	NTS1	4	33.643	104.859	4300	1134
CORN	NTS2	1	33.625	104.750	4063	1136
TOMCORN	NTS2	1	33.636	104.653	4131	1143
BM3794	NTS2	1	33.643	104.576	3794	1149
M1	NTS4	5	33.643	104.576	3794	1149
M2	NTS4	5	33.651	104.380	3620	1166
M4	NTS4	5	33.640	104.312	3730	1172
M8	NTS4	5	33.660	104.007	4035	1197
K2	NTS4	1	33.700	103.840	4241	1209
K3	NTS4	1	33.725	103.753	4405	1216
K5	NTS4	1	33.744	103.596	4414	1229
K6	NTS4	1	33.744	103.509	4340	1236
K7	NTS4	1	33.766	103.435	4308	1241
K8	NTS4	1	33.774	103.348	4215	1249

Table 4. Locations and configurations for each successful receiver station. The stations listed below the single line were plotted as a separate seismic section.

DATA PROCESSING

Several different processing procedures were required to assemble the raw data from the various types of recorders. The smoked-drum paper records from the MEQ-800's were first dipped in shellac to solidify the soot coating and were then removed from the recording drums. Once the first arrivals from the blast were located on the seismic trace, about two minutes of data, starting a few seconds before the first arrival, was digitized at a rate of 50 samples per second and stored in a format compatible with the seismic section program discussed below.

Several new programs were developed to process the digital data cassettes from the DR-100's. A UNIX shell and C program, GPIO, was developed to allow for a direct data transfer from Sprengnether DP-100 playback units to the Department of Geological Science's HP-9000. If more than one event occurred on a single tape, the program DPFILEGEN was used to separate them into separate data files. Once the transfer was completed, another program, DISPLAY, was used to assemble the raw data into a correctly formatted seismic trace. DISPLAY is an interactive program which runs on any of the HP graphics terminals. It extracts the raw data from the Sprengnether formatted data files and plots various portions of the seismic traces on the user's screen. The user may then use the interactive graphics capabilities of the terminal to identify key timing marks and time windows. The program will then demultiplex (if more than one channel is recorded) and process the selected data and create an output file (or files) compatible with the SECTION program. Care is taken to detect any data "dropouts" and to demultiplex only that portion of the trace critical for the experiment. For

this survey, the DR-100 recorders were set for sampling rates of 100 samples/second and two minutes of data were retained.

For the later deployments, the MEQ-800's were coupled with audio synthesizers and FM tape recorders developed at Purdue University. A system was developed at UTEP to playback the audio cassettes into a set of amplifiers which were in turn connected to a DR-100 recording unit and a DP-100 playback unit. The resultant data file can then be processed identically to the actual DR-100 records discussed above with one exception. After the DISPLAY program completed its processing, another program, FM.CLEANUP, was used to detect and adjust for the variable tape tracking rates of the FM recorders and to remove the wide timing marks generated by the MEQ-800.

Once all of the traces were assembled, they were processed and plotted together in a series of seismic sections using the SECTION program. Each digital trace was filtered with a low-cut filter at 0.1 Hz with a 0.2 Hz rolloff and a high cut filter at 10 Hz with a 4 Hz rolloff. The trace times were reduced at a velocity of 8.0 km/s and the resultant sections from NTS1/NTS2, NTS3, and NTS4 are shown in Figure 12.

Due to the various station configurations and the minimal calibration information available for each station, very little amplitude analysis is possible with these sections, especially when comparing actual amplitudes trace-to-trace. With this limitation in mind, the amplitudes of each seismic trace were normalized when the sections were plotted. Since shots NTS1 and NTS2 were located only 3.5 km away from each other and nearly equidistant from each station, the successful traces from each were combined into one section. NTS3

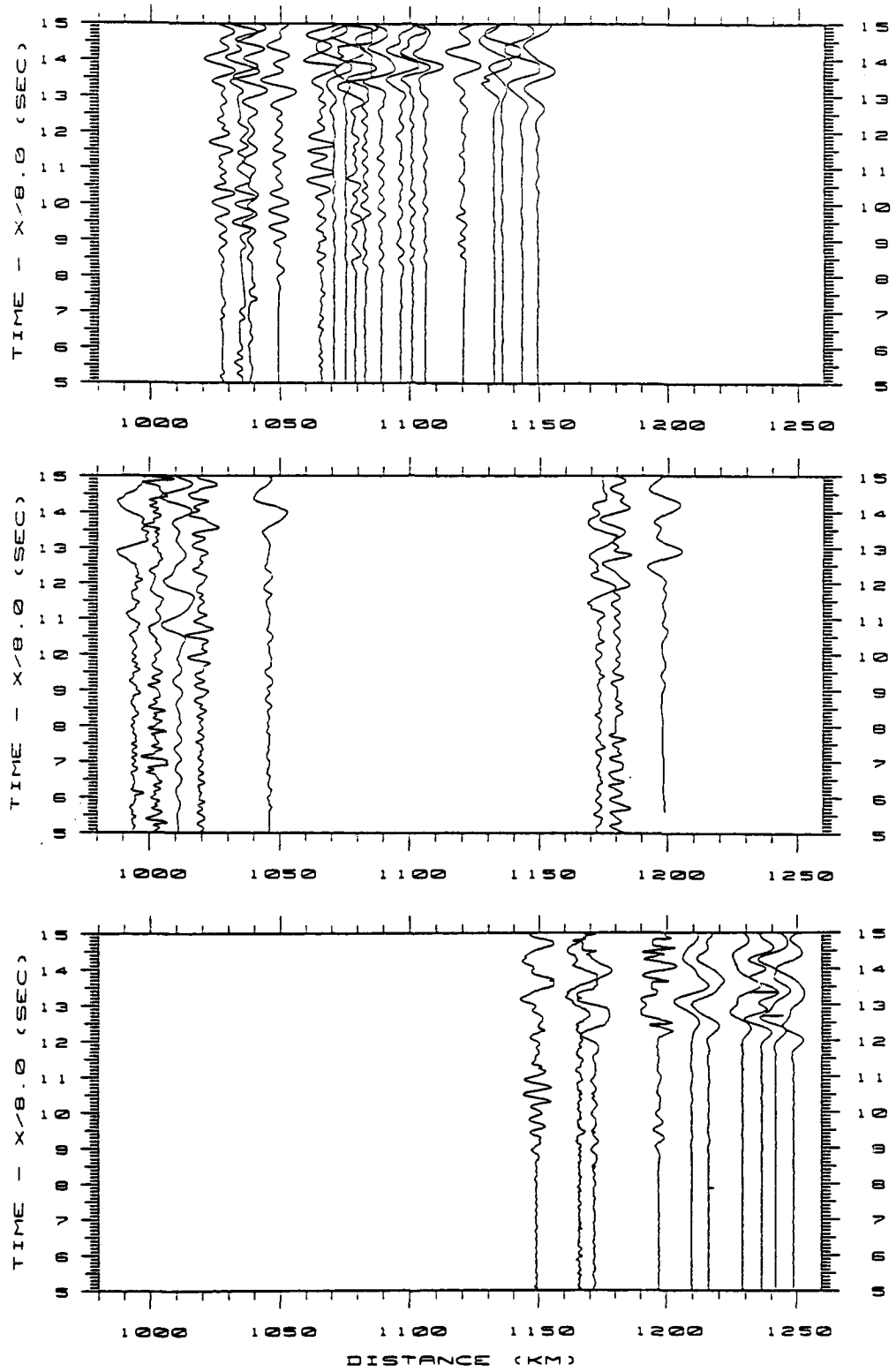

Figure 12. Seismic sections created from this work.

The top section is from shotpoints NTS1 and NTS2. The middle section is from shotpoint NTS3 and the bottom section is from shotpoint NTS4.

and NTS4 were located approximately 43.5 km and 7.5 km, respectively, closer to the recording stations. As Figure 12b shows, the quality of the traces from NTS3 was very poor. For this reason, the easternmost regions were re-occupied during NTS4. The success of the NTS4 survey and the lack of information provided by the westernmost stations of NTS3 make the NTS3 section obsolete.

MODELING

Modeling Technique

The long station offsets used in this survey provide the opportunity to examine the structure of the Rio Grande Rift/Great Plains transition down to depths of nearly 200 km. This is very advantageous since it is expected that the anomalous features of the rift extend throughout the lithosphere and into the asthenosphere. To generate an earth model consisting of two-dimensionally varying structures, the algorithm described by Cerveny et al (1971) and Cerveny (1979) and applied by Luetgert (RAY84 program, personal communication; see Hill et al., 1985) was used in an iterative manner to determine the ray paths and P-wave travel times through successive models until the modeled travel times matched with those extracted from the seismic sections. This ray-tracing technique, referred to as asymptotic ray theory (ART), has been used for seismic refraction surveys by scores of researchers and is well substantiated in the literature. However, the unusually long offsets of this survey required the consideration of a phenomenon not usually addressed in ART modeling -- the curvature of the earth's surface.

Chapman (1973) describes and compares several conventional earth "flattening" transforms. However, each of these methods is predicated on the use of a spherically symmetric earth model, i.e. one with no lateral velocity variation. Since the primary objective of this research is to examine the lateral transition from the Rio Grande Rift to the Great Plains, these techniques cannot be used. To alleviate this problem, a new technique for compensating for the earth's curvature was developed and implemented for

this study.

The simplest and most common method of referring to a sub-surface position is by depth and range. As Figure 13a shows, range, R, is a lateral distance along the earth's surface measured from some arbitrary reference point to the spot on the surface just above the sub-surface position. Depth, D, is then the vertical distance between this epicentral point and the buried point. The problem with this approach (especially in long offset surveys) is that it implies a cartesian relationship between range and depth. In reality, these points lie in a polar coordinate system (Figure 13b) where R is an arc distance along the great circle connecting the reference point and the epicentral point and D is a radial distance measured down from the surface. If the chosen modeling technique treats R and D as cartesian coordinates and R is more than 4^{o} or 5^{o} of arc, then significant errors can be introduced. If the (R,D) coordinates are first transformed into a true cartesian coordinate system, then the Earth's curvature no longer presents a modeling problem (i.e., as long as the chosen modeling technique allows for two-dimensional geometries). Figure 14 describes the mathematical relationship between the (R,D) coordinate system and the true cartesian system of the modeling space used in this survey. The following example illustrates how the transformation is applied in the ART modeling program, MENLORAY (the RAY84 program with the earth curvature approximation implemented).

Figure 15a is an example earth model with one horizontal sub-surface interface, one faulted interface, and one dipping interface. The X's represent the points used by the modeler to describe these interfaces. To apply the earth curvature approximation, the user must choose several intermediate

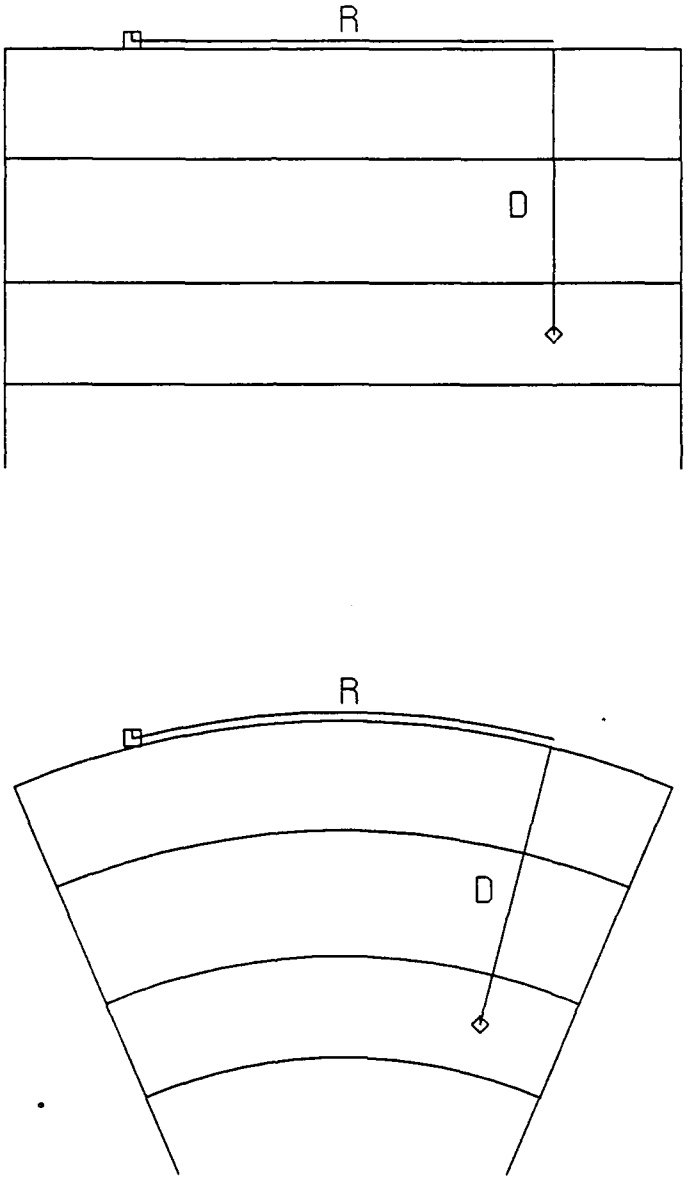

Figure 13. Geometric relationship between range and depth.

The top figure represents the idealized earth and the range (R) and depth (D) coordinates used to describe subsurface locations. The bottom figure illustrates the true polar relationship between R and D.

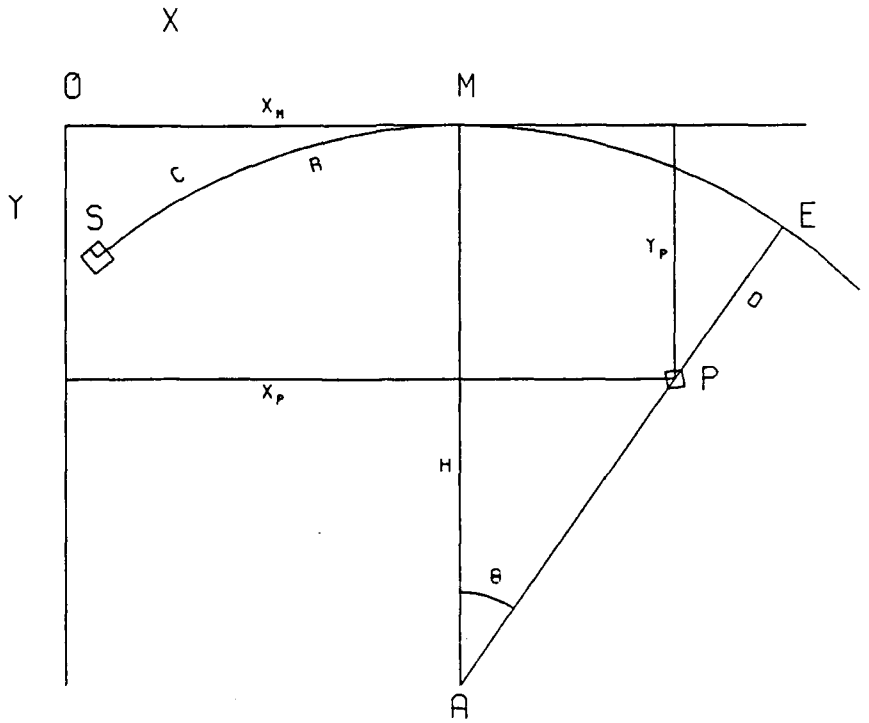

Figure 14. Graphic representation of earth curvature algorithm.

S = origin for user's range/depth coordinate system
P = subsurface position
R = arc distance from S to E (user input -- range)
D = radial distance from E to P (user input -- depth)
E = epicentral point
M = range at which the true cartesian coordinate system is tangential to the curved earth (user input)
A = center of the earth
C = arc distance from S to M
H = radius of the earth
O = origin of cartesian coordinate system
X_m = distance from O to M (= C)

$$\theta = (R - C) / H$$
$$X_p = X_m + (H - D) * \sin \theta$$

$$Y_p = H - (H - D) * \cos \theta$$

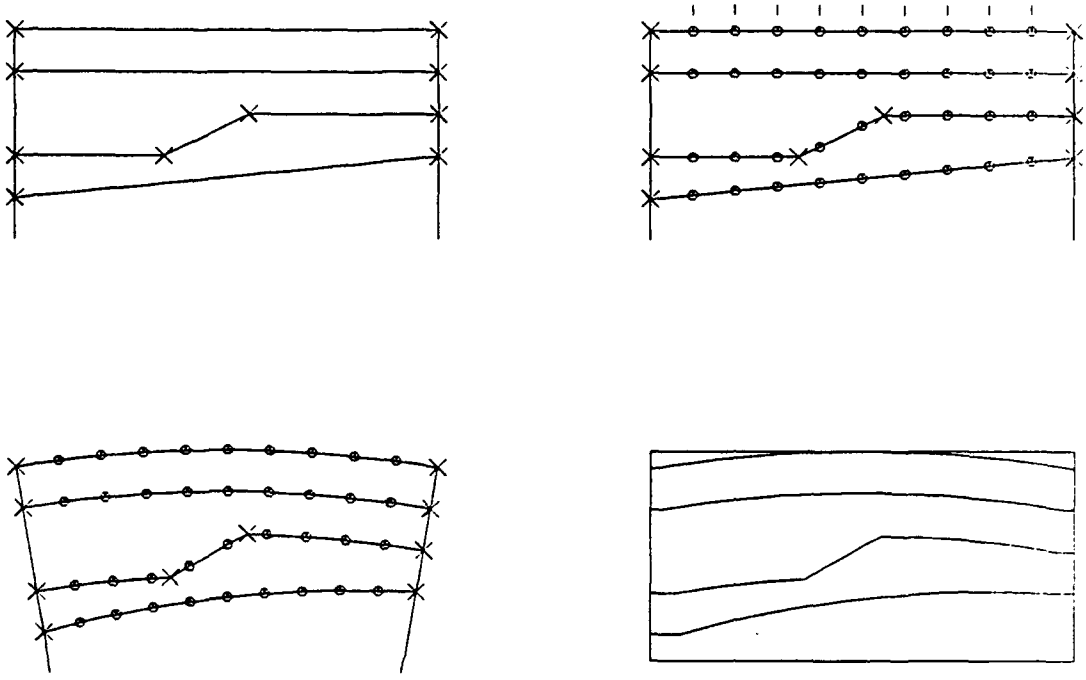

Figure 15. Example application of earth curvature algorithm.

The upper left figure shows the model as envisioned by the user. X represents a user supplied (R,D) coordinate. The upper right figure shows the interpolated ranges and depths. The lower left figure shows each of these points after conversion to the cartesian (X.Y) system. The lower right figure is the final curved model drawn in the cartesian (X,Y) system.

ranges, usually equally spaced, at which the program will interpolate the depth to each of the interfaces (Figure 15b). Each of the points in this dense range/depth (R,D) grid is then transformed into the true cartesian coordinate system (X,Y) using the algorithm described in Figure 14. The resultant model (Figure 15c) is best described as a spherical earth approximated by a series of pie wedges. The accuracy of the approximation is governed by the width of each wedge which, in turn, is a function of the spacing between the designated intermediate ranges. As Figure 15d shows, MENLORAY extrapolates the ends of each interface to the edge of the model space and the result is a series of curved surfaces drawn in a cartesian coordinate system.

MENLORAY then proceeds, using the (X,Y) coordinate system, to determine the appropriate ray paths and travel times. Each ray is stopped at the boundary corresponding to the earth's surface (as opposed to $Y=0$) and the final (X,Y) coordinates are inverse transformed to determine the range at which the ray exited the model.

To test this curvature technique, a spherically symmetric earth model was processed with the MENLORAY program and the SEIS4 program. SEIS4 is the 1D predecessor of the 2D ART program, MENLORAY (Sinno, personal communication; McMechan, personal communication). SEIS4 uses ART to trace rays through a laterally homogeneous earth model and then applies the principles of Disk Ray Theory to generate a synthetic seismic section. Since only 1D models are used, the program can also apply a standard earth curvature approximation when requested. The model chosen for the comparison is the western US crustal and upper mantle model of Burdick and Helmberger (1978; Figure 16).

Depth to bottom (km)	Velocity (km/s)
20.0	6.00
35.0	6.50
45.0	7.95
55.0	8.00
65.0	8.05
73.1	7.75
89.8	7.72
103.3	7.70
117.5	7.73
127.0	7.77
135.7	7.83
144.4	7.88
150.5	7.94
156.4	8.03
162.3	8.11
168.2	8.19
180.0	8.25
190.0	8.28
200.0	8.30

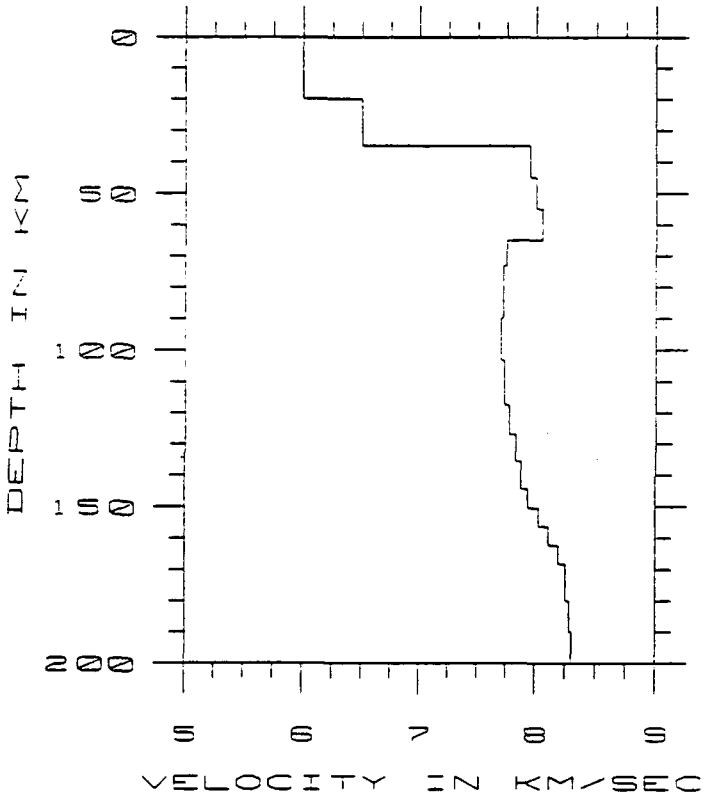

Figure 16. Velocity/Depth profile of western U.S. from Burdick and Helmberger (1978). These data correspond to their model T7.

Figure 17 shows the results obtained from the SEIS4 program along with the original and "flattened" earth models. Figure 18 shows the results obtained from the MENLORAY program and includes nine post-critical reflection, five refraction, and all pre-critical reflection phases. Figure 19 shows the synthetic seismic section generated from the MENLORAY amplitude output. Comparison of these figures leads to two conclusions. The first is that arrival times predicted by each of the methods are very similar. Second, noting that the amplitudes of several of the arrivals in Figures 17 and 19 do not match, is that the amplitude information from either SEIS4 or MENLORAY, or both, is suspect, especially at large offsets. This is not unexpected since neither of the techniques involves full wavefield modeling.

Analysis of Seismic Sections

Using the 1D synthetic sections discussed above as a guide (Figures 17 - 19), the first arrivals across the NTS1/NTS2 and NTS4 seismic sections (Figures 12a and 12b) are interpreted as Pn: critical refractions from the Moho discontinuity. The second arrival is P1: an arrival refracted below the upper mantle low velocity zone. The synthetic sections appear to indicate that the arrivals from several phases with arrival times of about 10 s are converging within the aperture of this work (1000 km to 1200 km). This is due partly to the nature of the test model (several thin layers at depth) and the modeling techniques but the observed sections indicate similar multiple arrivals. Further analysis of these tightly clusted phases will have to wait for additional traces to be added to this survey in order to increase the aperture and make phase correlation easier. For now, the earliest arrival within this packet was picked for modeling purposes. It should be noted however that

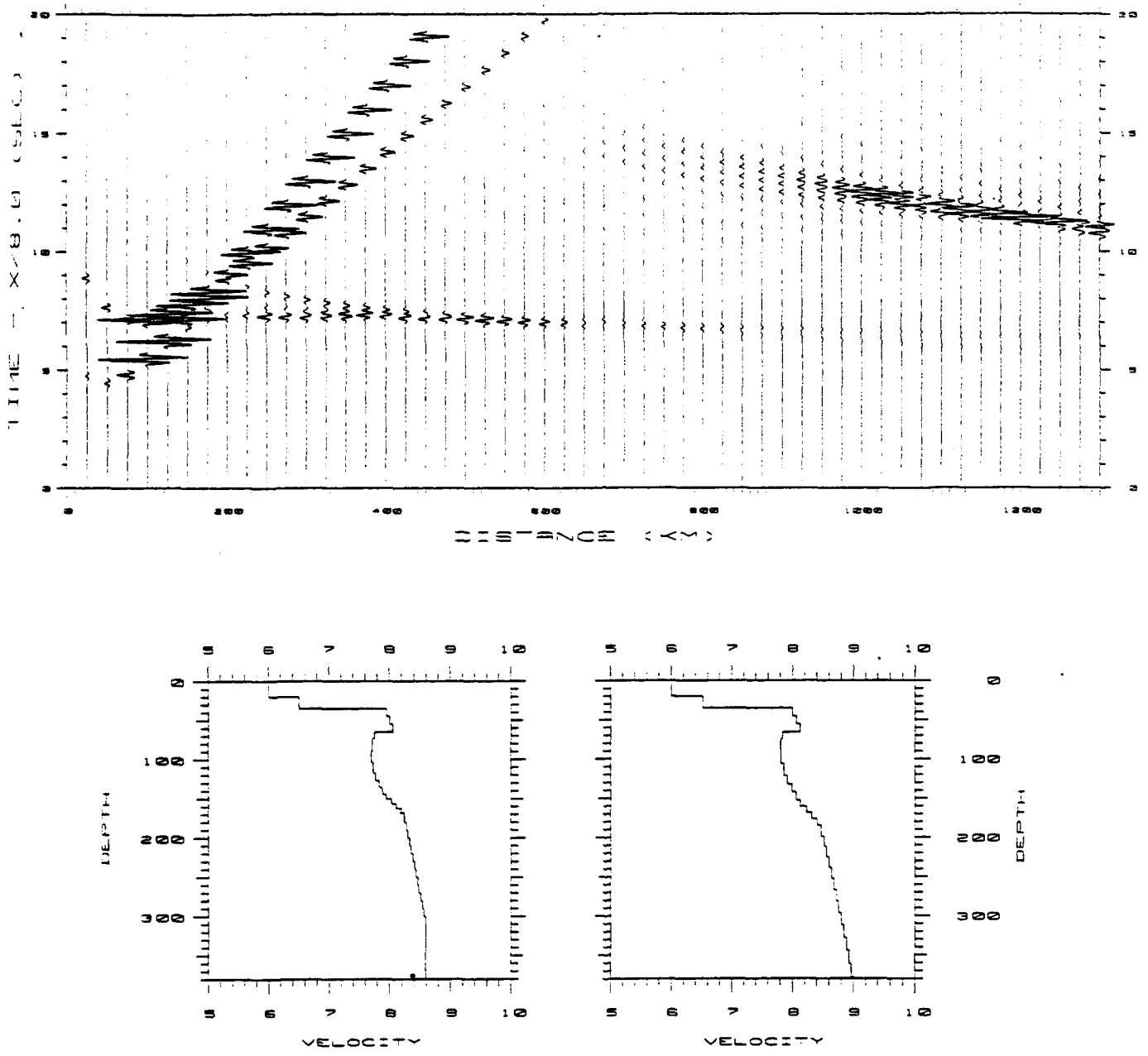

Figure 17.. Synthetic seismograms generated by SEIS4 program using the test model.

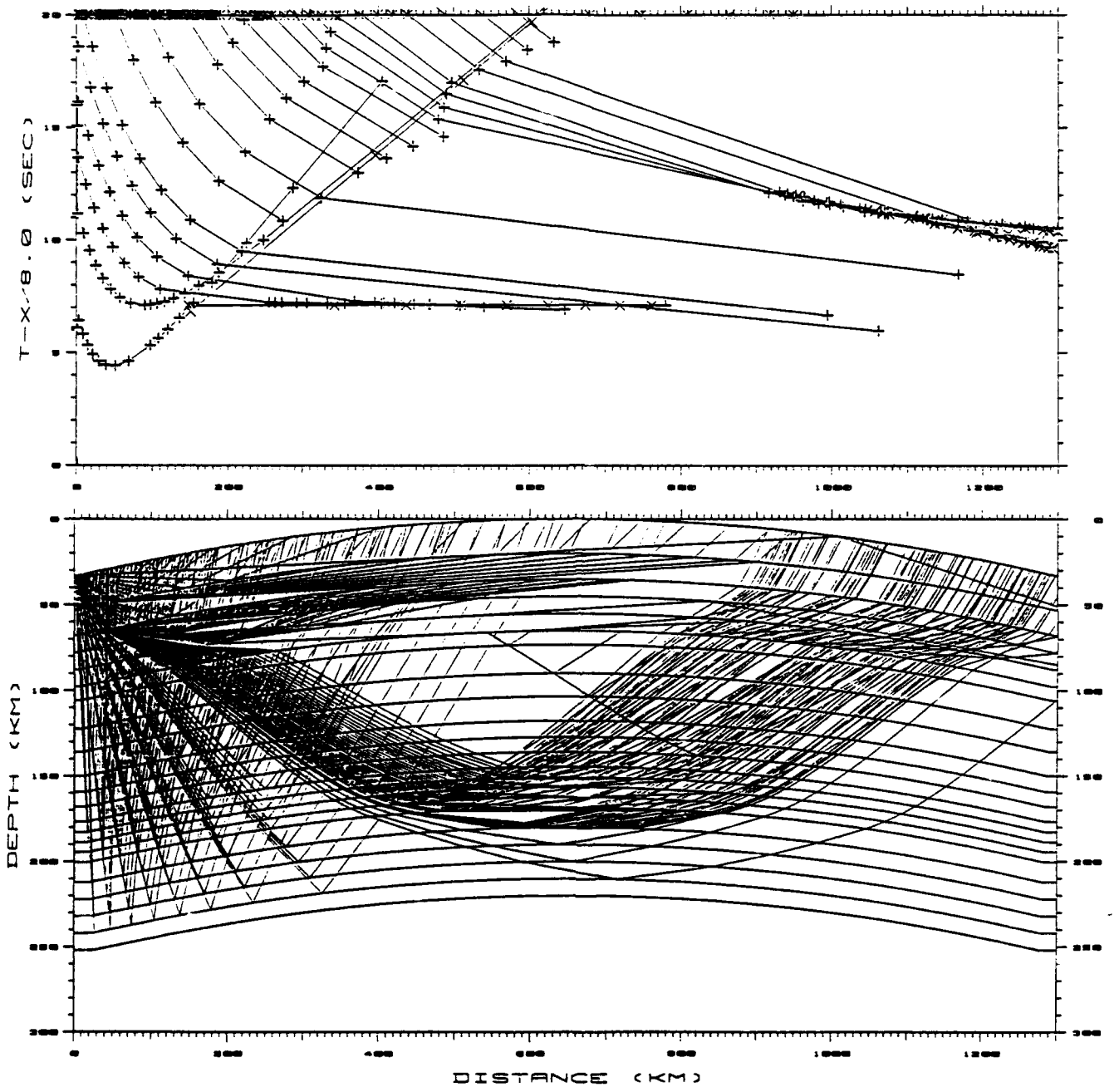

Figure 18. Raypaths and arrival branches generated by MENLORAY through the test model.

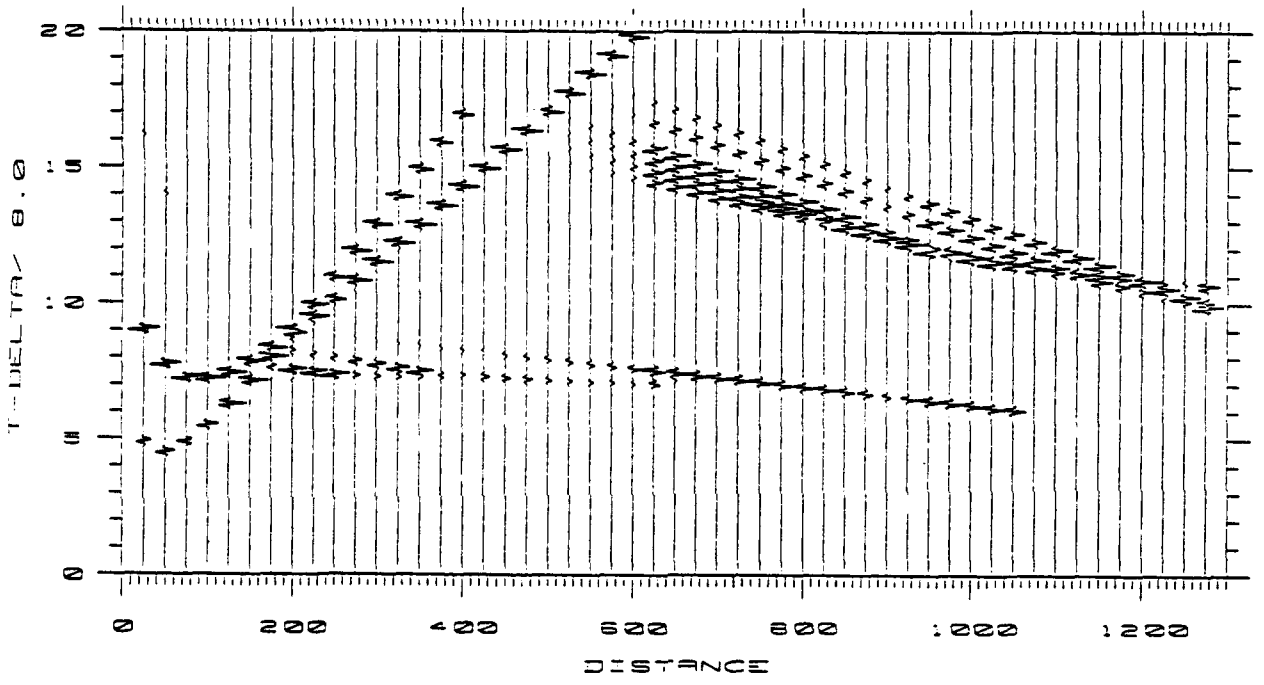

Figure 19. Synthetic seismograms generated by MENLORAY/RAY83PLT programs using the test model.

this packet of energy, as well as the Pn arrivals, all arrive several seconds later than that predicted by the 1D models, indicating the presence of major lateral variation in the lithospheric structure.

Two notable features of the NTS2 section are the decrease with distance in the difference between P1 and Pn arrival times and a decrease with distance in the Pn/P1 amplitude ratio. Similar characteristics appear on the 1D synthetic sections (Figure 17 - 19). The NTS4 section shows a similar decrease with distance in the difference between P1 and Pn arrival times but the amplitude ratios appear more complicated. At R = 1200 km, the Pn arrivals nearly disappear altogether. However, by referring to Table 4, one can quickly conclude that this abrupt feature is a manifestation of the varied instrument configurations between stations at R < 1200 km and stations at R > 1200 km.

Initial Model

The seismic waves recorded during this survey traveled through or under several geologic provinces within the western U.S. The shotpoints, located on the Nevada Test Site, are in the south central portion of the Basin and Range province and the seismic array begins in the Rio Grande Rift and ends within the Great Plains province (Figure 3). Between the shots and the receivers lie the Colorado Plateau and the Datil-Mogollon volcanic field. To accurately model the recorded wave forms, each of these provinces must be represented in the earth model.

At first glance, the task of generating an earth model using two-dimensional structures spanning each of these provinces appears somewhat difficult. However, upon further inspection it becomes clear that the trace-

to-trace variations in the phase arrival times apparent in Figure 12 are a result of variations in seismic properties within the RGR/GP transition region and are not strongly dependent on the provinces to the west. This is due to the very narrow band of take-off angles spanned by the packet of energy which reaches the seismic array. The seismic "rays" within this packet do not diverge appreciably until after their respective turning points. This means that any large structural anomaly encountered before the turning point will result in a constant shift in arrival time across the entire section and will create no trace-to-trace variation. This phenomenon simplifies the modeling task by accentuating RGR and GP structures while lessening the impact of BR, CP, and DMVF structures. If the starting model for these westernmost provinces is chosen wisely, then any discrepancies between the modeled arrival times and the measured arrival times can be attributed to anomalous structures within the RGR or the transition zone into the GP.

The initial model generated for this survey was derived from several sources. Crustal models were chosen from surveys within each of the separate geologic provinces (Taylor, 1983; Warren, 1969; Harden, 1982; Sinno et al., 1986; Stewart and Pakiser, 1963) and an upper mantle model was drawn from regional works in the western and central U.S. (Burdick and Helmberger, 1978; Green and Hales, 1968). The combined model consisted of three crustal layers and several mantle layers extending to a depth of about 200 km.

Shots NTS1, NTS2 (both located at R=0), and NTS4 (R=7.5 km) were located on Pahute Mesa and NTS3 (R=43.5 km) was located in the Yucca Flat, all within the Nevada Test Site. Taylor (1983) derives crustal models for each of the geologic regions within the NTS using teleseismic P wave

residuals and regional travel time data. Figures 20a and 20b summarize his results and also show the averaged NTS models extrapolated for this survey.

A crustal model for the Colorado Plateau was extracted from the seismic refraction work of Warren (1969). Figure 20c is a velocity depth curve deduced from his SW-NE trending line at a point southwest of Winslow, Arizona. This choice is relatively insignificant since none of the modeled arrivals travel through the Colorado Plateau crust.

The previously discussed work of Harden (1982) crosses this seismic line at R = 844 km and was used as a model for the DMVF. The initial model for the RGR itself was taken from Sinno et al. (1986). Their work extends to within a few tens of kilometers of the westernmost stations of this survey (Figures 2, 3, and 4). Farther to the east, the previously discussed work of Stewart and Pakiser crosses the array at R = 1225 km and provides control for the crust of the Great Plains province (Figures 2 and 3).

Burdick and Helmberger (1978) constructed a relatively detailed P velocity vs. depth curve for the upper mantle under the western U.S. (Figure 20d) by modeling long period body waves. Their final model, which they designate as model T7 (Figure 16), was used for the asthenospheric structure in this survey. The sub-Moho lithospheric model generated from the studies discussed above was extended to a depth of 65 km below each of the geologic provinces and T7 structures were incorporated beneath 65 km (corresponding to the top of the T7 low velocity layer) under the BR, CP, DMVF, and RGR provinces. Burdick and Helmberger (1978) describe the velocity structure of the asthenosphere as a series of "smooth" velocity gradient changes without any significant discontinuities. However, their model, as Figure 16 shows, consists of a number of constant velocity layers seperated by discrete

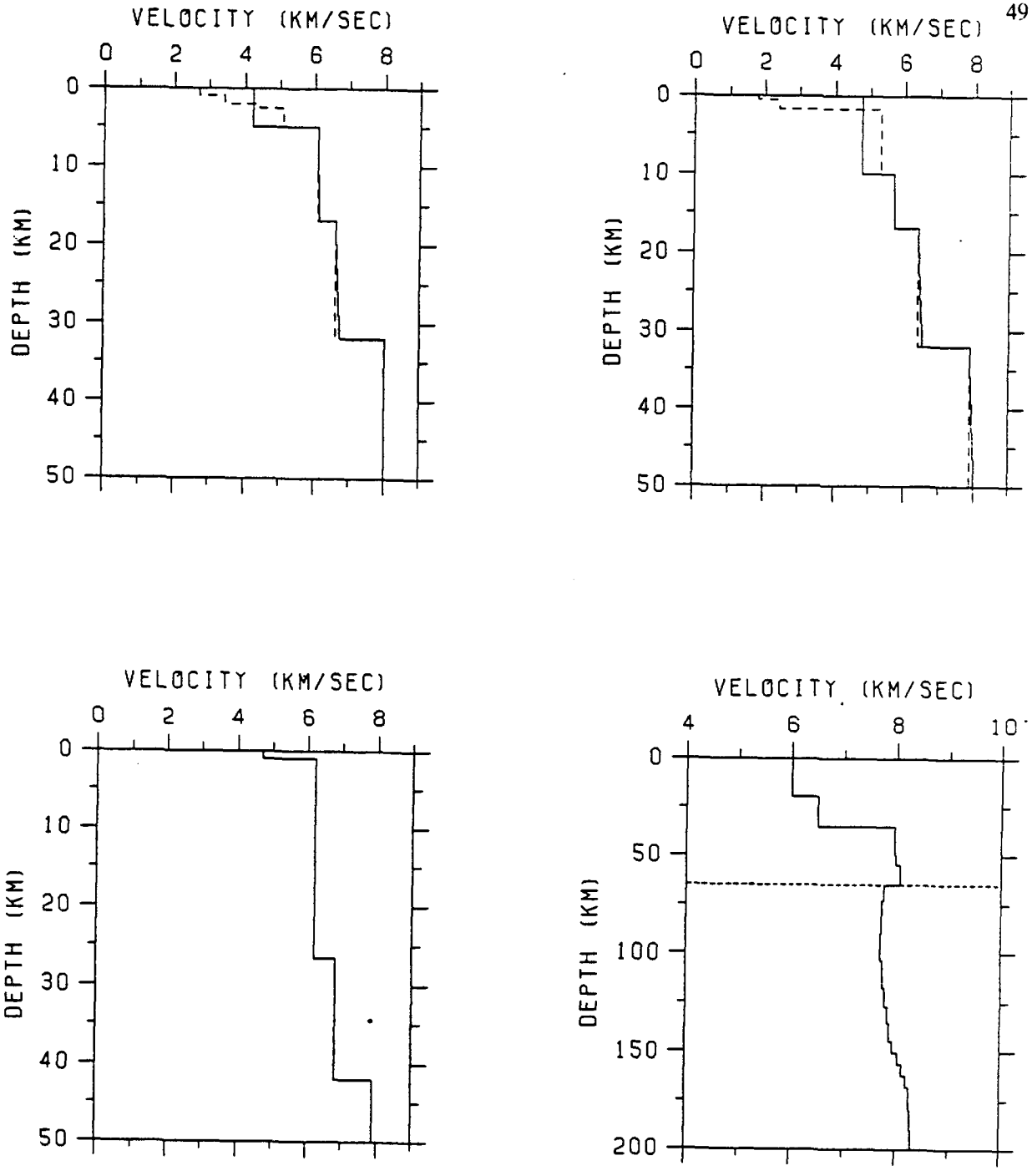

Figure 20. Published velocity profiles incorporated into the initial model.

The top two figures are the result of Taylor's (1983) work on Pahute Mesa (left) and Yucca Flats (right) in the Nevada Test Site. The dashed profiles represent Taylor's work and the solid profiles are the simplification of his models used in this work. The lower left profile is from Warren (1969) and shows his crustal model southwest fo Winslow, Arizona. The lower right figure is Burdick and Helmberger's (1978) T7 model. Only data beneath the dashed line was used in this work.

interfaces. This paradox results from the different scales between this work and that of Burdick and Helmberger. The complete model T7 extends to a depth of 885 km. On that scale, 10 km thick, constant velocity bodies can be used to approximate a smooth velocity gradient. For this work, 10 km is a more significant thickness. Therefore, the model T7 was modified slightly. The velocity given in Figure 16 was used at the top of each corresponding layer but the bottom velocity of that layer was taken from the adjacent deeper layer. The result is that the velocity remains the same on either side of the interfaces below 65 km but the velocity gradient may change.

The Great Plains mantle structure was derived from Green and Hales (1968), who monitored the Early Rise series of explosions in Lake Superior with a very widely spaced seismograph network. However, as with the Colorado Plateau crustal region, very little of the seismic energy recorded for this survey actually passed through the GP deep upper mantle.

Final Model

Figure 21b is a drawing of the final model derived from this work. The figure was drawn as a "flat earth," i.e. without the earth curvature approximations discussed above. Figure 21a shows all the rays which were used to construct the final model. Since the data had to be divided into 2 separate sections, the modeling was also divided. The solid rays are those that originated at shotpoint NTS1/NTS2 and the dashed rays are those that originated at NTS4. Figure 22 shows the NTS2 and NTS4 seismic sections plotted side-by-side and overlain by the modeled arrival branches.

The match between modeled and the observed first arrivals (Pn) is very good across both sections. The P1 arrivals are more complex. The modeled

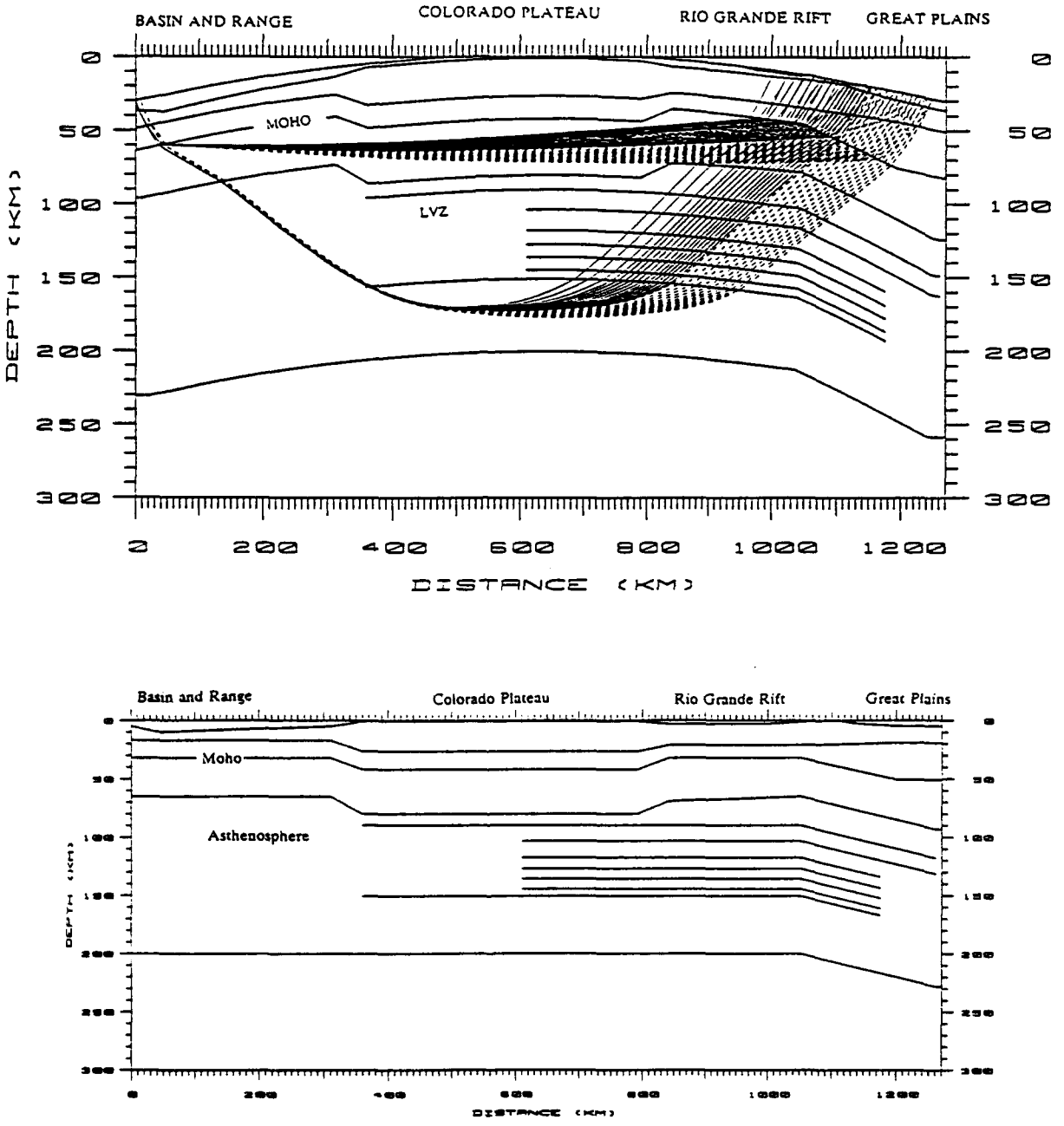

Figure 21. Modeled raysets and a plot of the final model from this work.

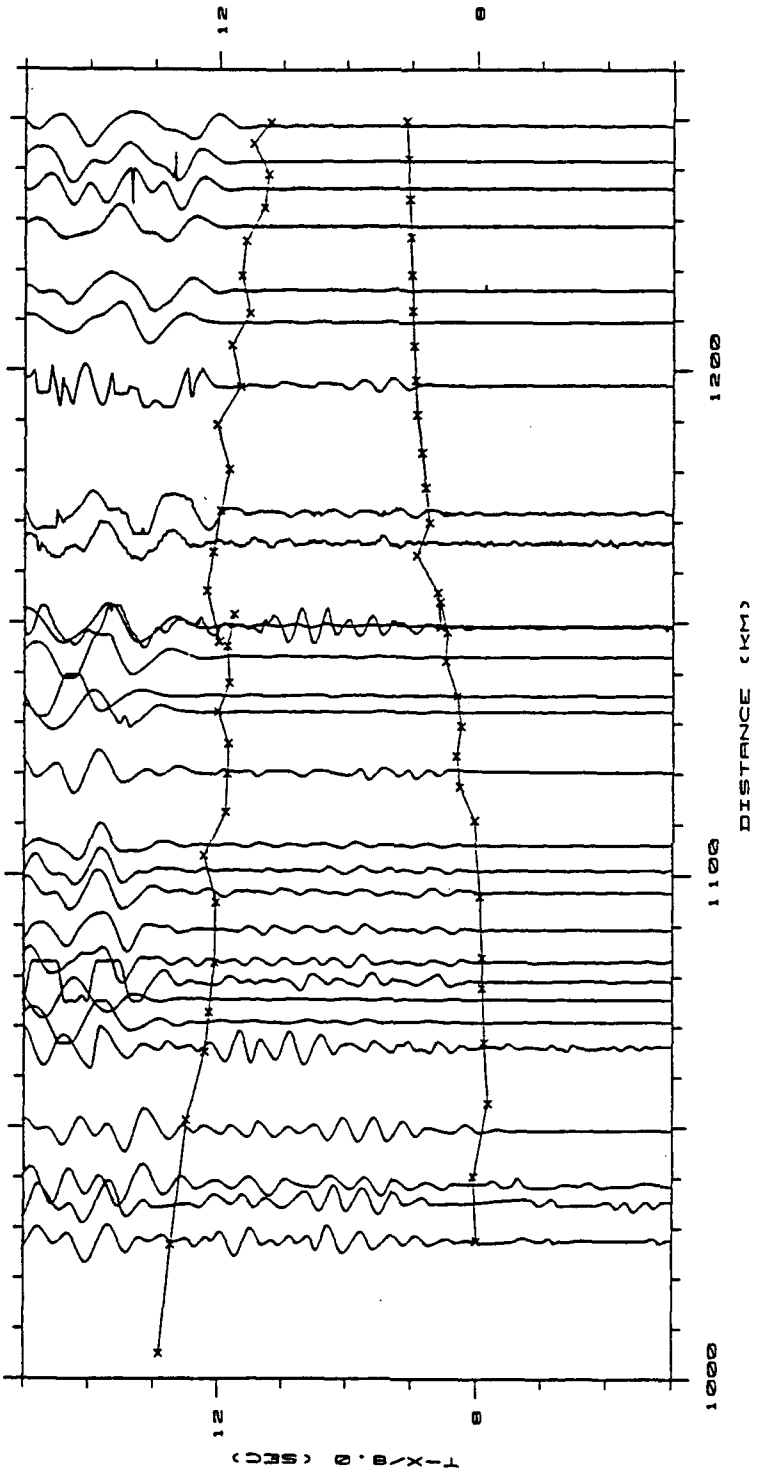

Figure 22. NTS1/NTS2 and NTS4 seismic section overlain by modeled arrival branches.

The station at 1049 km was occupied for both shots. Data to its left is from NTS1/NTS2 and the rest is from NTS4.

P1 arrival branch matches quite well with the first, weak arrival within the packet of energy observed at around 12 s. As previously discussed, the 1D modeling shown in Figures 17 - 19 indicates that several arrival branches converge several seconds after the first arrivals within the aperature of the seismic array and the observed sections (Figure 12) show a similar phenomena. The first of these arrivals was chosen for modeling. The observed sections show at least one strong, coherent arrival coming in slightly later than the modeled arrival. The modeling showed that the energy for all of these arrivals appears to bottom beneath the LVZ in the upper asthenosphere, but at slightly different depths. It is impossible to discern exactly which arrival is which at this point, but future extensions of this line to the east and the west will provide further data that will allow a more detailed analysis of these phases. The modeled P1 arrival bottomed at approximately 150 km.

Most of the crustal structure used in the initial model remained in the final model. This was expected since, unlike this survey, the previous surveys from which the crustal model was derived were specifically designed to resolve crustal detail. The only changes to the initial crustal model involved relocating boundaries between the various geologic provinces and the inclusion of Tularosa Basin structures around R = 1000 km.

The boundaries in the final model between the Colorado Plateau and its neighbors to the east and west are primarily asthetic since the energy reaching the seismic array traveled beneath the Colorado Plateau crust. However, the Pn arrivals at the western most stations do come close to exiting the upper mantle into the CP or DMVF lower crust.

East of the Plateau, the depth to the Moho discontinuity is steady at 32 km from R = 841 km to R = 1050 km (lon 105.7°W) and then drops steadily at an angle of about 7.6° until R = 1190 km (lon 104.1°W) where it reaches a depth of 51 km. The depths of 32 km and 51 km were taken from Sinno et al. (1986) and Stewart and Pakiser (1963), respectively, but the geometry of the interface between these two end members was determined during this study.

The next interface, at D = 65 km on the western end of the model, designates the base of the lithosphere and the top of the low velocity zone (LVZ) of the upper asthenosphere. As previously mentioned, the starting model for the asthenospheric region across most of the model was taken from Burdick and Helmberger (1978). For this reason, the initial model contained no asthenospheric discontinuities and the velocity gradient was varied according to the T7 model. The only asthenospheric interfaces drawn in Figure 21 are those that deviate from the initial model. Under the Colorado Plateau, the depth to the asthenosphere was lowered to 80 km, but, as with the Colorado Plateau crust, this depth was somewhat arbitrary since none of the modeled arrivals passed through that section of the interface. In the east, the same dip of 7.6° was used on the asthenosphere boundary which began to drop from 65 km at R = 1050 km to about 93 km at R = 1260 km. However, the resolution of details on this interface in the transition is limited.

The P-wave velocity beneath the crust within the rift begins at 7.7 km/sec at the Moho and increases very slightly to about 7.72 km/sec at the base of the lithosphere (D = 65 km). At the lithosphere/asthenosphere boundary, the velocity drops to 7.65 km/sec, then slowly decreases at a rate similar to the T7 model to a local minimum of 7.6 km/sec at D = 90 km. From that

depth downward, the geometry of the modeled interfaces is taken directly from the T7 model of Burdick and Helmberger (1978) with the velocities modified to fit the new data. Figure 23 shows velocity profiles for the Rio Grande Rift and the T7 model. The two profiles begin to match at a depth of 150 km but as Figure 21 shows, all of this region was not sampled by the seismic energy.

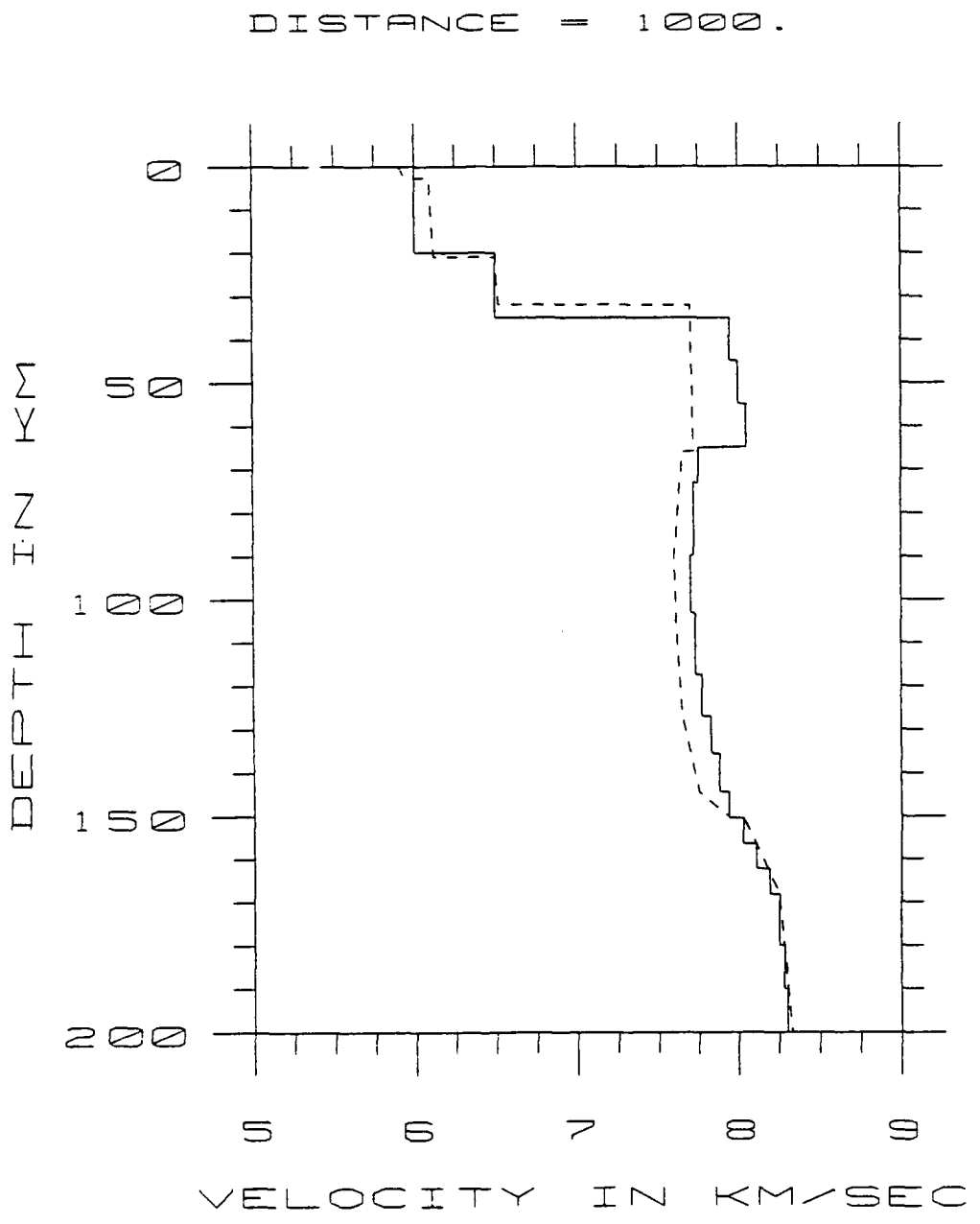

Figure 23. Velocity/Depth profiles within the Rio Grande Rift from the final model and the Burdick and Helmberger model T7.

CONCLUSIONS

The unreversed data presented in this thesis are not sufficient, by themselves, to yield a two dimensional model of the Rio Grande Rift/Great Plains transition. However, by careful construction of an initial model, a heavy reliance on previous studies, and some conservative modeling, some important information can be gleaned from the data concerning the transition. First, by comparing the synthetic sections generated from the 1D model of Burdick and Helmberger (1978; Figures 16 - 19) with the observed sections (Figure 12) it is clear that the recorded energy in the western portion of the study area traveled through significantly slower material than that predicted by the T7 model. As discussed above, this lower velocity is almost certainly under the Rio Grande rift. Modeling the Moho interface with no dip, i.e. extending the rift into eastern New Mexico and the western panhandle of Texas, and keeping the low upper mantle velocity of 7.7 km/s as well, is intuitively incorrect and yields later arrivals than those observed in the eastern half of the observed sections. Therefore, a lithospheric and presumably asthenospheric transition does occur within the study area.

The final location of the Moho transition (Figure 21) represents a best fit to the data using the Pn and P1 arrivals. Moving the interface significantly in either direction or changing its slope dramatically results in a less optimal fit to the observed sections. While the data will allow slight changes in the transition's location and slope, the chosen location represents a good fit and honors the data from Sinno et al (1986) taken just west of the interface and Stewart and Pakiser (1962) to the west. The data does not support a steep transition between the two provinces. The slope of 7.6^{o} is fairly gradual and

extends the effects of rifting under the physiographic Great Plains province of eastern New Mexico. As Figure 2 shows, this deep crustal structure begins significantly east of the eastern-most surface features attributed to the rift. This indicates that the Tularosa basin is definitely part of the Cenozoic extensional regime responsible for the rift.

These data also indicate a significantly lower seismic compressional velocity within the upper mantle under the Rio Grande Rift compared to the T7 model (Figure 23). This helps confirm the idea of higher mantle temperatures inferred from the anomalously high surface heat flow values within the rift and the large volumes of Cenozoic igneous rock within the area.

REFERENCES

Burdick, L. J. and Donald V. Helmberger, 1978, The upper mantle P velocity structure of the western United States, Jour. Geop. Res., vol. 83, no. B4, 1699-1712.

Cerveny, V., Ray theoretical seismograms for laterally inhomogeneous structures, 1979, Jour. Geophys., vol. 46, pp. 335-342.

Cerveny, V., E. A. Molotkov, and I. Psencik, Ray method in seismology, Praha, Univerzita Karlova.

Chapin, C. E., 1971, The Rio Grande rift, part 1: modifications and additions, New Mexico Geological Society, Guidebook 22, pp 191-202.

Chapin, C. E, 1979, Evolution of the Rio Grande rift: a summary, *in:* R. E. Riecker, ed., *Rio Grande Rift: Tectonics and magmatism,* Am. Geop. Union, pp. 1-5.

Chapman, C. H, 1973, The earth flattening transformation in body wave theory, Geop. Jour. Royal Astr. Soc., vol. 35, pp. 55-70.

Cook, F. A., D. B. McCullar, E. R. Decker, and S. B. Smithson, 1979, Crustal structure and evolution of the southern Rio Grande Rift, *in:* R. E. Riecker, ed., *Rio Grande Rift: Tectonics and magmatism,* Am. Geop. Union, p. 195-208.

Cordell, L., 1978, Regional geophysical setting of the Rio Grande Rift, Geol. Soc. Am. Bull., v. 89, p. 1073-1090.

Daggett, P. H., 1982, An integrated geophysical study of the crustal structure of the southern Rio Grande Rift, Ph. D. dissertation, New Mexico State University, Las Cruces.

Daggett, P. H., G. R. Keller, P. Morgan, and C. Wen, 1986, Structure of the southern Rio Grande Rift from gravity interpretation, Jour. Geop. Res., vol. 91, no. B6, p. 6157-6167.

Davis, P. M., E. C. Parker, J. R. Evans, H. M. Iyer, and K. H. Olsen, 1984, Teleseismic deep sounding of the velocity structure beneath the Rio Grande Rift, *in:* Jiri Zidek, ed., *Rio Grande Rift: northern New Mexico,* New Mexico Geol. Soc. Guide., no. 35, p. 29-38.

Gish, D. M., G. R. Keller, and M. L. Sbar, 1981, A refraction study of deep crustal structure in the Basin and Range : Colorado Plateau of eastern Arizona, Jour. Geop. Res., vol. 86, no. B7, p. 6029-6038.

Green, R. W. E. and A. L. Hales, 1968, The travel times of P waves to 30° in the central United States and upper mantle structure, Bul. S.S.A, vol. 58, no. 1, pp 267-289.

Hill, David P., E. Kissling, J. H. Luetgert, and U. Kradolfer, 1985, Constraints on the upper crustal structure of the Long Valley-Mono Craters volcanic complex, eastern California, from seismic refraction measurements, Jour. Geop. Res., vol. 90, no. B13, pp. 11,135-11,150.

Harden, S. N., 1982, A seismic refraction study of west-central New Mexico, master's thesis, University of Texas at El Paso.

Jaksha, L. H., 1982, Reconnaissance seismic refraction-reflection surveys in southwestern New Mexico, Geol. Soc. Am. Bull., vol. 93, p. 1030-1037.

Keller, G. R., L. W. Braile, and J. W. Schlue, 1979, Regional crustal structure of the Rio Grande Rift from surface wave dispersion measurements, *in:* R. E. Riecker, ed., *Rio Grande Rift: Tectonics and magmatism,* Am. Geop. Union, p. 115-126.

Keller, G.R., Paul Morgan, and William R. Seager, 1990, Crustal structure, gravity anomalies and heat flow in the southern Rio Grande rift and their relationship to extensional tectonics, Tectonophysics, vol. 174, pp. 21-37.

Kelley, V. C., 1972, Outcropping Permian shelf formations of eastern New Mexico, *in:* V. C. Kelley and F. D. Trauger, eds., *East-central New Mexico,* New Mex. Geol. Soc. Guide., 23rd field conference, pp. 811-818.

Kelley, V. C., 1979, Tectonics, middle Rio Grande rift, New Mexico, *in:* R. E. Riecker, ed., *Rio Grande Rift: Tectonics and magmatism,* Am. Geop. Union, pp. 33-56.

Kelley, V. C., and T. B. Thompson, 1964, Tectonics and general geology of the Ruidoso-Carrizozo region, central New Mexico, *in:* S. R. Ash and L. V. Davis, eds., *Ruidoso country,* New Mex. Geol. Soc. Guide., 15th field conference, pp. 110-121.

Olsen, K. H., G. R. Keller, and J. N. Stewart, 1979, Crustal structure along the Rio Grande Rift from seismic refraction profiles, *in:* R. E. Riecker, ed., *Rio Grande Rift: Tectonics and magmatism,* Am. Geop. Union, p. 127-143.

Reilinger, R. E., L. D. Brown, and J. E. Oliver, 1979, Recent vertical crustal movements from leveling observations in the vicinity of the Rio Grande rift, *in:* R. E. Riecker, ed., *Rio Grande Rift: Tectonics and magmatism,* Am. Geop. Union, pp. 223-236.

Reiter, M., C. L. Edwards, H. Hartman, and C. Weidman, Terrestrial heat flow along the Rio Grande Rift, New Mexico and southern Colorado, Geo. Soc. Am. Bull., v. 86, pp. 811-818.

Seager, William R. and Paul Morgan, 1979, Rio Grande rift in southern New Mexico, west Texas, and northern Chihuahua, *in:* R. E. Riecker, ed., *Rio Grande Rift: Tectonics and magmatism,* Am. Geop. Union, pp. 87-106.

Sinno, Y. A., P. H. Daggett, G. R. Keller, P. Morgan, and S. H. Harder, 1986, Crustal structure of the southern Rio Grande Rift determined from seismic refraction profiling, Jour. Geop. Res., vol. 91, no. B6, p. 6143-6156.

Sinno, Y. A., and G. R. Keller, 1986, A rayleigh wave dispersion study between El Paso, Texas, and Albuquerque, New Mexico, Jour. Geop. Res., vol. 91, no. B6, p. 6168-6174.

Stewart, S. W., and L. C. Pakiser, 1962, Crustal structure in eastern New Mexico interpreted from the GNOME explosion, Bull. Seis. Soc. Am., v. 52, no. 5, pp. 1017-1130.

Swanberg, C. A., 1979, Chemistry of thermal and non-thermal groundwaters in the Rio Grande Rift and adjacent tectonic provinces, *in:* R. E. Riecker, ed., *Rio Grande Rift: Tectonics and magmatism,* Am. Geop. Union, p. 279-288.

Taylor, Steven R., 1983, Three-dimensional crust and upper mantle structure at the Nevada Test Site, Jour. Geop. Res., vol. 88, no. B3, pp. 2220-2232.

Toppozada, T. R., and A. R. Sanford, 1976, Crustal structure in central New Mexico interpreted from the GASBUGGY explosion, Bull. Seis. Soc. Am., v. 66, n. 3, p. 877-886.

Veldhuis, J. H. and Keller. G. R. 1980, An interated geological and geophysical study of the Salt Basin graben, west Texas, New Mexico Geol. Soc. 31st Field Conf. Guideb., pp. 141-150.

Warren, David G., 1969, A seismic refraction survey of crustal structure in central Arizona, GSA Bul., vol. 80, no. 2, pp. 257-282.

A THERMOMECHANICAL MODEL OF THE COLORADO PLATEAU LITHOSPHERE

Juan Homero Hinojosa
Department of Geological Sciences
The University of Texas at El Paso
El Paso, Texas 79968-0555

(to be submitted to *Journal of Geophysical Research*)

Appendix D

ABSTRACT

The Colorado Plateau (CP) is a coherent and elastically strong lithospheric block surrounded in part by the weaker extensional regimes of the Basin and Range Province and the Rio Grande Rift. The CP has experienced a Cenozoic uplift of about 2 km. The exact physical mechanism responsible for isostatic uplift is still unclear. Previously proposed uplift mechanisms for the CP include, in general, some form of (i) thermal expansion, (ii) crustal thickening, and (iii) phase changes. An alternative thermomechanical uplift mechanism is proposed here. A finite difference solution to both the axisymmetric, time-dependent heat conduction equation with heat sources and the elastic flexure equation has been obtained. Heat flux boundary conditions are used at the base and sides of the model, while the upper boundary is isothermal. The time-dependent elastic thickness of the CP lithosphere model is computed at each time step, and the buoyancy produced by the heated material is used as the thermally-derived normal stress acting on the elastic lithosphere. The initial results of this study appear to indicate that the 2 km of uplift of the CP were produced by at least two sources of uplift: the first associated with the regional heating of the western Cordillera, and the second associated with the flexural response of the CP lithosphere to radial heating at the sides.

INTRODUCTION

The Colorado Plateau (CP) is a coherent lithospheric block in western United States. It is approximately 700 km in diameter, and is bounded by the extensional tectonic regimes of the Basin and Range Province (BRP) in the west and south, and the Rio Grande Rift (RGR) in the east. The CP remained relatively stable during the early stages of rapid extension in the BRP in the mid-Tertiary, and experienced a Cenozoic uplift of about 2 km. The interior of the CP is characterized by a crust 45 km thick, low to normal heat flow (55 to 65 $mW\ m^{-2}$) and low P_n velocities of about 7.8 $km\ sec^{-1}$. The margins of the Plateau, on the other hand, are characterized by very low upper mantle seismic velocities, anomalously thin crust (30 - 35 km thick), and late Cenozoic volcanism and faulting. The margins of the Plateau appear to be transition zones extending up to about 100 km into the Plateau, and resemble the extensional conditions more than the Plateau interior [*Keller et al.*, 1979; *Thompson & Zoback*, 1979; *Morgan & Swanberg*, 1985].

The nature of the Colorado Plateau as a separate tectonic entity amidst an extensional setting remains unknown. Even more importantly, the exact physical mechanism(s) responsible for isostatic uplift remain a mystery. Several uplift mechanisms have been proposed, all of which can be grouped into three classes: (i) thermal expansion, (ii) crustal thickening, and (iii) phase changes. *Morgan & Swanberg* [1985] conclude that no single uplift mechanism can satisfactorily explain the 2 km of uplift, and that the likely mechanism is some combination of thermal expansion and crustal thickening.

The primary objective of this study is to better understand the thermal evolution leading to the present structure of the lithosphere of the Colorado Plateau. To accomplish this, a numerical time-dependent thermal model of the CP lithosphere has been developed. The model predictions to be compared with the geophysical observables include: (i) isostatic uplift, (ii) surface heat flow, (iii) lithospheric thickness, (iv) elastic thickness, and (v) surface

deflection.

TIME-DEPENDENT ENERGY DIFFUSION EQUATION

We are using cylindrical symmetry in our treatment of both the energy diffusion equation and the elastic flexure equation. The axisymmetric energy diffusion equation with internal heat sources is given by

$$\frac{\partial T}{\partial t} = \kappa \left[\frac{\partial^2 T}{\partial r^2} + \frac{1}{r}\frac{\partial T}{\partial r} + \frac{\partial^2 T}{\partial z^2} \right] + \frac{\dot{q}(z)}{\rho c} \tag{1}$$

where $\dot{q}(z) = A_s e^{-(z/b)}$ is the exponential crustal heat production.

The initial and boundary conditions used are the following:

$$T = 0^{\circ}C \text{ at } z = 0, 0 \le r \le R, t = 0 \tag{2a}$$

$$T = 1024^{\circ}C \text{ at } z = L, 0 \le r \le R, t = 0 \tag{2b}$$

$$\frac{\partial T}{\partial r} = 0 \text{ at } r = 0, R; 0 \le z \le L, t \ge 0 \tag{3}$$

$$q_z(r) = 40\ mW/m^2 \text{ at } z = L, 0 \le r \le R, t > 0 \tag{4}$$

$$q_r(z) = 30\ mW/m^2 \text{ at } r = R, \frac{L}{2} < z \le L, t > 0 \tag{5}$$

The steady-state geotherm used as the initial temperature distribution is given by

$$T(z) = T_s + \frac{q_m z}{k} + \frac{A_s b^2}{k}\left(1 - e^{-(z/b)}\right) \tag{6}$$

The computational grid contained 101 nodal points in the radial direction, and 51 points in the z-direction. This leads to a resolution of 8 km in the radial direction, and 2.4 km in the z-direction.

The initial temperature distribution is a steady-state geotherm, with variation in the z-direction only (Fig. 1).

The reference (initial) density used for the crustal and mantle layers of the lithosphere is shown in Figure 2. The density in the crust increases from 2.7 $g\ cm^{-3}$ at the surface to 3.0 $g\ cm^{-3}$ at the base of the crust, while the density in the mantle decreases with temperature from 3.262 $g\ cm^{-3}$ just below the Moho, to 3.177 $g\ cm^{-3}$ at the base of the lithosphere.

The vertical walls of the computational domain (r=0 and r=R) were assumed to be adiabatic (i.e., dT/dr = 0). The top surface of the computational domain was held at $T = 0^{o}C$ for all times. A heat-flux boundary condition as a function of r was imposed at the base of the lithosphere as well as on the wall at r = R for t > 0.

AXISYMMETRIC ELASTIC DEFLECTION EQUATION

The deflection of the thin elastic plate being modeled here is given by

$$\nabla^2 \left(D(r) \nabla^2 w \right) + \rho g w(r) = \int_0^L \Delta\rho(r,z) g dz \tag{7}$$

The elastic deflection boundary conditions are

$$\frac{\partial w}{\partial r} = \frac{\partial^3 w}{\partial r^3} = 0 \ at\ r = 0; z = 0 \quad (Symmetry\ end) \tag{8}$$

$$\frac{\partial^2 w}{\partial r^2} = \frac{\partial^3 w}{\partial r^3} = 0 \ at\ r = R; z = 0 \quad (Free\ end) \tag{9}$$

MODEL PREDICTIONS

(i) The isostatic uplift was computated by assuming that isostatic compensation is point-wise (i.e., local), and by requiring that the net normal stress vanishes at the surface. That is, the upward buoyancy produced in the layers by thermal expansion is exactly balanced by the downward load of the uplifted surface material.

(ii) The surface heat flow was computed by taking a backward difference of the temperature at the surface over an increment dz.

(iii) The lithospheric thickness was obtained by monitoring the upward migration of the $1350^{o}C$ isotherm.

(iv) The elastic thickness was obtained by monitoring the upward migration of the $675^{o}C$ isotherm.

(v) The surface deflection was computed by numerically solving Eq. (7) with the variable elastic thicknesses obtained from (v) above.

At each time step of the calculation, a corresponding model prediction was obtained for the geophysical quantities mentioned above (i - v).

RESULTS

The temperature distribution within the axisymmetric computational domain is shown as a function of time in Figure 3 for the initial and boundary conditions described above. The contour interval in Fig. 3 is $100^{o}C$, and the variation in temperature with time is monitored in intervals of 20 Ma out to a maximum of 60 Ma. In Figure 4 the excess temperature is shown, that is, the temperature in excess of the initial temperature distribution. The contour interval is $10^{o}C$, and the time increments are also every 20 Ma.

In Figure 5 the isostatic uplift is shown as a function of radial distance and time. The uplift results from the thermal expansion of crustal and mantle material within the two-layer model. The uplift is larger over the region of higher basal and radial heat flux, as would be expected. The uplift increases with time because of the continued increase in temperature within the layers.

The surface heat flow is shown in Figure 6 as a function of radial distance and time. After about 40 Ma the effects of the basal and radial heating begin to reach the upper layer and the

heat flow begins to increase with time. Recall that the observed heat flow over the Colorado Plateau is in the range of 55 to 65 $mW\ m^{-2}$. The predicted heat flow reaches a value of about 70 $mW\ m^{-2}$ at the margins after 60 Ma of heating.

Figure 7 shows the lithospheric thickness as a function of radial distance and time. The lithospheric thickness is defined as the depth to the $1350^{o}C$ isotherm. The lithospheric thickness is smaller over the region of higher heat flux, and continues to decrease because of the continual increase in temperature.

The elastic thickness is here defined as the depth to the $675^{o}C$ isotherm. Note that the elastic thickness in this model is variable due to the temperature distribution within the model lithosphere. Figure 8 shows the elastic thickness of the lithosphere as a function of radial distance and time. Again, the elastic thickness decreases with time because of the input in heat.

Figure 9 shows the elastic deflection of the lithosphere due to the upward buoyancy produced by the heated rock layers. The deflection of the surface is low, and reaches a value of a little less than 1/3 km after 60 Ma.

CONCLUSION

The initial results of this study appear to indicate that the 2 km of uplift of the CP were produced by at least two sources of uplift: the first associated with the regional heating of the western Cordillera, and the second associated with the flexural response of the CP lithosphere to radial heating at the sides.

TABLE OF MODEL PARAMETERS

Parameter	Symbol	Value
Initial lithospheric thickness	L	120 km
Crustal thickness	L_c	39 km
Initial temperature at base of lithosphere	T_L	$1024^o\ C$
Radius of model	R	360 km
Coefficient of thermal expansion	α	$3.0\times10^{-5}\ C^{-1}$
Thermal diffusivity	κ	$8.0\times10^{-7}\ m^2\ s^{-1}$
Thermal conductivity	k	$4.0\ W/m^oK$
Crustal heat production	A_s	$2.47\ \mu W\ m^{-3}$
Radioactive length scale	b	14.17 km
Reduced heat flow	q_m	$30\ mW\ m^{-2}$
Mantle density (at $T=0^oC$)	ρ_m	$3.3\ Mg\ m^{-3}$

BIBLIOGRAPHY

Keller, G.R., Braile, L.W., and Morgan, P., 1979, Crustal structure, geophysical models, and contemporary tectonism of the Colorado Plateau; *Tectonophysics*, **61**: 131-147.

Morgan, P., and Swanberg, C.A., 1985, On the Cenozoic uplift and tectonic stability of the Colorado Plateau; *Journal of Geodynamics*, **3**: 39-63.

Thompson, G.A., and Zoback, M.L., 1979, Regional geophysics of the Colorado Plateau; *Tectonophysics*, **61**: 149-181.

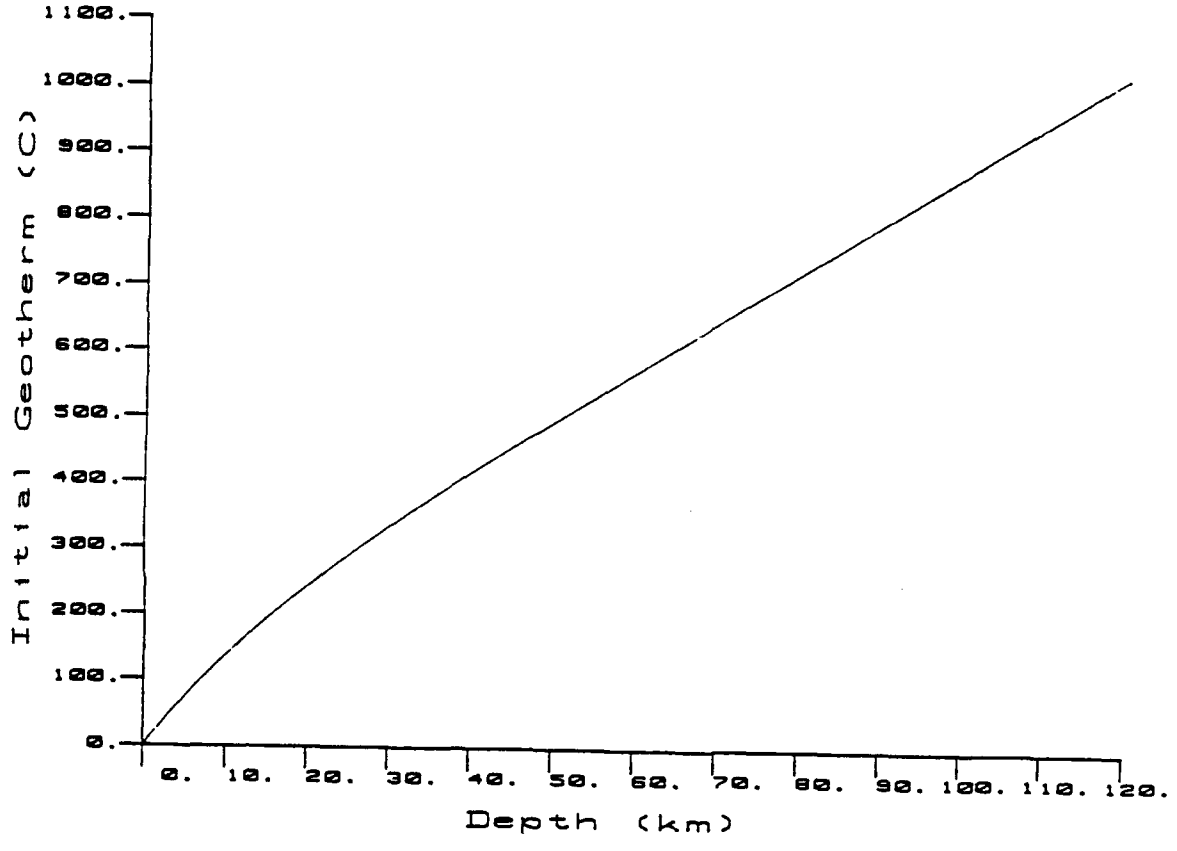
1100.
1000.
900.
800.
700.
600.
500.
400.
300.
200.
100.
0.
Initial Geotherm (C)
0. 10. 20. 30. 40. 50. 60. 70. 80. 90. 100. 110. 120.
Depth (km)

Figure 1

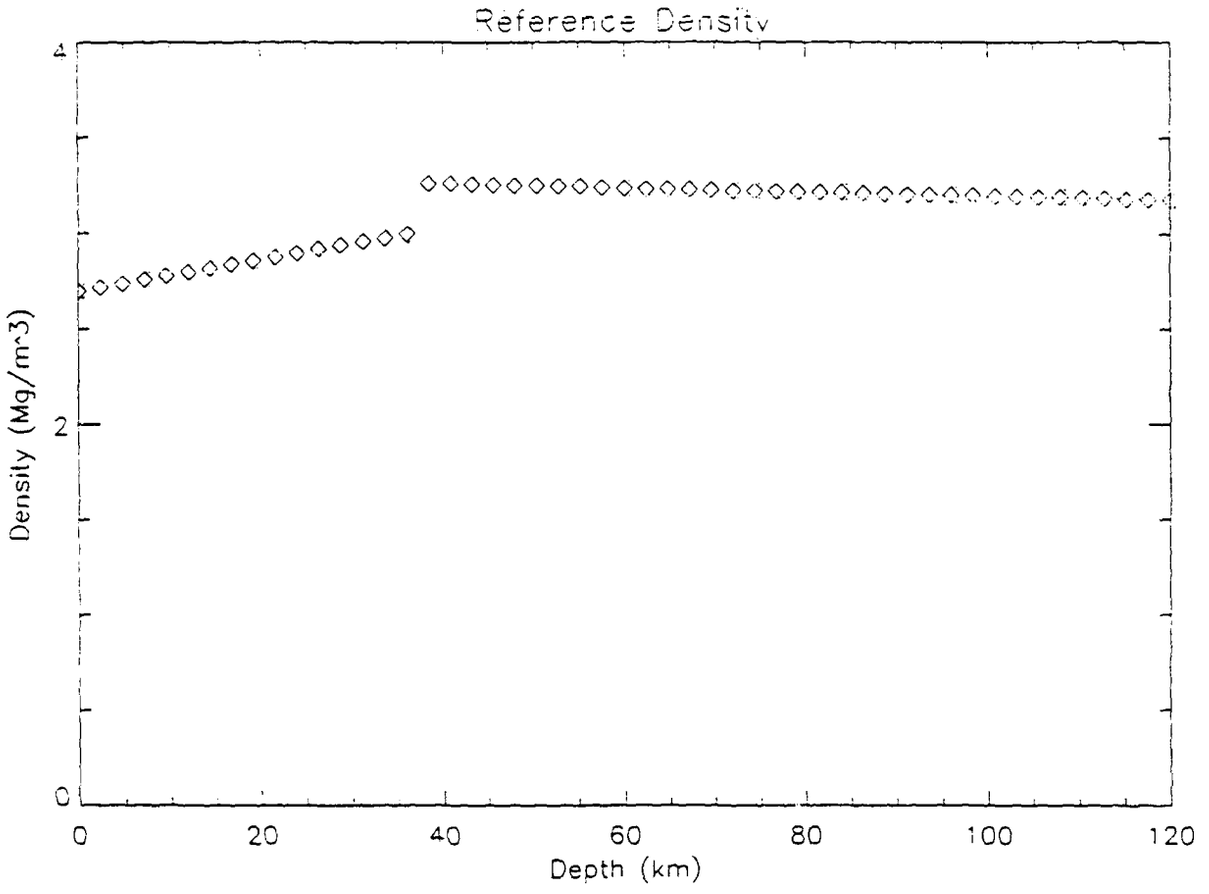
Reference Density
Density (Mg/m^3)
4
2
0
0
20
40
60
80
100
120
Depth (km)

Figure 2

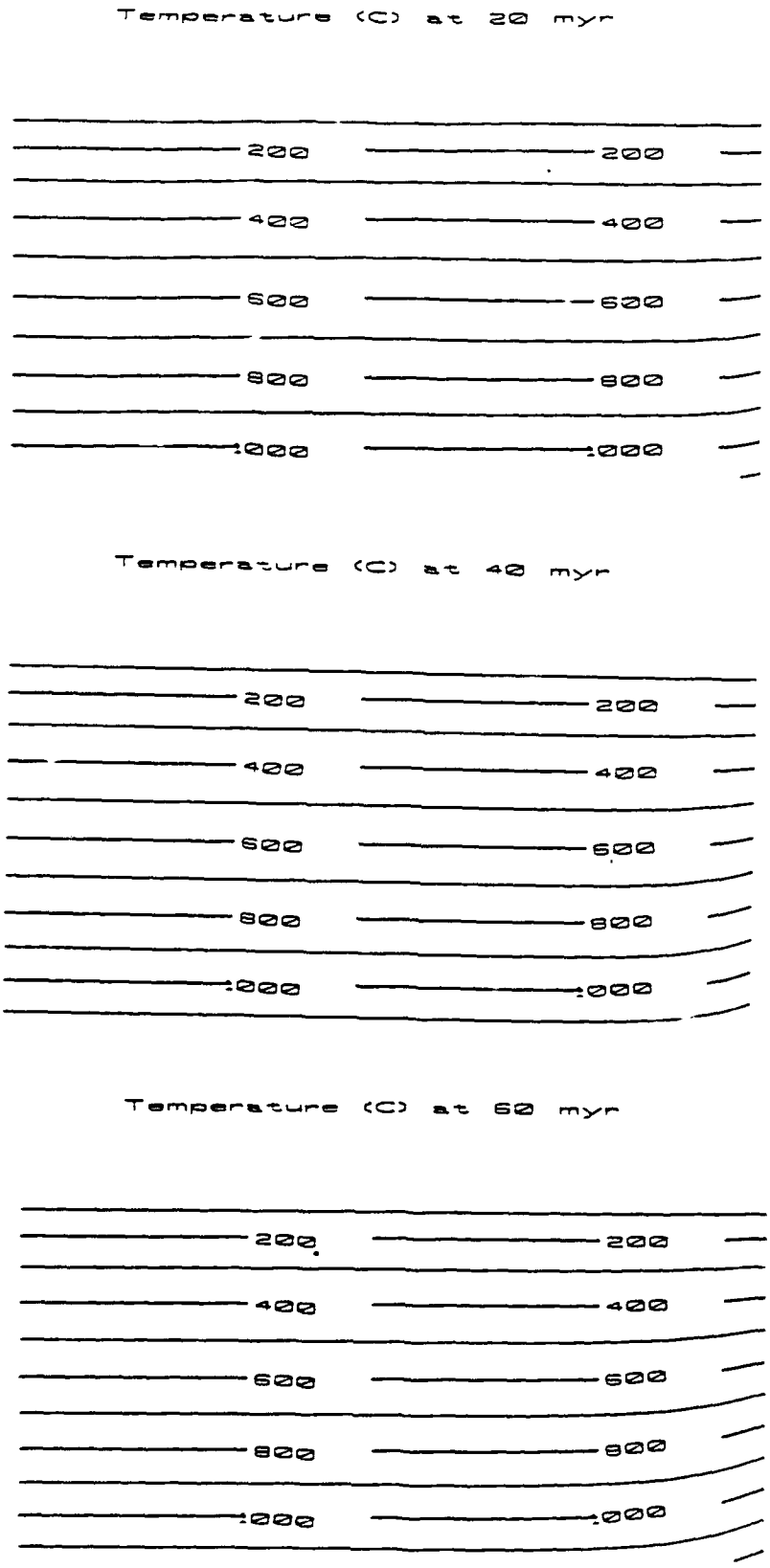
Temperature (C) at 20 myr
200
200
400
400
600
600
800
800
1000
1000
Temperature (C) at 40 myr
200
200
400
400
600
600
800
800
1000
1000
Temperature (C) at 60 myr
200
200
400
400
600
600
800
800
1000
1000

Figure 3

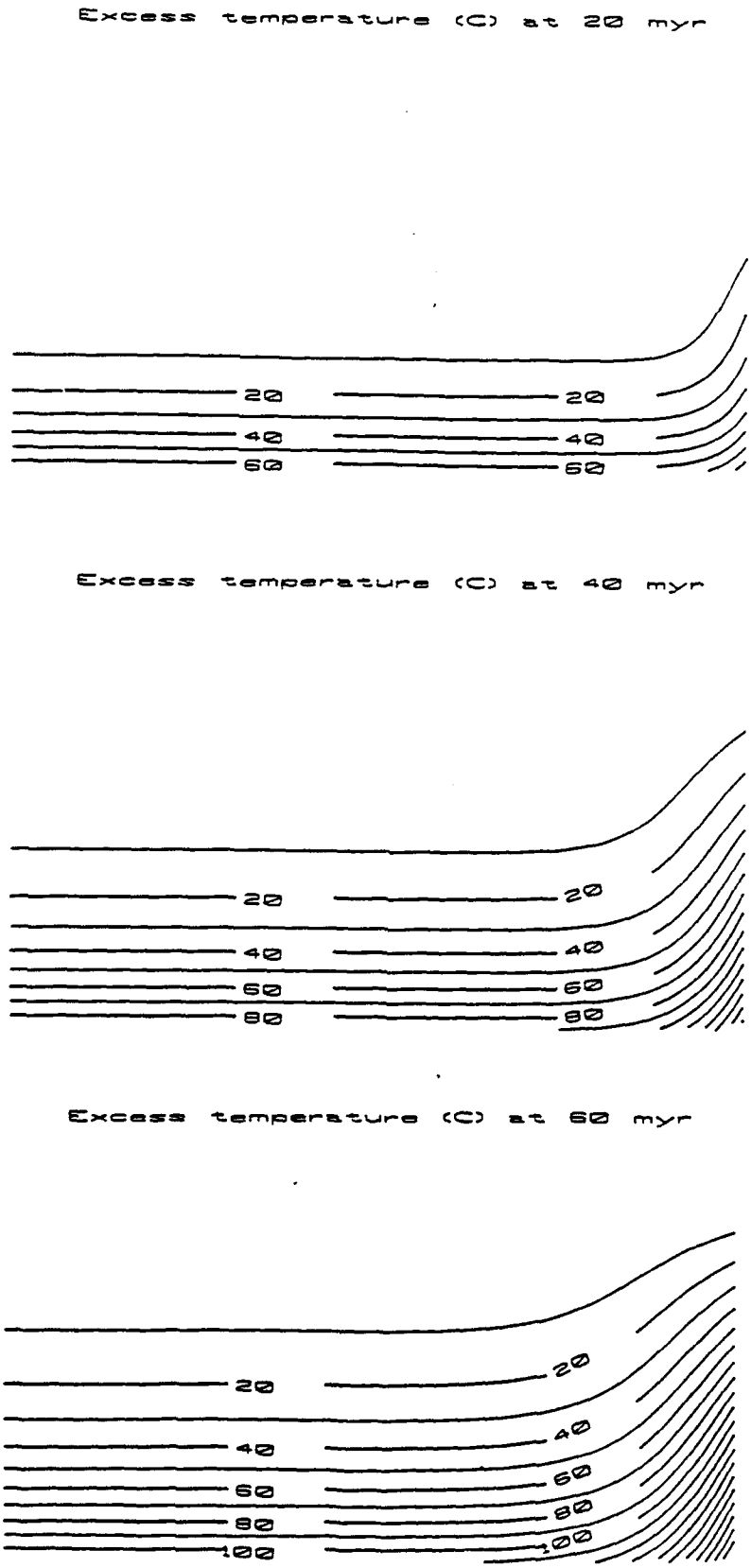
Excess temperature (C) at 20 myr
20
20
40
40
60
60
Excess temperature (C) at 40 myr
20
20
40
40
60
60
80
80
Excess temperature (C) at 60 myr
20
20
40
40
60
60
80
80
100
100

Figure 4

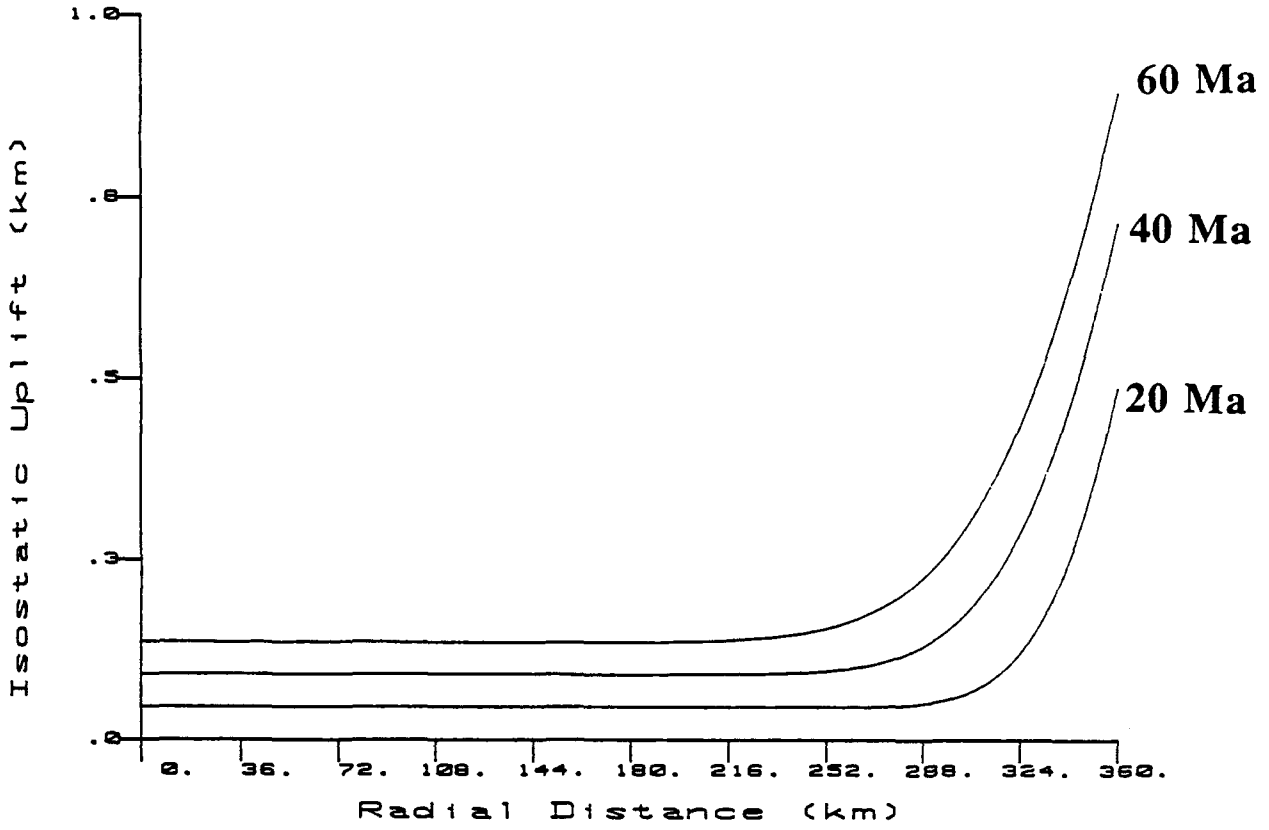
1.0
.8
.5
.3
.0
Isostatic Uplift (km)
60 Ma
40 Ma
20 Ma
0.
36.
72.
108.
144.
180.
216.
252.
288.
324.
360.
Radial Distance (km)

Figure 5

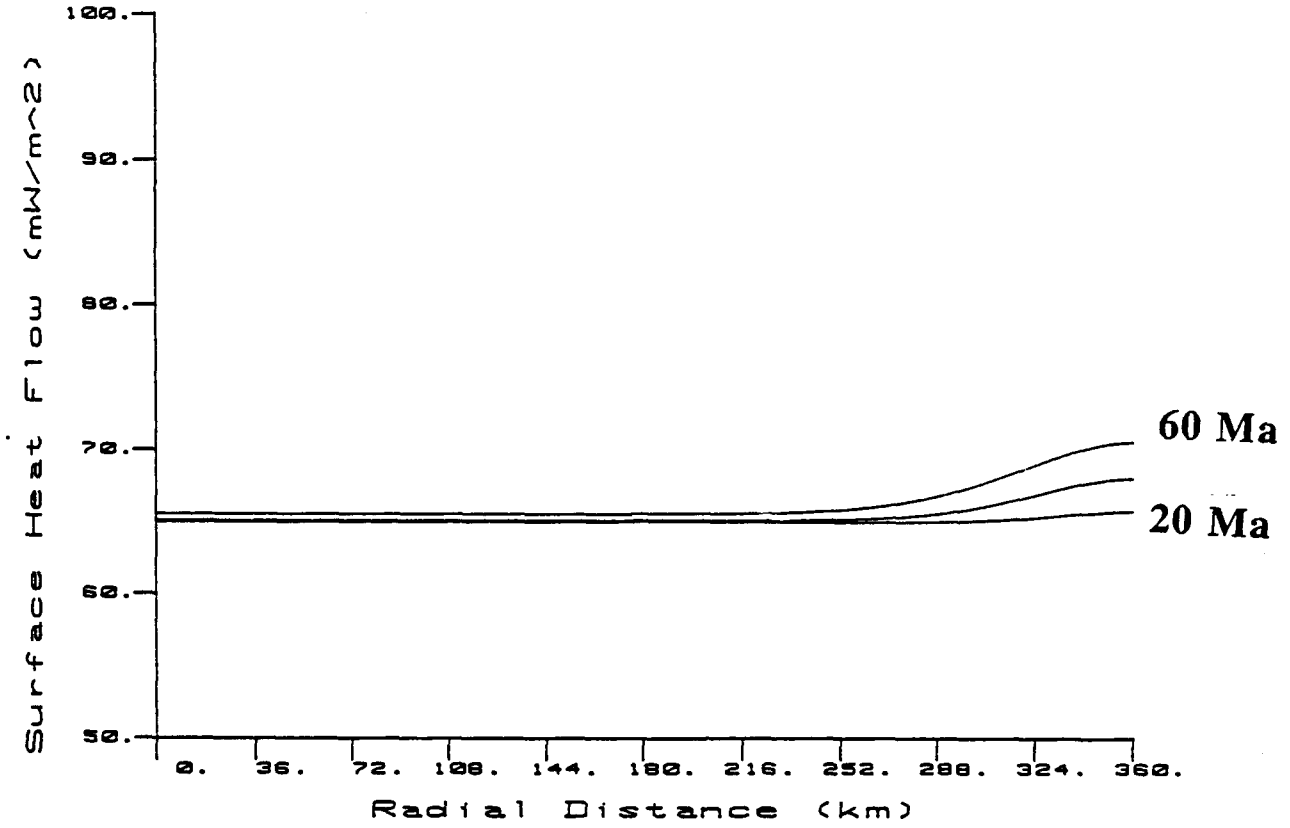
100.
90.
80.
70.
60.
50.
Surface Heat Flow (mW/m^2)
60 Ma
20 Ma
0.
36.
72.
108.
144.
180.
216.
252.
288.
324.
360.
Radial Distance (km)

Figure 6

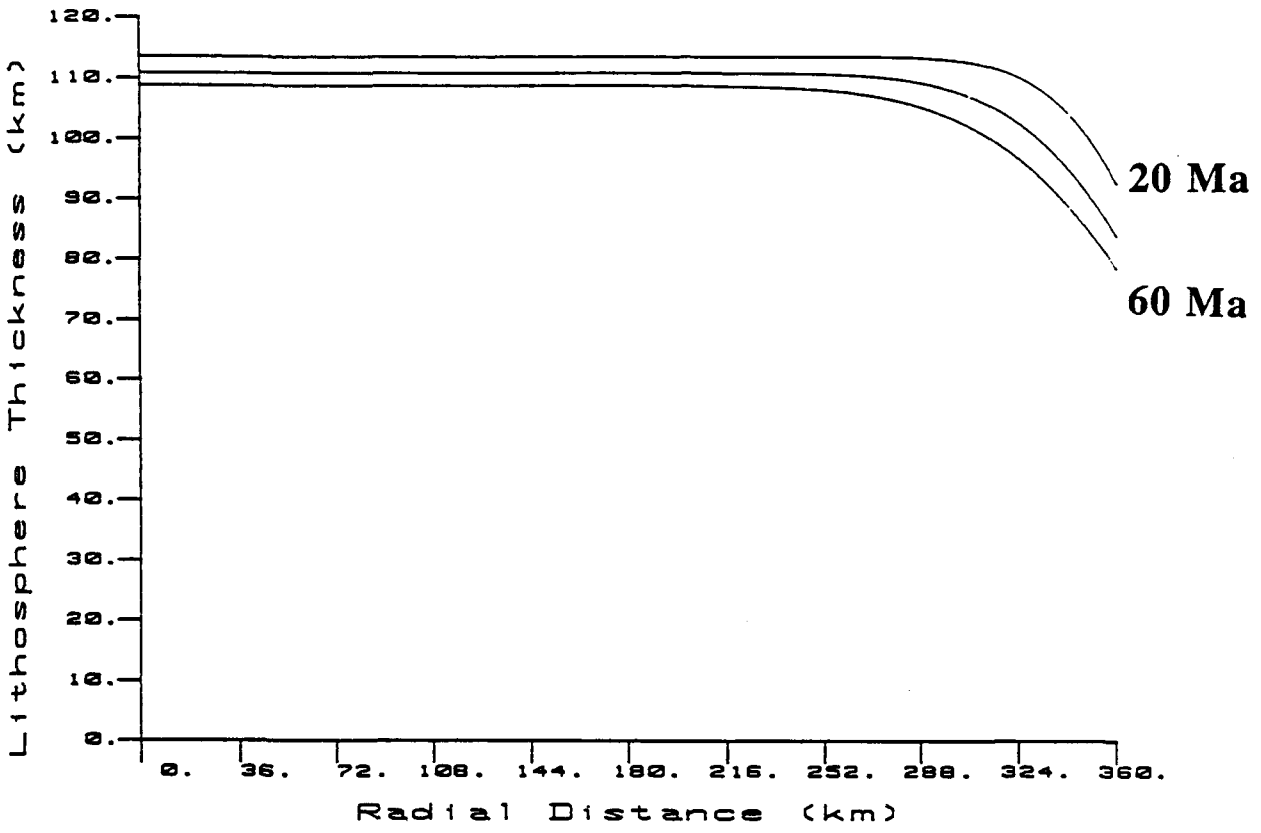
120.
110.
100.
90.
80.
70.
60.
50.
40.
30.
20.
10.
0.
Lithosphere Thickness (km)
0.
36.
72.
108.
144.
180.
216.
252.
288.
324.
360.
Radial Distance (km)
20 Ma
60 Ma

Figure 7

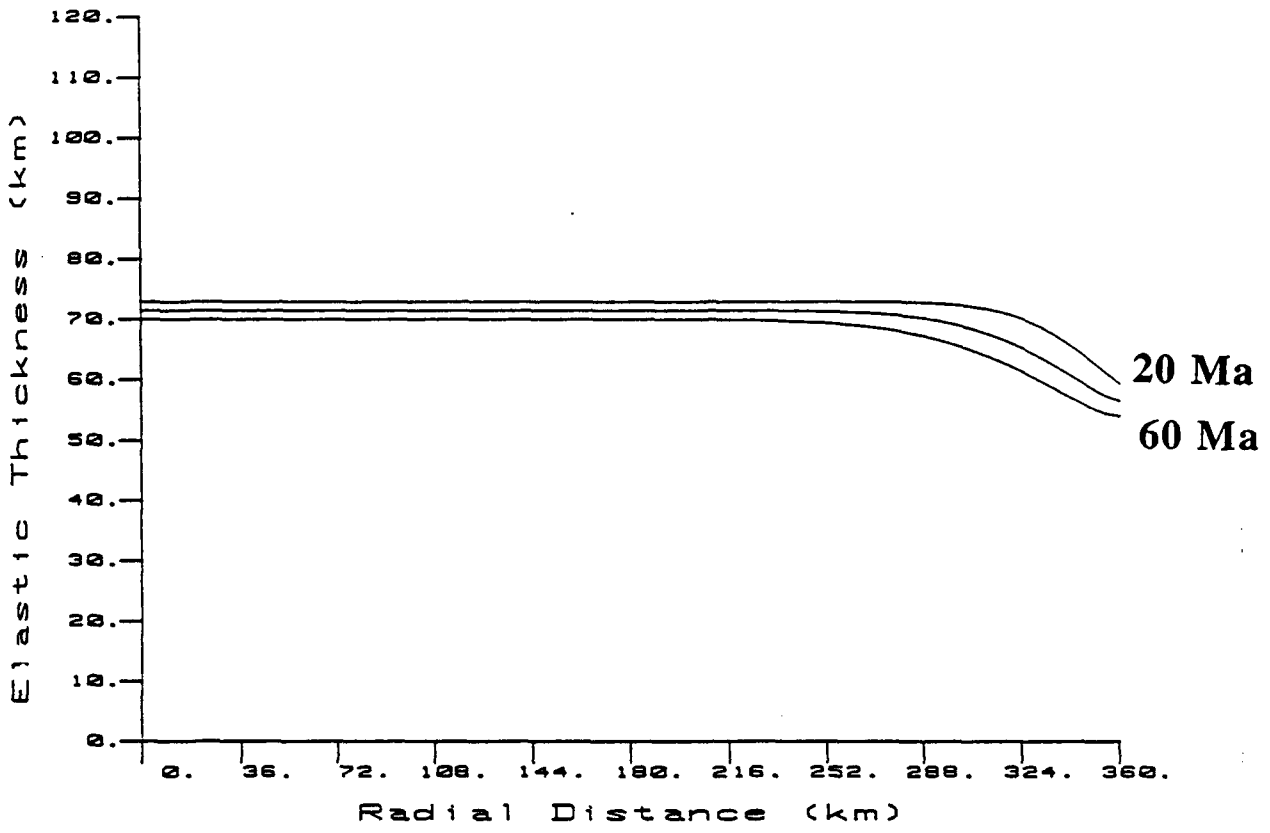
120.
110.
100.
90.
80.
70.
60.
50.
40.
30.
20.
10.
0.
Elastic Thickness (km)
0.
36.
72.
108.
144.
180.
216.
252.
288.
324.
360.
Radial Distance (km)
20 Ma
60 Ma

Figure 8

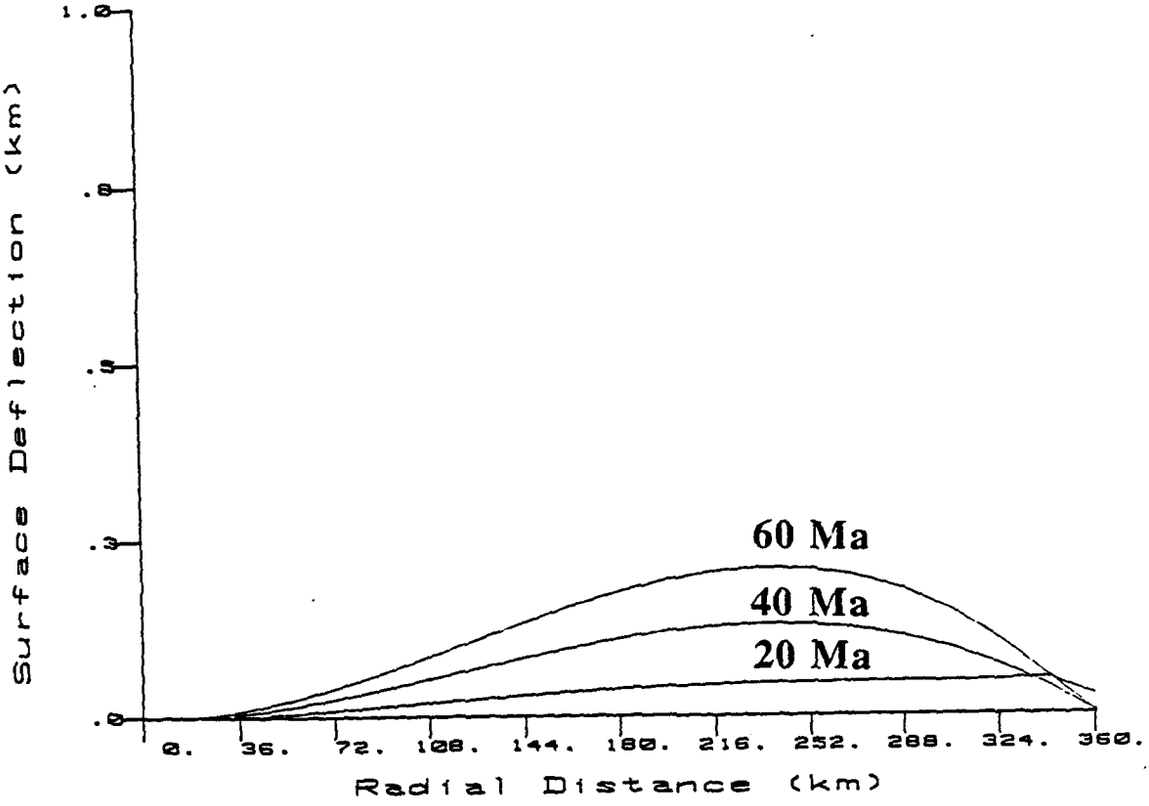
Surface Deflection (km)
1.0
.6
.3
.0
60 Ma
40 Ma
20 Ma
0.
36.
72.
108.
144.
180.
216.
252.
288.
324.
360.
Radial Distance (km)

Figure 9